University of Stavanger

Faculty of Science and Technology

MASTER'S THESIS

Study program/ Specialization: Master of Science in Petroleum Technology, Drilling Specialization	Spring semester, 2013 **Restricted Access**
Writer: **Anders Mikalsen**	.....
Faculty supervisor: **Mesfin Belayneh** External supervisor: **Leif Magne Stokland** **- Halliburton**	
Title of thesis: Analysis of drilled wells on the Norwegian Continental Shelf (NCS)	
Credits (ECTS): 30	
Key words: Post-run analysis, Torque and Drag, Drillstring Vibration, Model Calibration, Drilling, Real-time, Drilling Optimalization, Integrated Operations.	Pages: 80 + enclosure: 34 Stavanger, 17/06/2013 Date/year

Abstract

Safe drilling operations are a result of integrated geo-mechanical engineering and drillstring mechanical engineering. Torque and drag modeling is used by the oil and gas industry in all phases of drilling a well: Planning, operational and post-operation evaluations. There is an increase in the number of designer wells drilled with complicated wellpaths and extended reach. Good modeling is important to predict the drillstring operational window (ie. buckling or yielding of the drill string) and geo-mechanical well program (i.e collapse and fracture). For this the knowledge of mechanics and hydraulics is important. However, from literature study, and monitoring of real-time data, it is observed that the models do not perfectly capture measured data. Therefore, in order for the model to be reliable, it is important that it is frequently calibrated against high quality real-time field data.

A post-run analysis of a drilling operation is useful for determining friction factors and corrections needed to be made to other parameters in order to calibrate the model. When many wells in the same field have been analyzed it is possible to systematically use historic results and data for prediction use and for use in well planning. A post-run analysis of a recently drilled well in the North Sea is presented in detail in the thesis. In order for the results of such an analysis to be reliable, there has to be a systematic process for performing the analysis.

Acknowledgements

I would like to use this opportunity to thank several people that have contributed in the work of this thesis.

I would like to thank my external supervisor Leif Magne Stokland, Business Development - Landmark, for letting me participate in his Wellplan & Compass Software course at Halliburton, and for facilitating the necessary arrangements with ConocoPhillips.

I would also like to thank Mike Herbert, IO Advisor - ConocoPhillips, for letting me work on the thesis in their Real-Time Integrated Operations Centre.

My deepest gratitude goes to Even Tveit, Drilling Optimization Engineer - Halliburton, for letting me do a post-run analysis on my own. Along the way he provided me with excellent assistance and shared some of his deep knowledge on subjects within the thesis as well as other aspects of the industry. It was rewarding to see my results actually being used and inserted into their database. Thanks also goes to Kevin Boyle, Drilling Optimization Engineer - Halliburton, for assisting me with technical- and software questions during my work at ConocoPhillips.

In addition, I would like to thank my friends, family and girlfriend Monica for support in the months spent working on this thesis.

And last but not least, I would like to thank my faculty supervisor Mesfin Belayneh for constant motivation and positivity from beginning to the very end. I could not have asked for a more supportive and helpful supervisor.

Contents

List of Tables

List of Figures

Nomenclature

BHA – Bottom Hole Assembly

COF – Coefficient of Friction

DLS – Dogleg Severity

ECD – Equivalent Circulating Density

FF – Friction Factor

HPHT – High Pressure High Temperature

IRIS – International Research Institute of Stavanger

LCM – Lost Circulation Material

LWD – Logging While Drilling

MD – Measured Depth

MWD – Measurement While Drilling

OBM – Oil Based Mud

PDC – Polycrystalline Diamond Compact

POOH – Pull Out Of Hole

RIH – Run Into Hole

ROP – Rate Of Penetration

RPM – Revolutions Per Minute

TD – Target Depth

σ – Stress

WOB – Weight On Bit

1. Introduction

This thesis examines how a leading service company performs a post-run analysis of a drilling operation for a major operator.

1.1 Background and Problem Formulation

Safe drilling operation is a result of an integrated geo-mechanical engineering and drillstring mechanical engineering. Prior to drilling, a primary step in well planning is to perform a drillstring mechanical simulation study. The input data for the simulation is the planned section dimensions and lengths, historical data from nearby wells, drilling fluid properties, operational parameters and the drillstring components that are planned for the well. Landmark's WELLPLAN™ software is the commonly used industry standard simulator.

Wellplan's Torque Drag Analysis Module predicts the measured weights and torques while tripping in, tripping out, rotating on bottom, rotating off-bottom, slide drilling and back reaming. This is useful for determining if a well can be drilled or to evaluate the conditions during the drilling process. The module includes both soft- and stiff string models, and is applicable for analyzing drillpipes, casings, liners, tieback strings, tubing strings, and coiled tubing. [1]

An extended reach well is the preferred choice to cover a larger area of the reservoir and exploit more hydrocarbons. In addition, designer wells that can have a number of changes in inclination and azimuth throughout the wellpath are becoming the industry standard. In a field where a large number of wells are already drilled, there can be a need to navigate precisely to avoid collision with other wells. This is the case for this operator's field in the North Sea.

However, drilling long directional wells is challenging because of friction and the increasing drillstring lengths. The knowledge of a friction factors is valuable to predict how far it is possible to drill without buckling the string, and hence successfully reaching the target depth (TD). Without the knowledge of the friction factor, there is a possibility of not reaching the target. Another important issue is the calibration of the model. Hook load sensors on drilling rigs are known to have an uncertainty with regards to showing correct hook loads. This discrepancy is important to quantify in order for simulations to match real-time measurements.

When the operator has drilled a well, a post-run analysis is done by the service company's drilling optimization engineers. The objective is mainly to find friction factors and the uncertainty related to the hook load sensors. In addition, the detailed analysis of each drilling run can reveal the causes of drilling problems which may have been hard to explain during the operation. The field case presented is a post-run analysis of a recently drilled well performed in accordance with the service company's routines. The majority of the work of this thesis was carried out in the operator's real-time drilling center.

The International Research Institute of Stavanger (IRIS) has done extensive work on methods for calibrating different drilling models. Cayeux et al. (2012) [2] and Gravdal et al. (2010) [3] have shown that when computer models are used to analyze the differences between simulated values and observed values, the estimates deviate significantly from the actual measurements for most cases. This can be supported by experiences from the operator's real-time drilling center, in that it is often difficult to compare the initial well planning with the actual results because of sensor uncertainty.

Based on the issues examined by the operator's post-run analysis procedures and the findings of IRIS [2] [3] [4] some questions are raised:

- What is done in a post-run analysis?
- Is a post-run analysis useful?
- What is the importance of real-time data?
- Is the model trustworthy?
- What are the calibration issues of the model?
- Is the planning phase valid for operational phase?

2 Theory

In this section the theory of torque and drag will be presented. The two models presented are three dimensional models. The first model was presented by Johancsik et al. (1984) [5], and is the model which most commercial simulators like Wellplan are based on. The second model is a more recently derived model by Aadnoy (2010) [6]. A comparison of the models is made. In addition, the buckling and tensile limit models are reviewed.

2.1 Torque and Drag – Johancsik Model

Torque and drag is present to some extent in all wells drilled. The severity of torque and drag is connected in any particular well, because high drag forces and excessive torque loads normally occur together. [5] There are a number of causes for torque and drag [7]:

- Poor hole cleaning
- Direction or formation changes
- Increase in differential pressure
- Under gauged hole
- Bit or bottom hole assembly (BHA) balling
- Metal to metal contact
- Cuttings bed on low side of a high-angled hole
- Excessive buildup of filter cake
- Reactive swelling formations (shale)
- Dogleg severity
- Sliding wellbore friction [8]
- Key seats [8]

Most of these causes are due to poor wellbore conditions. The main cause of torque and drag in wells with good hole conditions is sliding wellbore friction. The problems related to torque and drag are usually more severe in directional holes. [5] The most challenging wells are modeled in real-time.

The torque and drag model developed by Johancsik et al. (1984) is still considered as the only "standard" drillstring model in use in the industry today. The model assumes that sliding friction is the primary cause of torque and drag forces in a directional wellbore, and that the friction forces result from contact of the drillstring with the wellbore. [9] [10]

2.1.1 Model Assumptions

For the modeling, the following assumptions are made:

- The bending stiffness of the drillstring is neglected, i.e. the string is modeled as a cable or rope. The contact force in inclined and vertical sections is because of the normal component of the weight of the drillstring. This is called a **soft string**.
- The friction force is between the drillstring and the wellbore in the presence of drilling fluid. This is called **Coulomb friction**.
- The drag force will be affected by flow of fluid in the annulus. This is called the **fluid flow effect**.
- The drillstring is assumed in continuous contact with the wellbore, neglecting the effects of tool joints, coupling and wellbore irregularities and tortuosity. This is called a **slack string**.

2.1.2 Drag Model

Drag is the additional load compared to free rotating drillstring weight. This additional load is usually positive when pulling out of hole and negative when running into hole. The drag force is mainly due to friction generated by the drillstring contact with the wellbore. [10]

Oil wells comprise of vertical, inclined and curved sections. When calculating buckling loads and torque & drag forces, all loads must be computed with respect to a given well geometry (inclination, azimuth and measured depth). The drillstring is assumed to be divided up into a number of short segments (cells) jointed by connections, through which the transmission of tension, compression and torsion are allowed. [11] This is shown in figure 2.1 (left).

Figure 2.1 also shows a simple free-body diagram of a drillstring segment with respective loads (right). The basic Coulomb frictional force, axial forces and other effects are applied to each segment. The loads can be computed from bottom to top or top to bottom. Each of the short

elements contributes small parts of axial drag, weight and other effects. The sum of these forces produces the total loads on the string. [11]

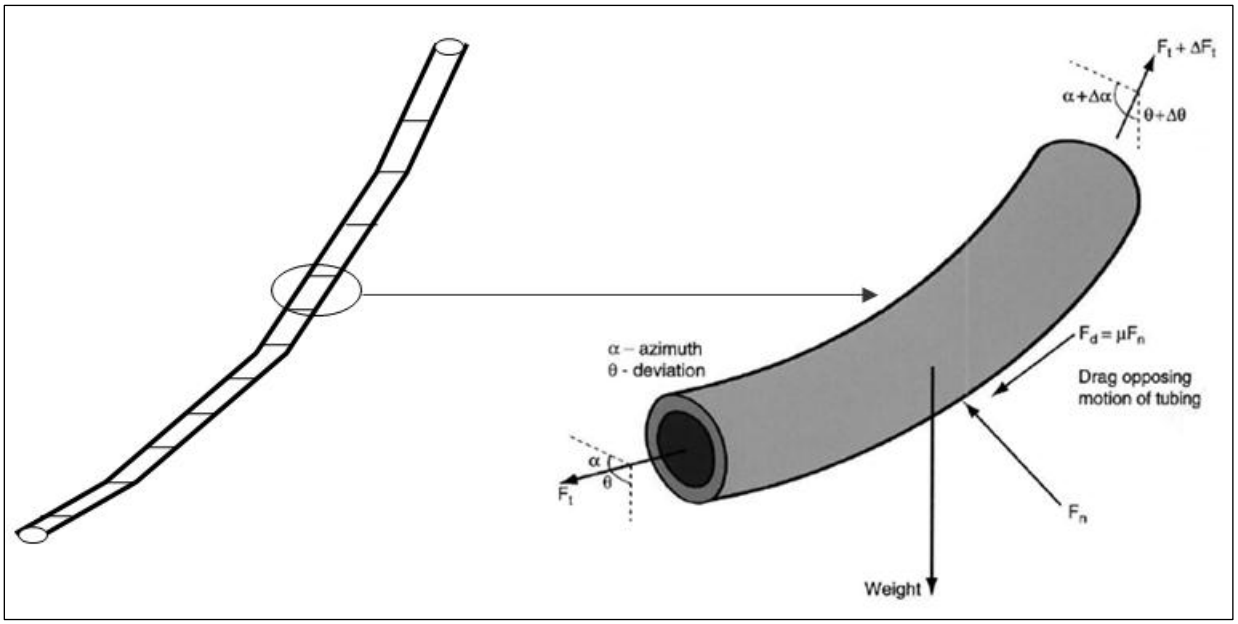

Figure 2.1 – Segmented drillstring and the loading of a single segment [12]

From force balance, applying the condition of equilibrium along the axial and normal directions, the effective force along the axial direction is [5]:

$$\frac{dF}{ds} = \pm\mu_a N + \beta w_s \cos\bar{\theta} \tag{1}$$

Johancsik et al. (1984) derived the normal force in any curved well geometry with variation in inclination and azimuth [5]:

$$N_i = \sqrt{\left(\beta w_{si}\sin\left(\frac{\theta_{i+1}+\theta_i}{2}\right) - F_i\left(\frac{\theta_{i+1}-\theta_i}{S_{i+1}-S_i}\right)\right)^2 + \left(F_i\sin\left(\frac{\theta_{i+1}+\theta_i}{2}\right)\left(\frac{\varphi_{i+1}-\varphi_i}{S_{i+1}-S_i}\right)\right)^2} \tag{2}$$

When drilling at various angular rotational speeds and when tripping in and out, the drillstring is at various axial speeds. These dynamic parameters affect the axial and tangential friction coefficients, and will be considered in the torque and drag model as the following [5]:

The buoyancy factor is defined as: $\beta = 1 - \frac{\rho_{mud}}{\rho_{pipe}}$

The axial friction factor is defined as: $\mu_a = \mu \sin\alpha$

Where the angle α is given by: $\tan\alpha = \frac{v_a}{r\Omega}$, r is the drillstring radius, Ω is the angular velocity of rotation and v_a is the axial speed. v_a is defined positive for tripping in and drilling, and negative for pulling out [5]:

$$F_{i+1} = F_i + \sum_{i=1}^{n}\left[\beta w_i \cos\left(\frac{\theta_{i+1}+\theta_i}{2}\right) \pm \mu_{ai} N_i\right](S_{i+1} - S_i) \quad (3)$$

$F_{a(i)}$ is the bottom weight when integrating from bottom to top. The friction force always has a sign opposite to the direction of the applied axial load on a tube. For running into the hole, the axial load is in the direction of the component of the weight of the tube. For this case the friction causes a compressive (negative) force to be added to F_a. For pulling out of the hole, the axial load is in the opposite direction of the component of the tube along the axial direction. For this case the friction causes a tensile (positive) force to be added to F_a. [13]

2.1.3 Torque Model

Torque is the moment required to rotate the drillstring. The same drillstring-wellbore contact friction that causes drag, will reduce the surface torque that is able to reach the bit. [10]

The torque for both buckled and non-buckled string is given as [5]:

$$T_{i+1} = T_i + \sum_{i=1}^{n} \mu_t r_i . N_i . (S_{i+1} - S_i) \quad (4)$$

$\mu_t = \mu \cos\alpha$

where the tangential friction factor is always positive. N_i is the contact force per unit length.

2.1.4 Friction Factor

The friction factor (FF) is a key parameter for modeling torque and drag. This parameter may also be referred to as the coefficient of friction (COF). Ideally the FF would represent the roughness between the drillstring and the wellbore as a purely mechanical friction. However, drilling introduces a number of forces contributing to the total friction [11] [14]:

- Viscous drag
- Stabilizers/centralizers
- Pore pressure
- Circulation losses
- Tortuosity
- Mud properties
- Temperature effects
- Cuttings bed
- Pipe stiffness effects (for stiff-string models)

The friction factor is often called a fudge factor because of these unwanted effects being included. The belief is that friction factors will to a great extent depend on mud type and whether the hole is cased or open. [5] In addition, the rotating speed of the string, the revolutions per minute (RPM), will affect the friction factors. A well will usually have sections of both cased and open hole, so two friction factors are used when simulating in Wellplan: One inside the casing and one for open hole. Common friction factors for rotary drilling range between 0.10 and 0.30, but values as low as 0.05 and as high as 0.50 can also be found. [11]

2.1.5 Effect of Hydrodynamic Viscous Force

Circulation of mud causes an additional "uplift" effect on the drillstring, resulting in lower effective weight of the string. The effect of this hydrodynamic viscous force is dependent on a combination of hole size, string size and flow rate. The fluid flow will affect pick-up, slack-off and rotating off-bottom weights, but will not have a significant effect on the torque. [11]

To include the effect of hydrodynamic viscous force, Eq. 1 is modified:

$$\frac{dF}{ds} = \pm\mu_a N + \beta w_s \cos\bar{\theta} + \frac{dF_{fl}}{ds} \tag{5}$$

Maidla and Wojtanowicz (1987) also derived the effect of viscous pressure gradient for each pipe element. The hydrodynamic viscous drag force can be calculated to be included in the drag equation [15]:

$$F_{fl} = \frac{\pi}{4}\sum_{i=1}^{n}\left(\frac{\Delta P}{ds}\right)\Delta s_i d_i^2 \tag{6}$$

Where the pressure loss term with fluid velocity and density in the annulus is given as:

$$\frac{\Delta P}{ds} = \frac{f\rho V_{av}^2}{D-d} \tag{7}$$

Where D is the well diameter and d is the outer diameter of the drillstring.

The frictional pressure loss is the loss in pressure during fluid flow due to contact between the fluid and the walls of the flow channel. The frictional pressure loss for both drill-string and annulus flow is calculated using the relation. [3]

$$K = c \times \frac{2f}{D_{hy}}\rho_{mix} v_{mix}^2 \tag{8}$$

Where D_{hy} is the hydraulic diameter, $D_{hy} = D$ for drillstring and $D_{hy} = D_o - D_f$ for annulus and v_{mix} is the fluid mixture velocity. The Fanning friction f is calculated according to the rheological model chosen, and the prevailing flow regime. The coefficient c is a calibration factor that can be used to adjust the model to the measurements in real-time if a proper calibration technique is chosen. The initial value is 1. The friction factors can be used to adjust the flow model if a proper estimation algorithm is implemented. The factors will then be updated in real-time by chosen algorithm to obtain an optimal match between measurement and calculated results. [3]

In the case of non-circular flow conduits, the diameter parameter is replaced by the equivalent diameter. [3]

$$D_e = 4 \times \frac{A_f}{P_w} \quad (9)$$

Where:

D_e= equivalent diameter

A_f = cross-sectional area

P_w = wetted perimeter

In addition the wall roughness, pipe inclination and flow regime is important. In single phase and multiphase flow the difference between laminar and turbulent flow plays an important role for the frictional pressure loss. The type of flow is determined from the Reynolds number [3]:

$$N_{Re} = \frac{\rho v D_{eff}}{\mu_{app}} \quad (10)$$

In Eq.10, D_{eff} is the effective diameter that accounts for both geometry and the effects of non-Newtonian fluid. μ_{app} is the apparent viscosity.

The effective diameter for the drillstring is given by [3]:

$$D_{eff} = D \frac{4N}{3N + 1} \quad (11)$$

les

And for the annulus [27]:

$$D_{eff} = 2/3(D_o - D_i) \frac{3N}{2N + 1} \quad (12)$$

Where:

N= generalization power law index

The definition between flow model regimes:

$R_e \leq 2000$ Laminar flow

$2000 < R_e \leq 4000$	Transition between laminar and turbulent flow
$4000 < R_e$	Turbulent flow

The coefficient f in laminar flow is given by the Reynolds number N_{Re} as [3]:

$$f = \frac{16}{N_{Re}} \tag{13}$$

To find the turbulent friction the equation below is used [3]:

$$\frac{1}{\sqrt{f}} = -4\log_{10}\left[\frac{0.27\varepsilon}{D_{eff}} + 1.26^{N^{-1.2}}/\left(N_{Re,G}f^{1-N/2}\right)^{N^{-0.75}}\right] \tag{14}$$

Where:
ε is wall roughness.

2.2 Torque and Drag - Aadnoy's 3D Model

Aadnoy (2010) recently derived a three dimensional torque and drag model. The model defines the hook loads for hoisting and lowering operations, in addition to torque, for a string in a wellbore. There are two sets of equations, one for straight well sections and another for arbitrary well orientation. [6]

The idea behind the model is to first compute the dog leg severities. The newly developed model was implemented on the simple models presented in Appendix A. The newly derived model takes into account several parameters such as the effect of combined axial motion and drill string rotation. [6] Figure 2.2 is an illustration of drill string in a curved well showing 40, 25 and 73 bend angle.

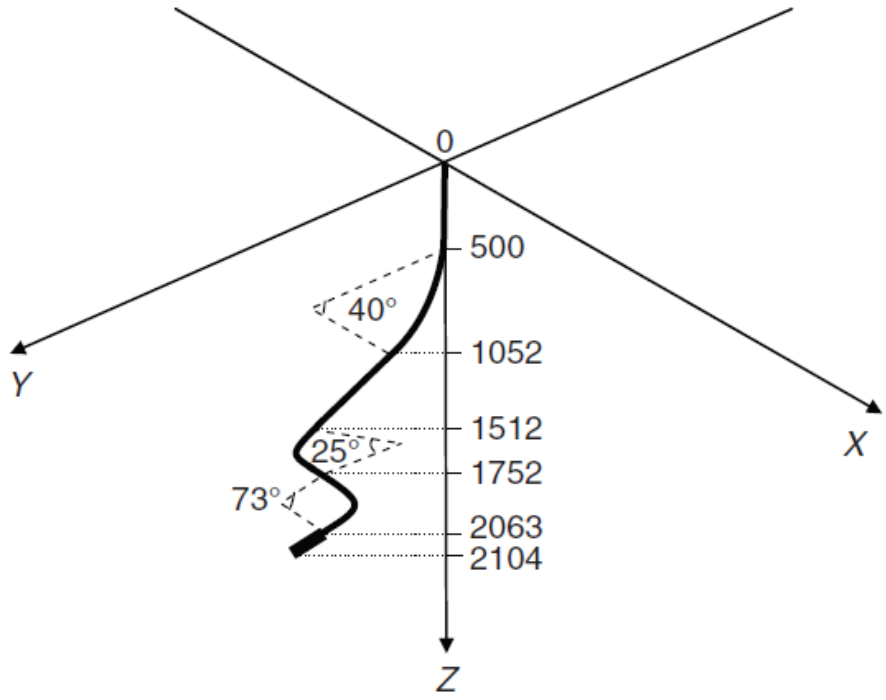

Figure 2.2 – A 3D well shape [6]

Combined -Axial motion and Rotation:

For combined motion, axial velocity will be V_h and tangential pipe speed will be V_r, giving a resultant velocity of V.

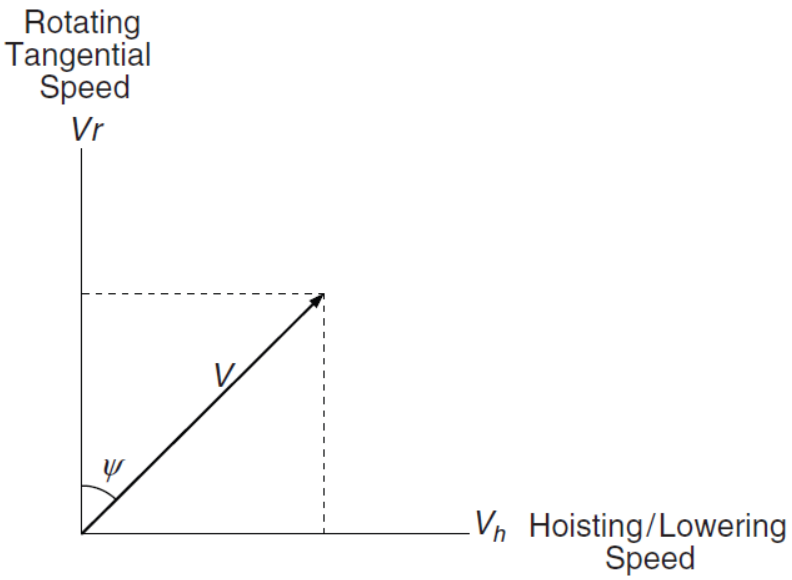

Figure 2.3 – Resultant velocity of axial and tangential velocity [6]

The angle between axial and tangential velocity is [6]:

$$\psi = \tan^{-1}\left(\frac{V_h}{V_r}\right) = \tan^{-1}\left(\frac{60V_h(m/s)}{2\pi N_r(rpm)r(m)}\right) \tag{15}$$

The torque and drag for combined motion in a straight section is [6]:

$$F_2 = F_1 + \beta w \Delta L \cos\alpha \pm \mu\phi w \Delta L \sin\alpha \sin\psi \tag{16}$$

$$T = r\mu\beta w \Delta L \sin\alpha \cos\psi$$

And the torque and drag for combined operation in a curved section is [6]**:**

$$F_2 = F_1 + F_1\left(e^{\pm\mu|\theta_2-\theta_1|} - 1\right)\sin\psi + \beta w \Delta L\left\{\frac{\sin\alpha_2 - \sin\alpha_1}{\alpha_2 - \alpha_1}\right\} \tag{17}$$

$$T = \mu r N = \mu r F_1|\theta_2 - \theta_1|\cos\psi$$

2.3 Application and Comparison of Johancsik and Aadnoy's Model

Aadnoy et al. (2010) performed a field case study of an offshore well in the North Sea. The 3D model presented in section 2.2, the Johancsik model (also referred to as the Exxon model) presented in section 2.1, and the modified Texas A&M model were compared against real-time hook load data. Figure 2.4 shows the result of the comparison for tripping out and Figure 2.5 shows the result of the comparison for tripping in. A friction coefficient of 0.2 was used for the entire section. [8]

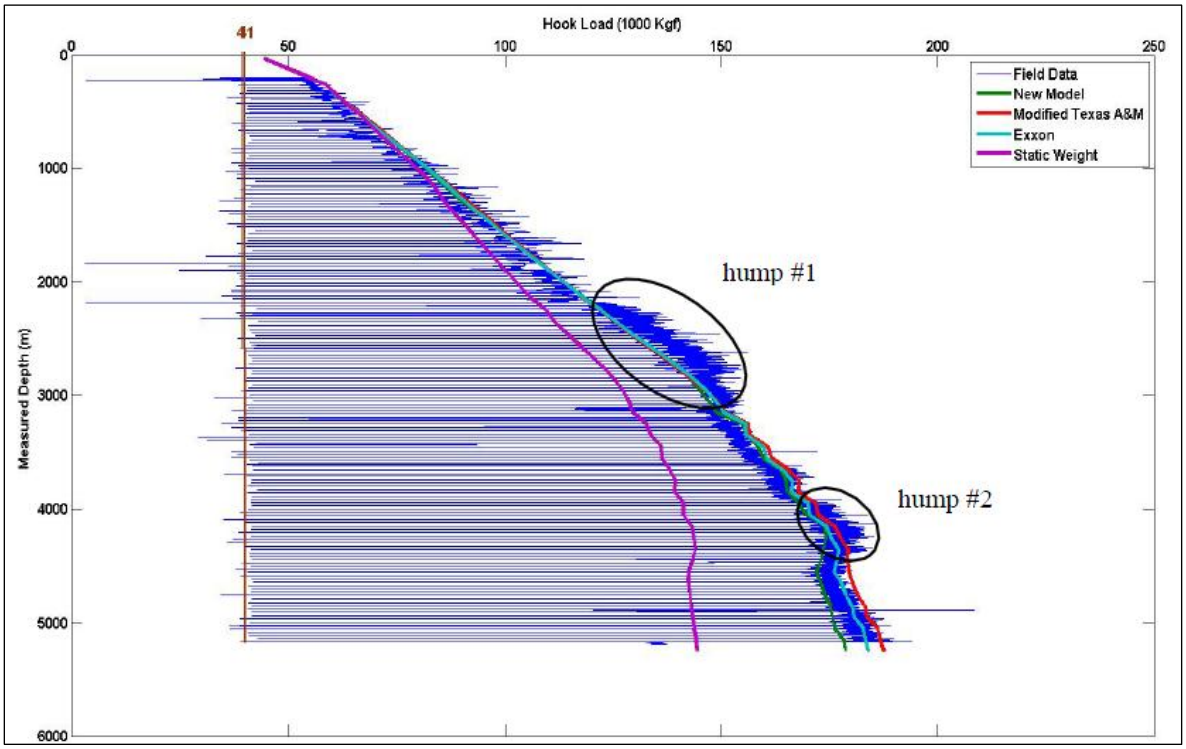

Figure 2.4 – Comparison of models and field hook load data for tripping out [5]

As can be seen in Figure 2.4, the three models match the field data excellently except for the two humps indicated on the graph. In these two intervals is where the well builds angle. The Johancsik model gives a good match for the last length of the well, below hump #2, while the new 3D model is below the real-time hook loads.

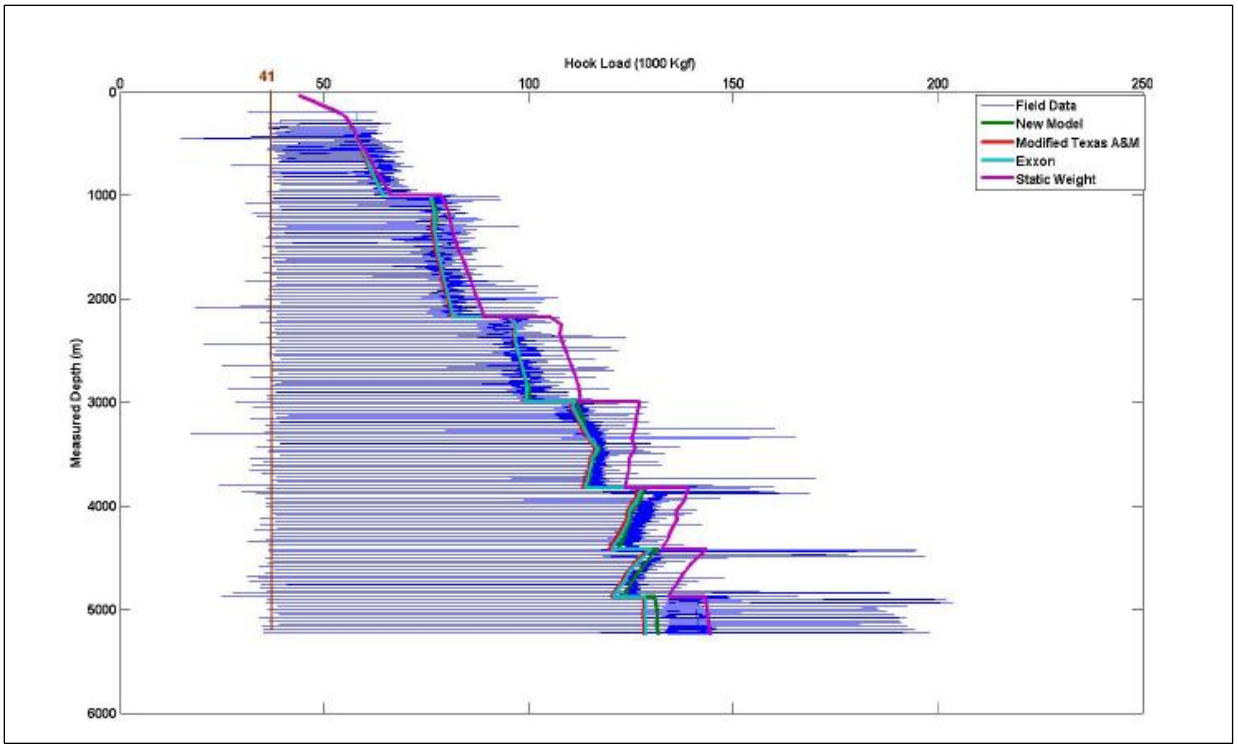

Figure 2.5 – Comparison of models and field hook load data for tripping in [5]

For running in hole operations a drillstring is usually filled with drilling fluid a number of times throughout the operation. For this example well the string is filled almost every 1000 m MD of sting run in. This can be seen in the stepwise manner of the graph in Figure 2.5. Every time the string is filled with fluid there is a sharp increase in the hook load equal to the weight of the fluid added. The models match the first 3000 m MD, but after this point the hook load data is slightly more to the right of the simulated lines. Aadnoy et. al. investigated this and found that a friction factor of 0.1 gave a better match for the interval below 3500 m MD. This was not the case for tripping out, in which a friction factor of 0.2 gave good results for the entire length. [8]

Tripping in is more complex than tripping out. The pipe will change between tension and compression and will not be on the high side or the low side of the wellbore, but somewhere in between. The contact force will then be reduced, leading to a reduction in friction. This is something a normal soft string model cannot predict. [8]

From the study performed by Aadnoy et al. (2010) it is found that the new 3D model and the Johancsik model give similar results. This is not unexpected as they have many similarities:

- In straight sections the equations used are the same
- In curved sections the only difference is the way side force is calculated
- Both models assume a linear Coulomb friction
- Both models assume a drillstring made up of short segments jointed by connections

However, some differences are present:

- The new 3D model handles dogleg in a simpler way
- The new 3D model has some inaccuracy for the lower part of the string with low tension

2.4 Buckling

If a drillstring is put under sufficient compressive stress, it will buckle. Modes of buckling include sinusoidal buckling and helical buckling. In this section buckling models are reviewed. The models predict the loads necessary for the onset of sinusoidal and helical modes of buckling. The models give different predictions for vertical, inclined and curved well sections. The models were reviewed and presented by Belayneh (2006). [16]

2.4.1 Non-Rotating Buckling Models

Section	Buckling	
	Sinusoidal	Helical
Vertical	Lubiniski (1962): $F_{sin} = 1.94(EIw^2)^{1/3}$ $I = \frac{\pi}{64}(OD^4 - ID^4)$ • E youngus modulus • W Weight per unit length	
	Wu et al. (1992): $F_{sin} = 2.55(EIw^2)^{1/3}$	Wu et al. (1993): $F_{hel} = 5.55(EIw^2)^{1/3}$

Table 2.1 – Buckling in the vertical sections

Section	Buckling	
	Sinusoidal	Helical
Curved	Mitchell (1999): $F_{sin} = \frac{2EIk}{r}\left[1 + \sqrt{\frac{wsin\alpha r}{EIk^2}}\right]$ • $k = 1/R$ (build or drop) • $r = \frac{1}{2}(ID_{well/casing} - OD_{tubing})$ • r = Radial clearance	Mitchell (1999): $F_{hel} = 2.83F_{sin}$

Table 2.2 – Buckling in the curved sections

Inclined	Dawsons and Paslay (1984): $F_{sin} = 2\left(\frac{EIwsin\alpha}{r}\right)^{0.5}$ • r = Radial clearance • α= incllination	Chen et al. (1989): $F_{hel} = 2\sqrt{2}(EI)^{0.5}(wsin\alpha)^{0.5}\left({}^{1}/_{r}\right)^{0.5}$ $\sqrt{2} \times F_{\text{Dawson Paslay sinusoidal}}$
		Wu and Juvkam-Wold (1993): $F_{hel} = 2\left(2\sqrt{2}-1\right)(EI)^{0.5}(w)^{0.5}\left({}^{sin\alpha}/_{r}\right)^{0.5}$ $2\left(2\sqrt{2}-1\right) \times F_{\text{Dawson Paslay sinusoidal}}$
		Kyllingstad (1995): $F_{hel} = 2.90(EI)^{0.5}(w)^{0.5}\left({}^{sin\alpha}/_{r}\right)^{0.5}$ $1.45 \times F_{\text{Dawson Paslay sinusoidal}}$
		Miska et al. (1996): $F_{hel} = 4\sqrt{2}(EI)^{0.5}(w)^{0.5}\left({}^{sin\alpha}/_{r}\right)^{0.5}$ $2\sqrt{2} \times F_{\text{Dawson Paslay sinusoidal}}$
		Aasen and Aadnoy (2002): $F_{hel} = 3.75(EI)^{0.5}(w)^{0.5}\left({}^{sin\alpha}/_{r}\right)^{0.5}$ $1.875 \times F_{\text{Dawson Paslay sinusoidal}}$

Table 2.3 – Buckling in the inclined sections

2.4.2 Rotating Buckling Loads

He et al. (1995) developed a model for critical buckling loads under presence of torque on the tubing. Their model reads [17]:

$$F = F_c\left(1 - \frac{T}{\sqrt{EIF_c/2}}\right) \tag{18}$$

where F_c is the buckling load in the absence of the applied torque. Because the torque, T, applied decreases the critical buckling load.

2.4.3 For Any Change in Azimuth and Inclination

Typical oil well geometry comprises of both inclination and azimuth gradients. The contact force per unit length, given in Eq. 19, is a simple expression and does not take the mentioned gradients into account. Kyllingstad (1995) generalized the contact force of a string for any given inclination and azimuth as [18]:

$$f_o = \sqrt{[(bW_s \sin\theta - F\theta')]^2 + [F \sin\theta \varphi']^2} \tag{19}$$

Where $\theta' = (d\theta/ds)$ is Inclination gradient and $\varphi' = d\varphi/ds)$ is Azimuth gradient.

When there is no inclination and azimuth gradient, i.e.: $d\theta/ds = 0$ and $d\varphi/ds = 0$.

For general use the Dawson-Paslay-Bogy model is used [19], but for other conditions that have practical applications Kyllingstad (1995) summarized the buckling equation as:

$$P_{cr} = \sqrt{\frac{KEIf_0}{r}} \tag{20}$$

Where the factor K is:

For sinusoidal buckling K = 4 – 12.25

For Helical buckling K = 8 – 7.5

2.5 Tensile Limit

Drillpipes and drill collars are designed to satisfy a series of operational requirements. Downhole tubulars must be able to withstand maximum expected hookload, temperature, torque, internal pressure, external collapse pressure and bending stresses. [20] Figure 2.6 shows a stress-strain curve for steel. When a steel drillpipe is loaded, it will have an elastic deformation up to a certain point, known as the yield point or tensile limit. When the drillpipe is loaded within this region and the force is removed, it will return to its original dimensions. In other words, this process is fully reversible. If the force exceeds the tensile limit, the pipe will yield and a plastic deformation takes place. In this region the drillpipe stays permanently deformed when the force is removed. The upper limit of plastic deformation is the ultimate tensile strength. If this point is exceeded, the drillpipe will fail. [13] [20]

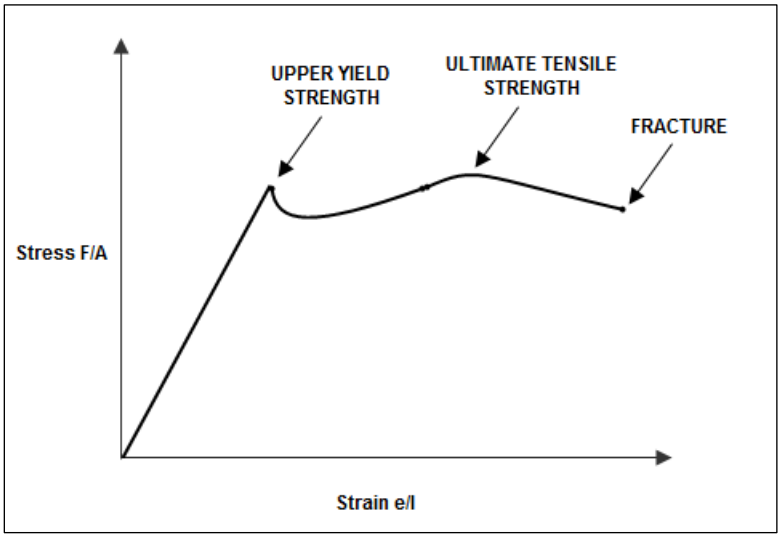

Figure 2.6 – Stress-strain curve

2.5.1 Single Load Theory

Tensile load is the maximum allowable force applied on a drillstring before yielding occurs. This tensile load is referred to as tensile limit. The tensile load is given as [13]:

$$\sigma_{max} = \frac{F_{max,tensile}}{A} \tag{21}$$

$$F_{tensile} = \frac{\sigma_{max}\, A}{SF} \tag{22}$$

2.5.2 Combined Load Theory

A one-dimensional strength assessment of a drillstring often has limited value because several types of loading are usually applied simultaneously. A drillstring can be subjected to loading from axial loads, torsion, pressure and temperature at the same time. Resulting in tangential, axial and shear stresses in the pipe. [13]

The two normal stresses and the shear stress can be presented in as stress matrix [13]:

$$[\sigma] = \begin{bmatrix} \sigma_t & \tau \\ \tau & \sigma_a \end{bmatrix} = \begin{bmatrix} \sigma & 0 \\ 0 & \sigma \end{bmatrix} \tag{23}$$

This can be determined from principal stress and von-misses failure criteria [13]:

$$F_{tensile} = \frac{A}{SF}\left(\sigma_y + \frac{\tau^2}{\sigma_t^2 - \sigma_y^2}\right)$$

Where, the σ_t and the τ are the hoop stress and the torsional stresses.

2.6 Measurements

2.6.1 Hook Load

The primary means of moving pipe in and out of a well on a drilling rig is a hoisting machinery called the drawworks. The system is shown in Figure 2.7. The drilling line (thick wire/cable) goes from the drawworks cable drum to the crown block. This length of the line is called the fast line. The line then runs between the crown- and the travelling block multiple times through a number of sheaves. This creates a "block and tackle" arrangement that provides the mechanical advantage needed for the large loads. The drilling line exits the last sheave in the crown block and is anchored on the rig floor. This length of the line is called the dead line. The hook load is measured by a load cell mounted on the dead line or incorporated into the dead line anchor. On some rigs the hook load is measured by sensors in the top drive. [21] [22]

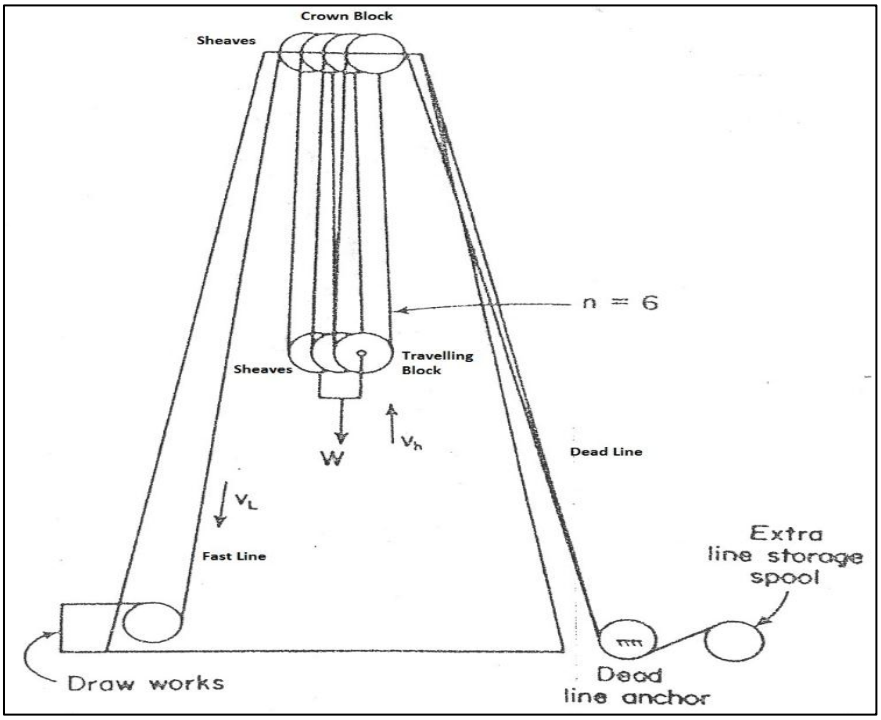

Figure 2.7 – Drawworks on a drilling rig [23]

The hook load can be calculated by multiplying the dead line tension, F_{dl}, with the number of lines, n, between the crown block and travelling block. The traveling equipment is subtracted to get the drillstring weight [5] [21]:

$$W = F_{dl}n - W_{TravellingBlock} \tag{24}$$

2.6.2 Sheave Friction

Eq. 24 would give a precise result of hook load if there was no friction present in the system. Hook load measurements will in addition to dead line tension and number of lines between the blocks, be affected by block-movement direction and sheave efficiency. Luke & Juvkam-Wold (1993) showed that friction in the sheaves has a significant effect on the accuracy of the conventional weight indicator. The hook load readings also depend on whether the type of dead line sheave is active or inactive. [8] [21] When pulling out of hole the drawworks have to overcome the friction in the sheaves, and the fast line will have higher tension than the dead line. Oppositely, when running into hole the dead line will have higher tension than the fast line. This friction effect results in hook load readings being too low when RIH and too high when POOH. [21]

Inactive dead line sheave.

When raising the blocks:

$$W = F_{dl}\frac{e\left(1-\left(\frac{1}{e^n}\right)\right)}{(e-1)} - W_{tb} \tag{25}$$

When lowering the blocks:

$$W = F_{dl}\frac{(1-e^n)}{(1-e)} - W_{tb} \tag{26}$$

Active dead line sheave

When raising the blocks:

$$W = F_{dl}\frac{(1-e^n)}{(1-e)e^n} - W_{tb} \tag{27}$$

When lowering the blocks:

$$W = F_{dl}\frac{e(1-e^n)}{(1-e)} - W_{tb} \tag{28}$$

2.7 Drillstring Vibrations

2.7.1 General

Because drillstrings are not stable, downhole vibration due to drilling is bound to occur. Vibrations at a low level are not an issue, but high levels of vibrations over time can cause a number of serious problems. Drillstring vibrations and high shock loads are a significant factor contributing to poor drilling performance, and create both visible and invisible nonproductive time. [24] Drillstring vibrations are very complex because they have such a random nature of a number of factors. The vibrations are usually induced by two excitation forces: bit/formation and drillstring/borehole interactions. As a result, three primary modes of vibrations can occur during drilling, axial, torsional and lateral. Within these modes there are several mechanisms. [25]

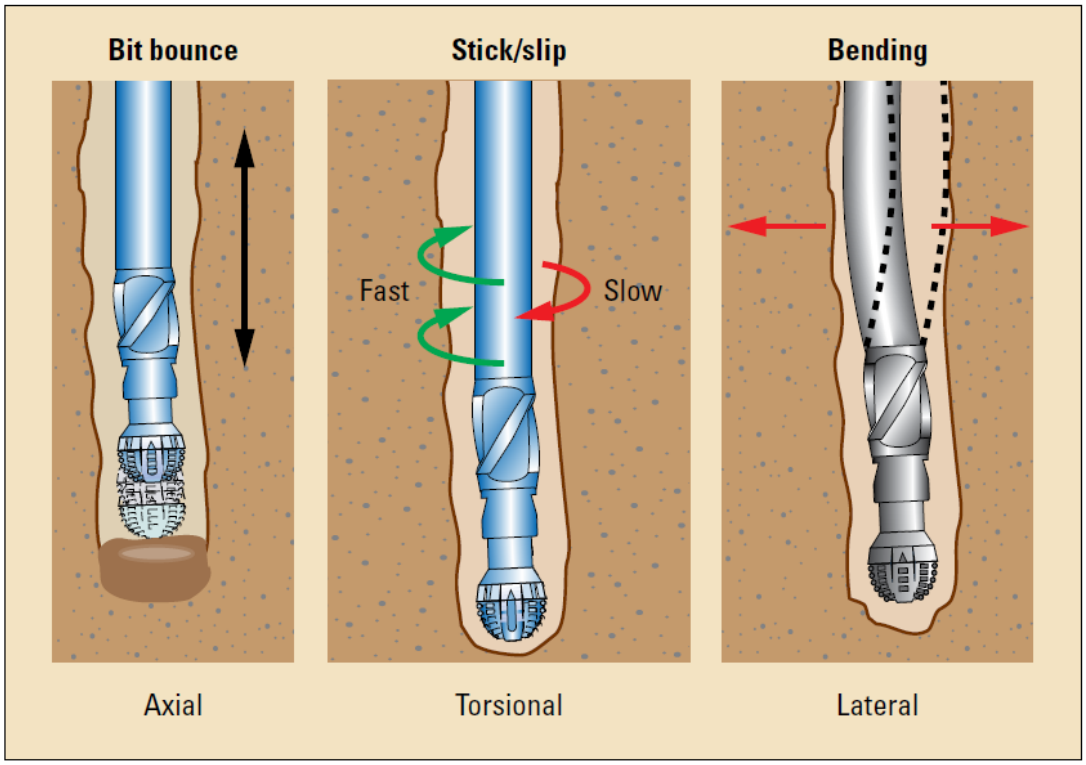

Figure 2.8 – Vibration modes [16]

In order to compress the main report, a detailed review of the different vibration mechanisms with causes and consequences can be found in Appendix B. A field case example will be presented here to illustrate the significance of vibration for modeling and management.

2.7.2 Vibration Mechanisms

The following is based on information presented in the Halliburton ADT Vibration Brochure [26]

Stick-Slip – Torsional vibrations

Frictional torque on bit and BHA causes the drillstring to periodically twist up and then spin free. Variations in downhole RPM can be as large as 3 to 15 times the average surface RPM. Stick-slip is the main cause of torsional vibrations, and usual consequences of stick-slip are fluctuations in the surface torque readings, reduction in rate of penetration (ROP), connection over-torque, and back-off and drillstring twist-offs.

Bit Bounce – Axial vibrations

Large variations in weight on bit (WOB) cause the bit to repeatedly lift off-bottom and then drop, impacting the formation. Bit bounce is connected to the axial stiffness of the drillstring and the mass of the BHA. It usually occurs when drilling hard formations with tricone bit. Bit bounce will impact the hook load reading when the bit moves upward, causing the string to compress.

Bit Whirl – Lateral vibrations

Occurs when the bit has cut a hole larger than its own diameter, causing the bit to *walk* around the hole producing unusual bottomhole patterns. The bit is not rotating around its natural geometric center. PDC bit-wellbore gearing resulting from excessive side-cutting forces causes this. When the BHA is whirling, it continuously impacts the wellbore.

Torsional Resonance

This is “drill collar torsional resonance” to be more specific. This mechanism is a natural torsional frequency of the drill collar which is being excited. This specific type of vibration usually occurs when drilling with PDC bits in very hard formations.

2.7.3 Vibration Consequences

Drilling vibrations will cause damage to the downhole equipment and the drillstring itself. In addition vibrations will cause an energy loss from rotary table/top drive to the bit, so that less energy will be available for destroying rock. [27]

Another consequence is that the vibrating drillstring can cause significant damage to the wellbore. The industry has traditionally had the conception that wellbore instabilities are due to the chemical reaction between the formation and the drilling fluid. Santos et al. (1999) performed a field case study of two wells in Brazil to document the effect of drillstring vibrations on wellbore- stability and enlargement as well as ROP and drillstring fatigue. [27]

Vibrations were measured in real-time with surface sensors on the rig. The results from the vibration data were compared to the caliper logs of the two wells [27]:

Well I

The caliper log showed a hole diameter varying from 6” to 16”. The bit size of this section was 8,5”. This indicates considerable hole enlargement. The formation is diabasis, so the enlargement was not from chemical interaction between the formation and drilling fluid. Vibrations are the likely cause of the wellbore instabilities. Figure 2.9 shows the vibration measurements at depth 1944 m and caliper log of a 50 m interval from 1900 m to 1950 m.

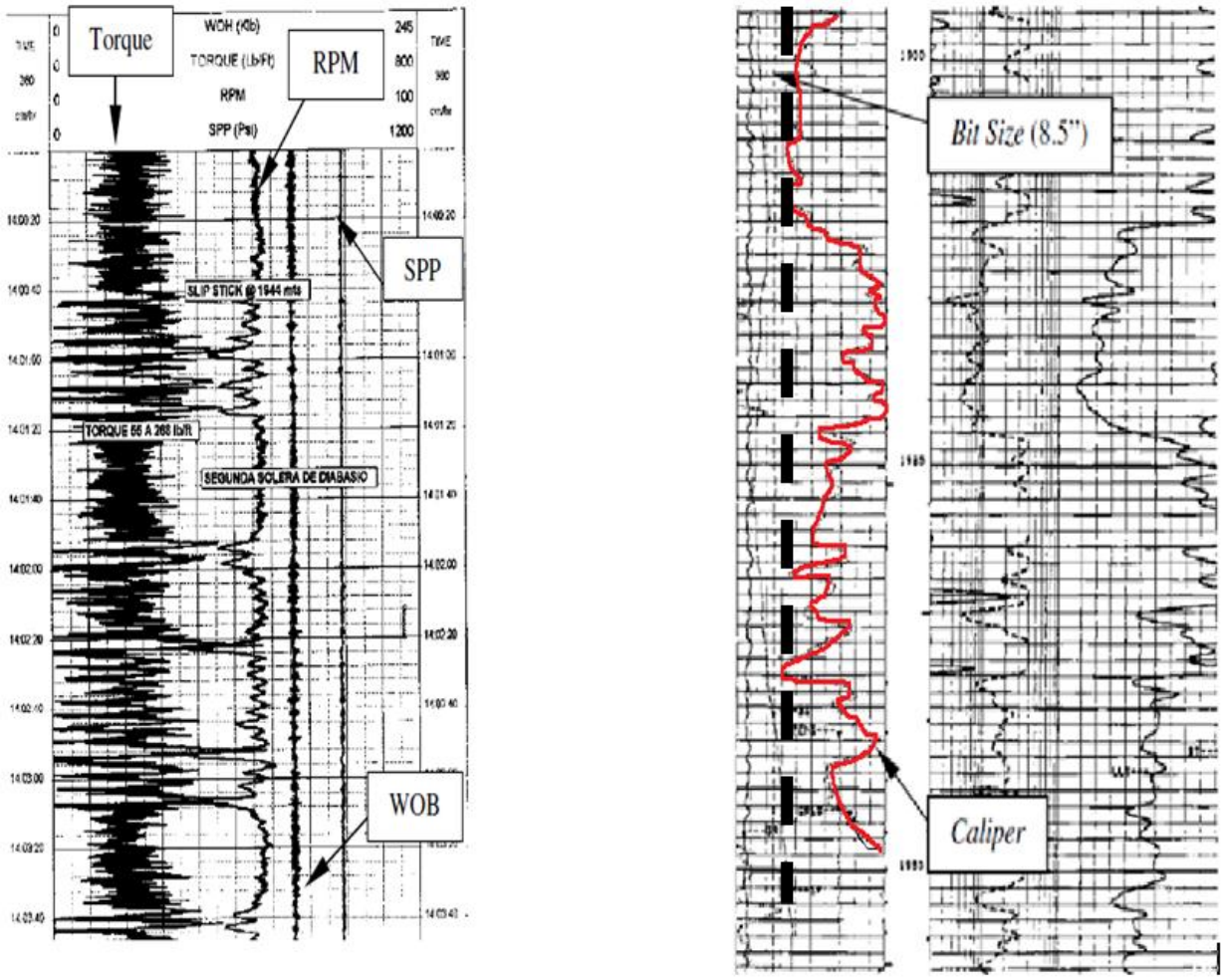

Figure 2.9 – Vibration measurements and caliper log of Well I [27]

Well II

The caliper log showed a hole diameter without significant enlargement. A 4,5" drill bit was used, and the widest diameter found was 5,3". The surface sensors detected minor vibrations downhole. Figure 2.10 shows the vibration measurements and a caliper log from 3000 m to 3250 m.

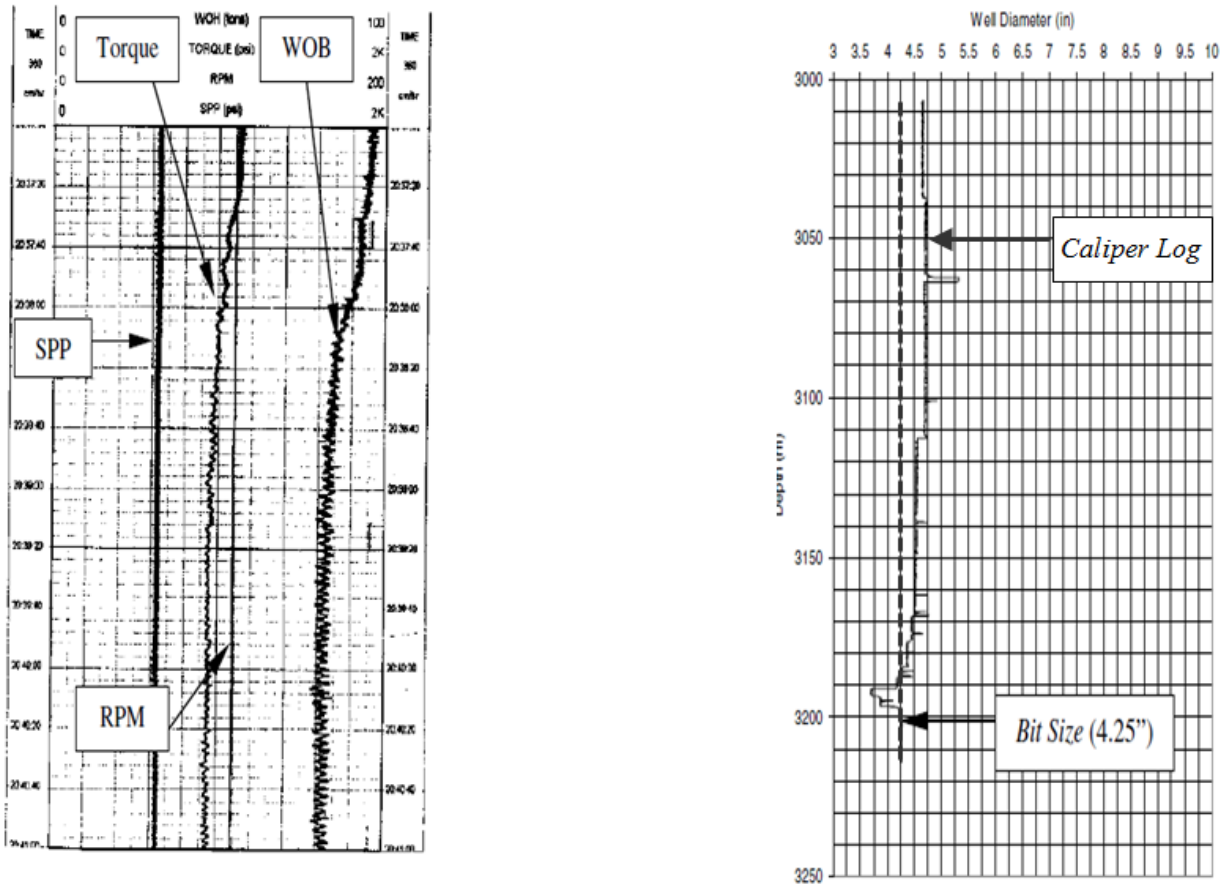

Figure 2.10 – Vibration measurements and caliper log of Well II [27]

Conclusion

Well I experienced excessive drillstring vibrations along with extensive hole enlargement. Well II on the other hand had considerably less of both vibrations and hole enlargement. Considering both wells were drilled in a non-reactive formation, the study gives a clear indication that drilling vibrations have a major impact on wellbore stability and hole enlargement.

2.7.4 Post-Run Analysis and Vibrations

After the drilling is done it is important to analyze the data in the memory of the measurement while drilling (MWD) tools. Then it is possible to confirm the vibration mechanisms encountered during the run. The point of the vibration analysis is to transfer the experience gained to the next well.

3 Post-Run Analysis

Wellplan's Torque Drag Analysis Module predicts the measured weights and torques while tripping in, tripping out, rotating on bottom, rotating off-bottom, slide drilling and backreaming. This is useful for determining if a well can be drilled or to evaluate the conditions during the drilling process. The module includes both soft- and stiff string models, and is applicable for analyzing drillstrings, casing strings, liners, tieback strings, tubing strings, and coiled tubing. [1]

The purpose of a post-run analysis is to improve modeling and provide valuable learning points for future well planning. It gives information on what actually happened on each run of the drilling process. It is also a way to see if the well planning turned out to be valid for the well, or if deviations from the plan had to be done during the drilling operation. Hook load sensor discrepancy and friction factors for cased and open hole are of special interest when doing a post-run analysis.

3.1 What Is Required for a Post-Run Analysis?

3.1.1 Data Quality

In order to do a realistic and useful post-run analysis, or any other analysis for that matter, it is important with good data quality. It doesn't matter how good the T&D model or the simulations are if the real-time data available for comparison is not correct. As the drilling optimization engineers from the service company say: "If you put garbage in, you get garbage out". Obtaining accurate field data of drillstring loads is mainly dependent on the accuracy of the sensors used for measurements on rigs. [5]

The amount of data recorded has grown with the technological developments in recent years. The ever-increasing stream of data has made it more important to measure and evaluate the data quality and choosing the appropriate selection. [28] It is a well-known fact that data from oil well drilling is often noisy and of poor quality. Bad data quality is a cost driver, but it is also a potential drilling hazard if it leads to bad decisions. [29] Real-time operation centers are becoming more common in the petroleum industry. In order for the centers to provide decision support for the rig operations, the assurance of good data quality is an increasing need. [28]

For a post-run analysis, one of the most important steps is assuring that the data used in the analysis is reliable. This is done at the start of the analysis to calibrate the model.

3.1.2 Model Calibration

The torque and drag model must be calibrated in order to be used in software simulation and analysis. Sensors need to be calibrated frequently to provide good data quality. [5] The preferred calibrations of the model is done using real-time data. In this section an example of a model calibration done in the industry and three examples of model calibration by IRIS are presented.

3.1.2.1 Correction for Hook Load Sensor Discrepancy – Service Company Procedure

Hook load sensors on drilling rigs are rarely calibrated. To get simulated and real-time loads to match, the service company's drilling optimization engineers need to make up for this when doing a post-run analysis by introducing a hook load discrepancy. All rigs used by the operator have discrepancies ranging from -18% to +9% deviation compared to theoretical free rotating weight. Correcting for this discrepancy is done by subtracting or adding a percentage of the string weight in Wellplan. Trial and error method is used until a percentage that gives the best fit between real-time and simulated data is chosen. Calculating this discrepancy does not work, as it is not a linear relationship. The reduction of string weight is done by subtracting or adding the weight percentage of the discrepancy from the string elements of notable length. The elements chosen is usually the drillpipe, heavyweight drillpipe and drill collars.

The real-time rotating off-bottom weights are chosen for fitting the simulated curve when adjusting the discrepancy. Wellplan calculates the free rotating weight using bit depth, string components, pipe specifications, mud weight and flow hydraulics. Theoretically, the free rotating weight should match the hook load readings from the rig. In a rotating drillstring there will be no axial-friction drag, making a rotating drillstring the zero-drag reference point. [10] The discrepancy can only be trusted if compared to good rotating off-bottom rotation readings. Until a new run with good rotating off bottom readings is recorded, the last discrepancy found is used in the following runs. Figure 3.1 shows an example of discrepancy correction for one of the operator's rigs. The different points are real-time readings of actual hook loads for tripping out, tripping in and rotating off-bottom. The green lines are the theoretical simulated values for the

three operations without hook load sensor discrepancy. The red lines are the theoretical simulated values with a hook load sensor discrepancy of -13%.

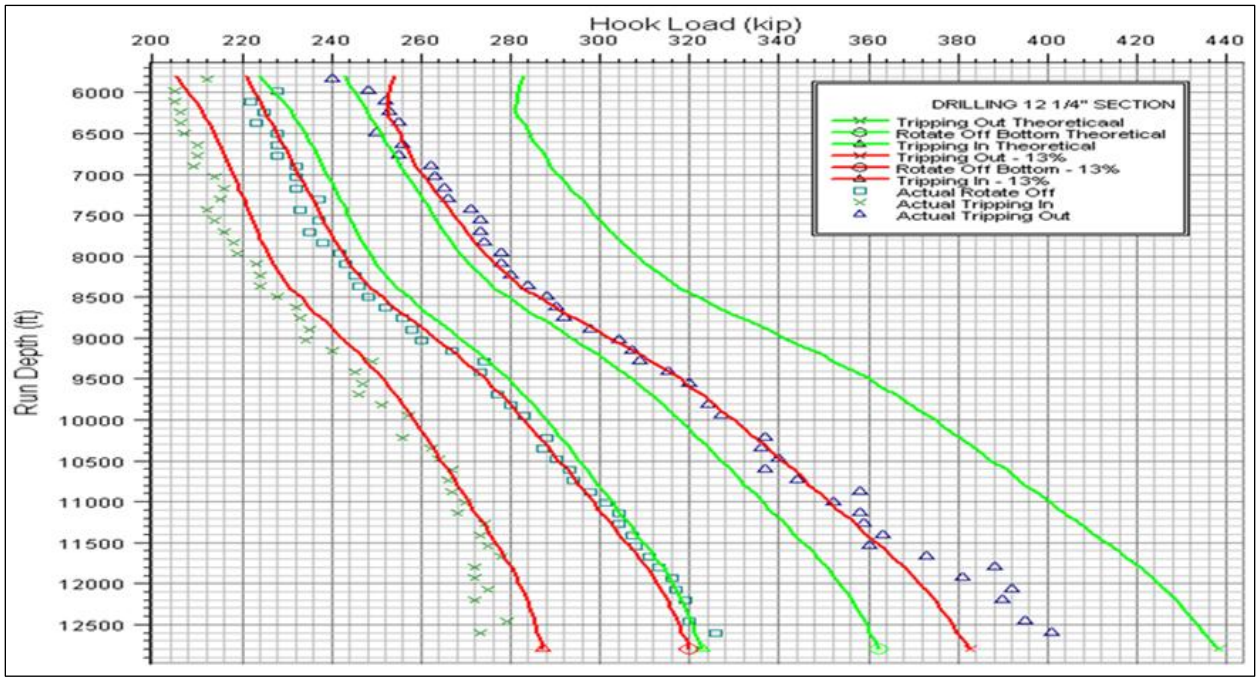

Figure 3.1 – Example of Hook Load Sensor Discrepancy Correction

All measurements taken during connections must be taken above the stretch distance. With no stretch left in the string and the buoyancy subtracted, the full weight of the string can be recorded. The distance from bottom must also large enough to avoid a lift effect from the drilling fluid pumping against the bottom of the hole. In the event of a slip-and-cut operation performed on the rig, a new hook load discrepancy may have to be found. In a slip-and-cut operation the drilling line in the drawworks is replaced to prevent failure due to fatigue. [30] Beacause the hook load sensor is mounted in the dead line anchor or on the last part of the drilling line, a slip-and-cut may affect the value of the measurements. [21] When a slip-and-cut operation is performed it will be noted in the Daily Drilling Report (DDR).

3.1.2.2 Example Illustrations of Torque and Drag Model Calibration – IRIS

The following calibration models are not included in the field case, and are not used by the service company or the operator. They are included to illustrate different examples of how models can be calibrated.

IRIS has published several works regarding automatic model calibration using real-time data.

A global calibration model has been developed to deal with imprecise configuration of parameters and to manage the inefficiency of model prediction. The global calibration module includes [4]:

- Linear weight of the drill-pipes.
- Hydraulic effect on the mechanical forces.
- Frictional pressure losses inside the drill-string

The system's automatically performed calibration can be considered global because it does not vary with time. Calibration values are only refined as additional measurements become available. [4]

Linear Weight Calibration

Figure 3.2 shows an example of the effect of linear weight calibration. The three curves on top are the rotate off-bottom roadmap for three different flow rates. From the figure one can see that calculation and measurement do not match. Linear weight of the drillpipe and the hydraulic effect are calibrated, until the difference between modeled hook loads and the measured hook loads is minimized. After calibration it is seen that there is a much better correspondence between modeled hook loads and real-time measurements (blue triangles). The three curves on the bottom of the figure show the same roadmap after calibration is done. [4]

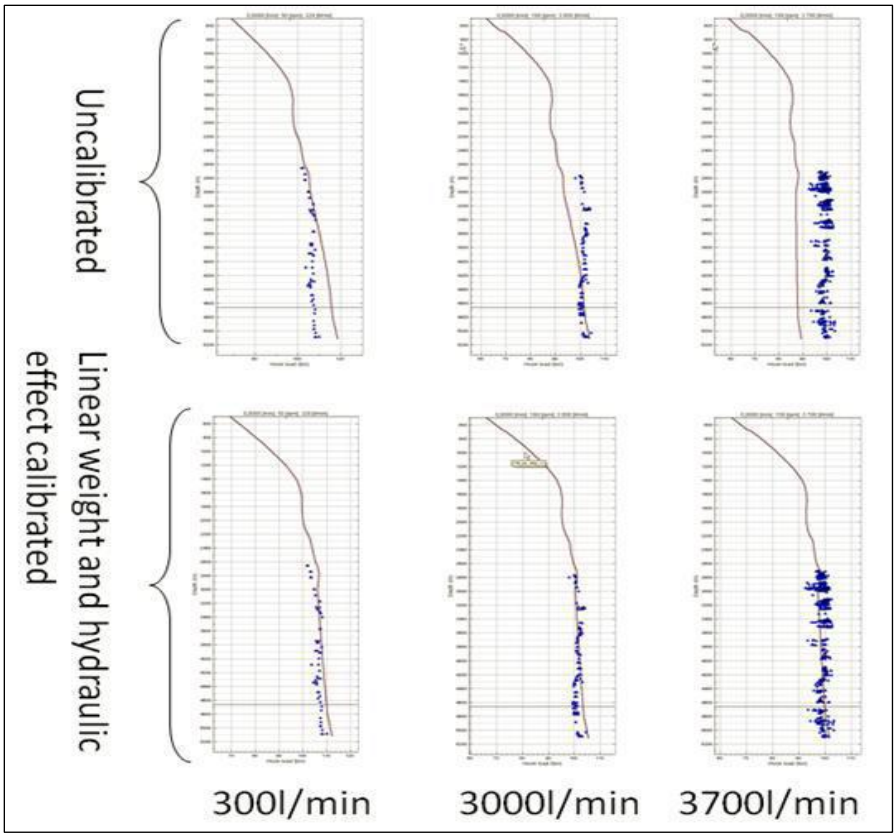

Figure 3.2 – Torque and drag global calibration [4].

3.1.2.2 Example Illustrations of Hydraulic Model Calibration – IRIS

Hydraulic Model Calibration

Pressure loss is dependent on flow rate and mud properties. Even with a perfect configuration of the drillstring properties, the model-based calculations may need to be adjusted to match the measured pump pressure to account for small discrepancies. An example of hydraulic calibration is presented in Figure 3.3. The colored circles indicate the SPP at different depth and flow rate, and the color bends corresponds to calculated values. The color code corresponds to the flow rate of the measurements and to the flow-rate used for the calculation (the same color coding is used). If a correctly calibrated model is used, the measurement circles should fall into an area with the same color. In that case, it means that the model predicts the correct standpipe pressure for the given flow rate. The left plot in the figure shows a non-calibrated model in which there is no

match between the measurement circles and calculations. The right plot in the figure shows a calibrated model in which the measurement circles and calculations match well. [4]

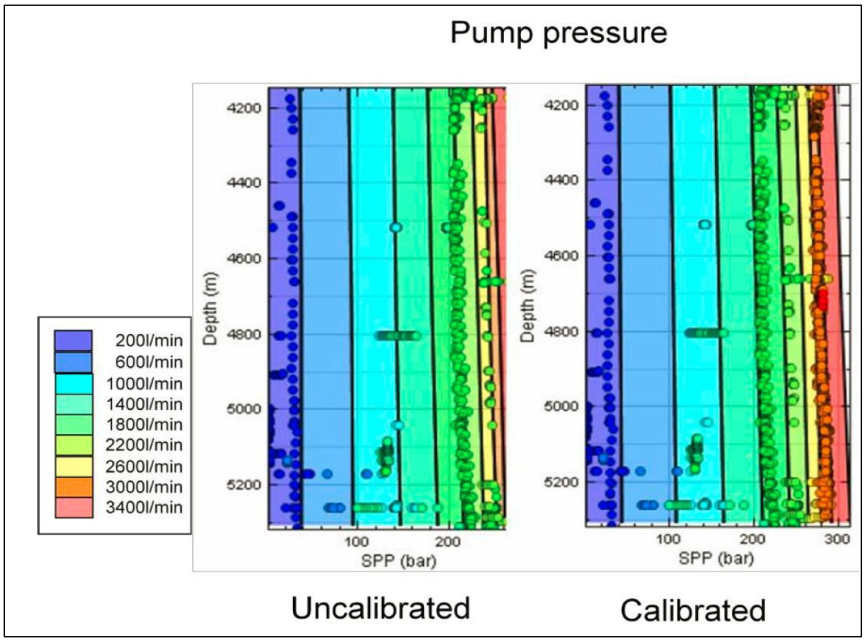

Figure 3.3 – Hydraulic global calibration [4]

Another IRIS's model calibration example is the work presented by Lohne at. al. (2008), in which the WeMod flow model was used to model a historic case. As seen in Figure 3.4, the model did not match the measurements for the selected case. The authors have focused on estimation of the friction parameter which scales the frictional pressure loss given for the drillpipe and for the annulus. In addition to the friction factor, there is uncertainty in the temperature of the well, dynamic characteristics of the pump, pressure loss through BHA and bit, and the density and rheology of the drilling fluid as functions of temperature and pressure. Because the detailed knowledge of these parameters is difficult du determine, the authors use a calibration factor, c, to fit the model to the measurements. This factor will then make up for the hidden physical parameters that the model does not account for. After computing the calibration factor, the results of comparison can be seen in Figure 3.5. After calibration the authors match the model and measurements perfectly. [2]

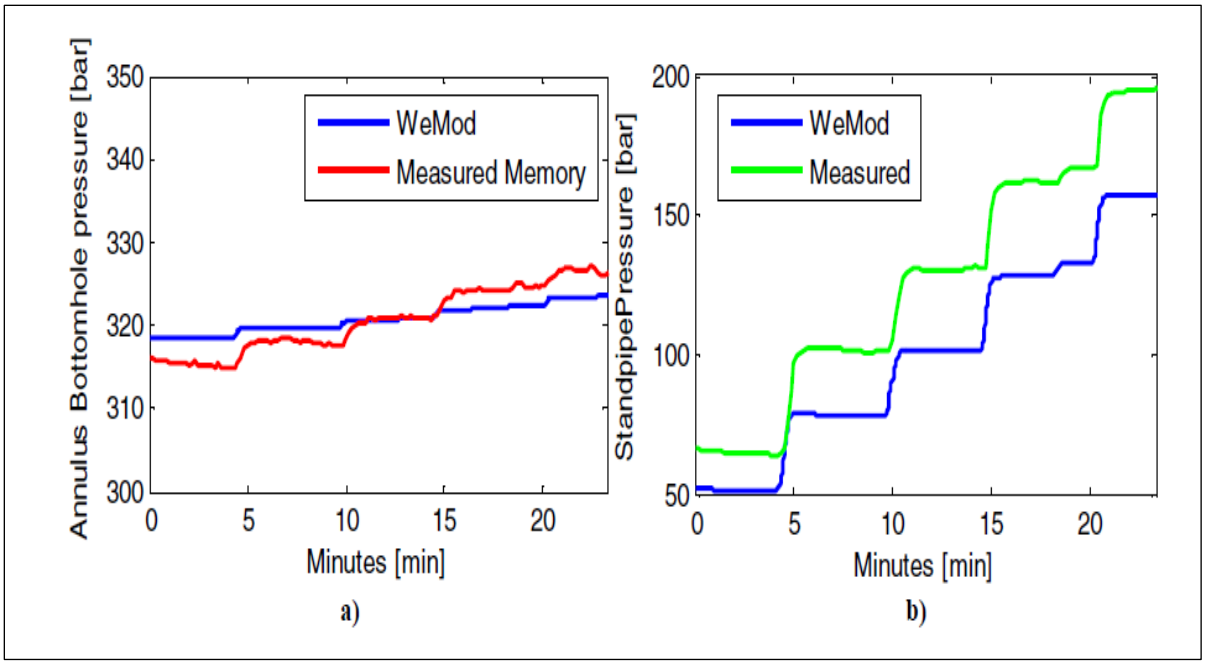

Figure 3.4 – Comparison of model and measurements without calibration [2]

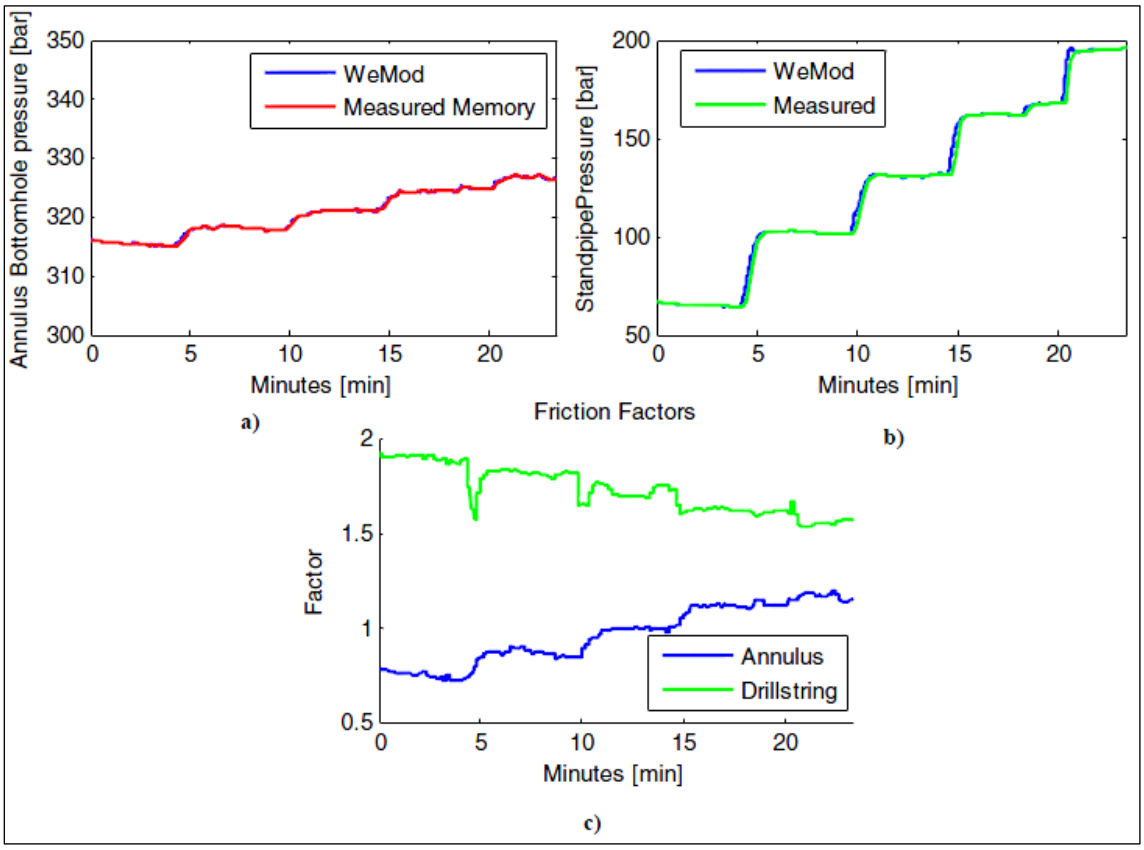

Figure 3.5 – Comparison of calibrated model and measurements, and the factor in bottom chart [2]

3.2 Integrated Operations

The concept of integrated operations is an ever increasing area of focus for the oil and gas industry. Most operators are devoting resources to develop integrated operations in their company, and some of the different names used are: Field of The Future (BP), Smart Fields (Shell), Real-Time Integrated Operations (ConocoPhillips), i-field (Chevron) and Integrated Operations (Statoil).

The operator considered in this thesis has an integrated operations center with 24/7 drilling monitoring for ongoing operations, and a visualization center for well planning. One of the primary focuses of the operator's integrated operations is drilling optimization. Chen (2004) defines drilling optimization as:

"Drilling optimization is a process that employs downhole and surface sensors, computer software, Measurements-While-Drilling (MWD), and experienced expert personnel – all dedicated to reduce trouble time and increase drilling effiency." [31]

Rig downtime is one of the main cost drivers of a drilling operation, and statistics have shown that rig downtime accounts for approximately 25% total of rig time. This is equivalent to an estimate of 1.5 million dollars per well. [31] Subsequently, a reduction in rig downtime will have a huge cost saving potential. The trouble time can be even higher in challenging cases such as HPHT, extended reach horizontal wells and deepwater/ultra-deepwater drilling. Drilling optimization is also beneficial for HSE and drilling efficiency. [31]

Chen (2004) states that a comprehensive drilling optimization in general should include solutions for [31]:

- **Drillstring Integrity:** The most important issues of drillstring integrity are downhole vibrations, BHA buckling and torque and drag.
- **Hydraulics Management:** The focus of hydraulics management is maintaining the hydrostatic and dynamic drilling mud pressure within the operating limits and optimizing hole cleaning.
- **Wellbore Integrity:** The focus of wellbore integrity is determining the upper and lower circulating limits through predicting pore pressure, fracture pressure and collapse pressure.

Figure 3.6 shows the drilling optimization process presented by Chen (2004):

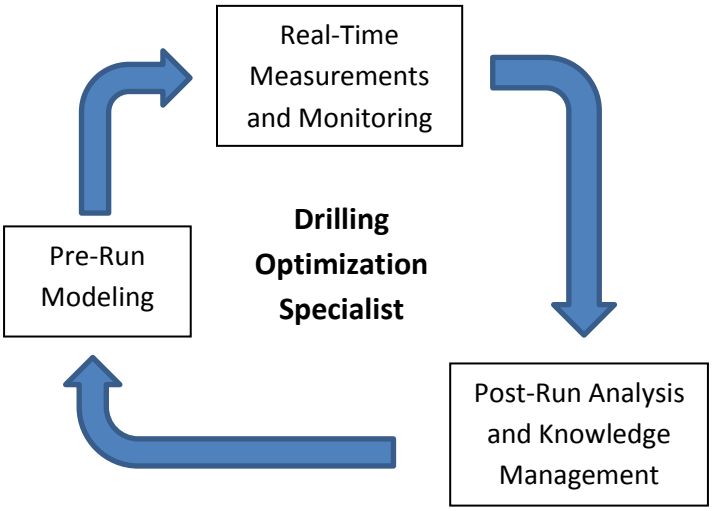

Figure 3.6 – Drilling optimization process

The drilling optimization engineers from the service company working in the operator's real-time drilling center have developed their own take on the drilling optimization process. It's in many ways the same process, only they call it the Model-Measure-Optimize loop. The loop can be applied in all phases of the drilling operation, planning, real-time and post-drilling. The loop is shown in Figure 3.7:

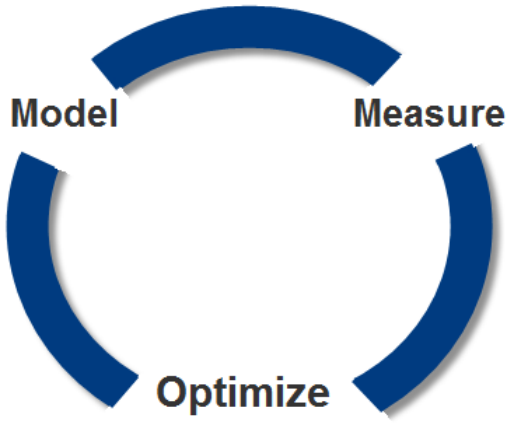

Figure 3.7 – Modified drilling optimization loop

Within the drilling optimization of the operator's integrated operations, improving torque and drag modeling has been a focus area. Continuous sharing of knowledge and training are key values for building competence.

The large increase in available bandwidth in recent years has made it possible to transfer readings from any sensor to locations worldwide at high speeds. This has revolutionized the communication between offshore and onshore, as well as communication between global offices and sites. The different operators mentioned using integrated operations take an advantage of this. [32] For instance, during Norwegian nighttime the operator's operations in the North Sea are monitored from the company's real-time center in Alaska when extra assistance is needed.

Although the name of the integrated operations may differ from company to company, the goal is the same: Making better decisions, and making them faster. This is achieved by multidisciplinary teamwork. In the integrated operations center there are well planners, data engineers, drilling optimization engineers/specialists, geomechanics- and pore pressure specialists, IT support and drilling fluids engineers. These positions are filled by various service companies and they work closely with the operator's drilling engineers as well as communicating directly to the various workers on the rigs.

Benefits of integrated operations are networking competencies, increased communication, increased recovery and reserves, improved HSE, global collaboration, effective use of the resources and competencies available and reduced costs. [32]

4. Field Case

4.1 Introduction

The well selected for the field case study is a recently drilled injector well in the North Sea. A Post-Run Analysis of the well has been done in this thesis, and the findings presented in the following sections. The well is drilled from a fixed platform which is a combined drilling- and water injection rig. The well was drilled with the service company's drilling optimization service, with well planning and real-time support from the operator's real-time drilling center. All depths refer to measured depths, MD, unless other is mentioned.

Well A is a sidetrack with kickoff at 2525 ft, and was drilled in six runs before encountering gas problems. The well was plugged at 7390 ft, and the technical sidetrack A T2 was drilled from cement plug out of casing shoe with a kickoff at 5752 ft and target depth (TD) of 12865 ft. A T2 was drilled in two runs. The total eight runs are numbered from 100 to 800, with these subcategories:

- 00A – Tripping in to previous section TD
- 00 – Drilling
- 00B – Tripping out from section TD
- 40 – Running casing or liner
- 50 – Cementing runs

In addition, it is common practice to divide the directional wells into three sections. The tophole section is the first section of the well. The next section is the overburden section, which is the longest section. The wellpath trough the overburden is designed to position the well for optimal penetration of the reservoir. The last section is the reservoir section. In this section the well penetrates and enters the reservoir. The goal of a well is to achieve optimal production- or injection flow.

The field case well A and A T2 is divided into these sections:

- Tophole section: Runs 100 and 200. Depth 2550 ft to 5710 ft.
- Overburden section: Runs 300, 400, 500, 600 and 700. Depth 5310 ft to 11715 ft.
- Reservoir section: Run 800. Depth 11715 ft to 12940 ft.

All runs were well inside the buckling and yield limits. Figures with buckling and yield lines are found in Appendix D. The Field Case Rig does not have any issues with sheave friction in its drawworks. Sheave correction is therefore not applied when simulating this well.

Figure 4.1 shows the well schematic of the final drilling run for the reservoir section.

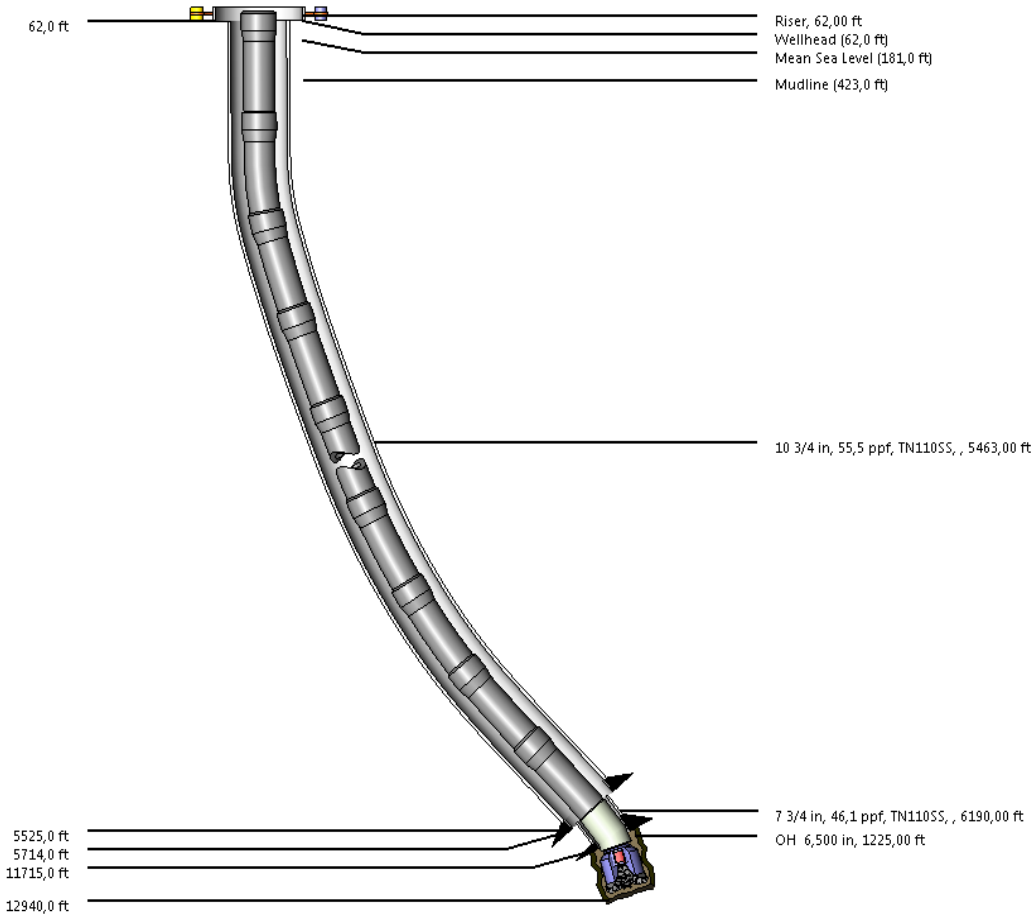

Figure 4.1 – Well Schematic of final drilling run

The wellpath undergoes several changes in inclination and azimuth, as displayed in the following figures:

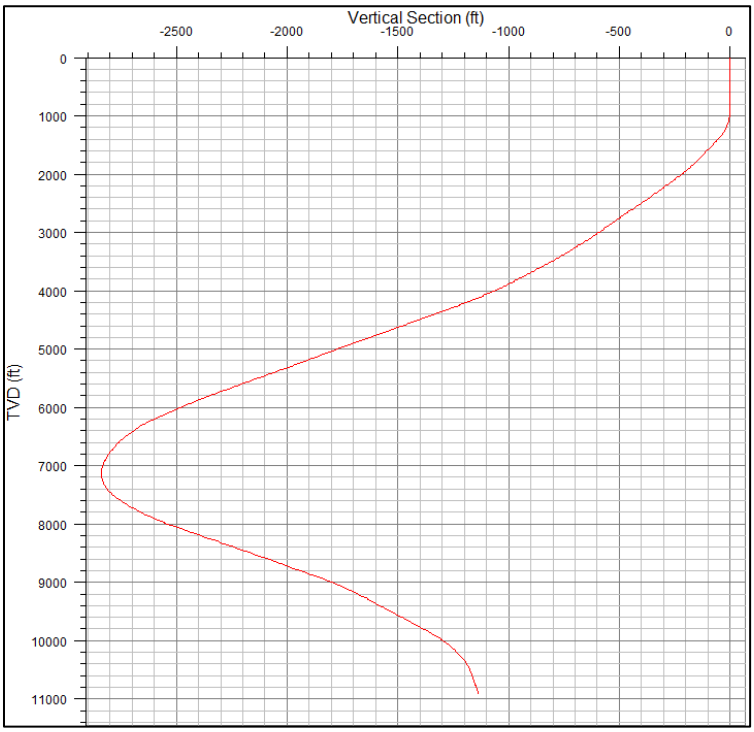

Figure 4.2 – Vertical section plot

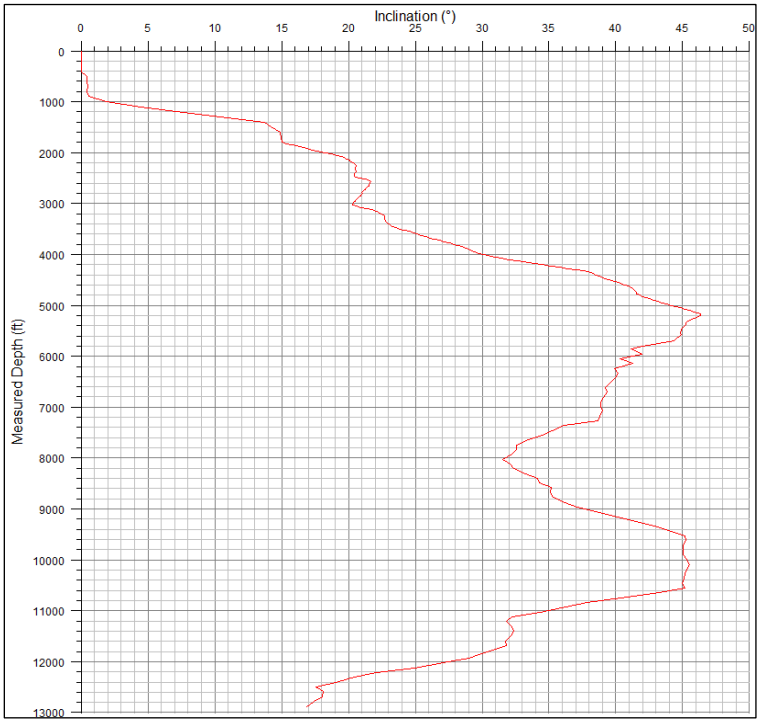

Figure 4.3 – Measured depth vs. inclination plot

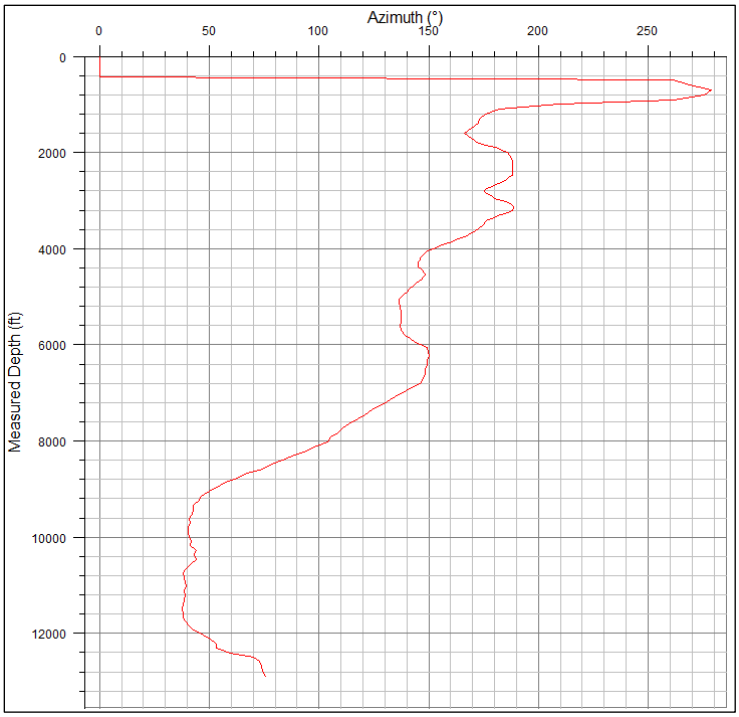

Figure 4.4 – Measured depth vs. azimuth plot

The dogleg severity reaches a maximum of approximately 4 degrees/100ft three times, as shown in Figure 4.5:

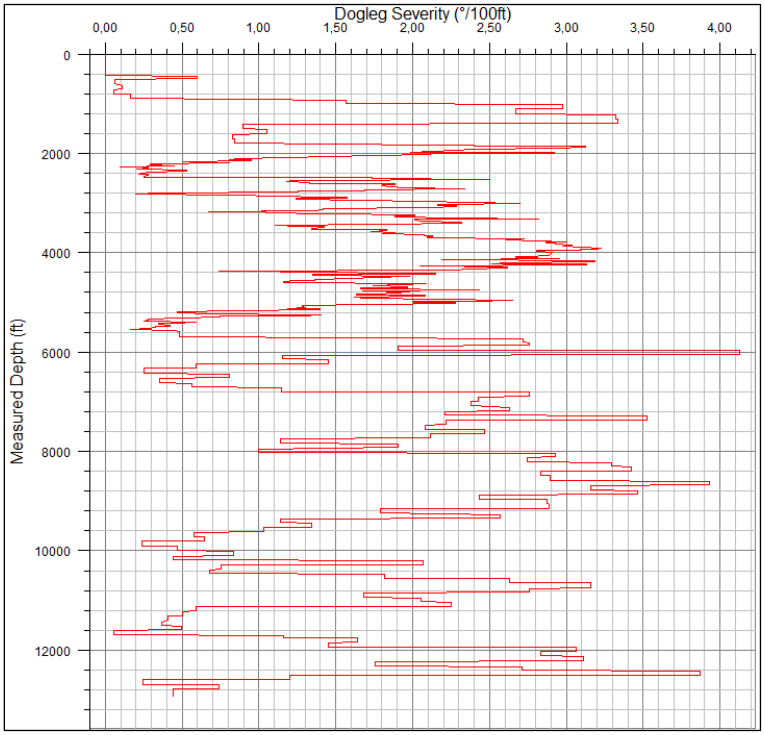

Figure 4.5 – Measured depth vs. dogleg severity plot

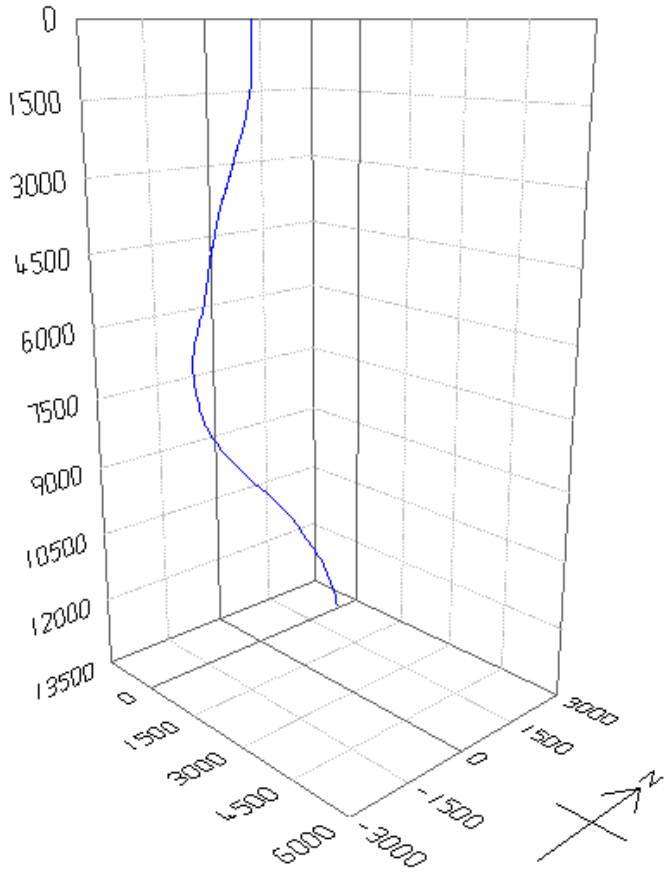

Figure 4.6 – 3D view of well from Landmark Compass™

4.2 Post-Run Analysis Process

In the field case a post-run analysis was performed in the same way the service company's drilling optimization engineers perform it. A post-run analysis is done every time operator has completed the drilling of a well. Simulating and modeling is done in Landmark's WELLPLAN™ Software. The Torque Drag Module is used with the Drag Charts setting. Real-time data, string- and BHA information, drilling records and run details are obtained from the service company's data management system. The Daily Drilling Report for the well is also used for detailed description of the day to day activities on the rig.

The analysis was started with the Wellplan files from the planning phase. The string components used in planning are often not the same as the actual components used when drilling the well. This is because the planning is done months in advance, and the components at the rig might change in the meantime. For this reason it is important to import the correct string components from the data management software into Wellplan before doing any post simulations. Having the wrong drillpipe- and casing specifications, bit type, stabilizers, rotary steerable assembly etc. will give inaccurate results.

The next thing to do is to get the real-time data of the actual loads from the run into Wellplan. For most runs there are already actual loads in Wellplan. These are taken manually in real-time and can have some inaccuracies. In the post-run analysis it is important to take these manually or at least check that the ones already there can be trusted, to ensure good data quality. The actual free rotating torque and the actual hook loads for pick-up weight, slack-off weight and free rotating weight are the data points that are the objective to match with the simulations done in the post-run analysis. The values for the actual loads are found in the data management software's real-time plot, and are taken at every connection of a drilling run. The connections are made every 90-120 feet depending on the pipe used, and are carried out according to the operator's connection procedure. The complete procedure can be found in Appendix C. The connection procedure is the same for all rigs, and was made to ensure specific and high quality data collection. Readings are also taken on trip-runs: Slack-off weights for tripping in and pick-up weights for tripping out.

Trip-out operations give many high quality measurements. Trip-in operations are more difficult. The string is filled with drilling fluid for every given length of string tripped in as explained in

section 2.3. Uncertainty in how much mud is filled, how often and if the density of mud in the string is the same as the mud in annulus are reasons why trip-in runs are not analyzed as detailed as the other runs. To find friction factors for trip-in, the slack-off measurements for drilling runs are used. Cases in which trip-in runs are analyzed in detail are casing- and liner runs.

Figure 4.7 shows the real-time plot the actual loads are taken from and where to take them during a drilling run. Because the data quality is such an important part of a post-run analysis, it is important to be precise when taking the readings. The readings are taken for every connection on every run. The number of connections per run ranges from 10 to 130 depending on the depth of the run. Taking these readings is a time-consuming but essential part of the work. Points that are not above stretch distance or for other reasons have values that seem unreasonably high or low are neglected. In these cases the connection procedure has been poorly followed and the hook load values seen on the plot will not be correct for that point.

Other parameters that need to be checked and inserted into Wellplan before doing simulations are: Drillstring information, pump rates, block weights, mud density and rheology, RPM, the start and end MD of the run, running speed and survey data. When all required input paramaters and data are in place, the simulations can start. The first step is finding the hook load sensor discrepancy for the first drilling run. This will often turn out to be a temporary discrepancy. A well usually has a number of drilling runs, and the discrepancy found in the first run might not be representative for the following runs. For instance, if one of the following runs has better rotating off-bottom readings, the discrepancy of this run will be the most reliable. The discrepancy used on the previous runs must then be changed to the new discrepancy. This was done several times throughout the field case post-run analysis.

When a discrepancy is chosen for a run, the different friction factors can be found. This is like the hook load sensor discrepancy done by starting with some probable values, and then adjusting them to get the best fit for the simulations against real-time data. All data for the runs and information found from the post-run analysis is inserted into a large spreadsheet called the Friction Factor Table when the analysis is done. This is done for every analysis and the Friction Factor Table contains enormous amounts of information from the wells drilled on the operator's field.

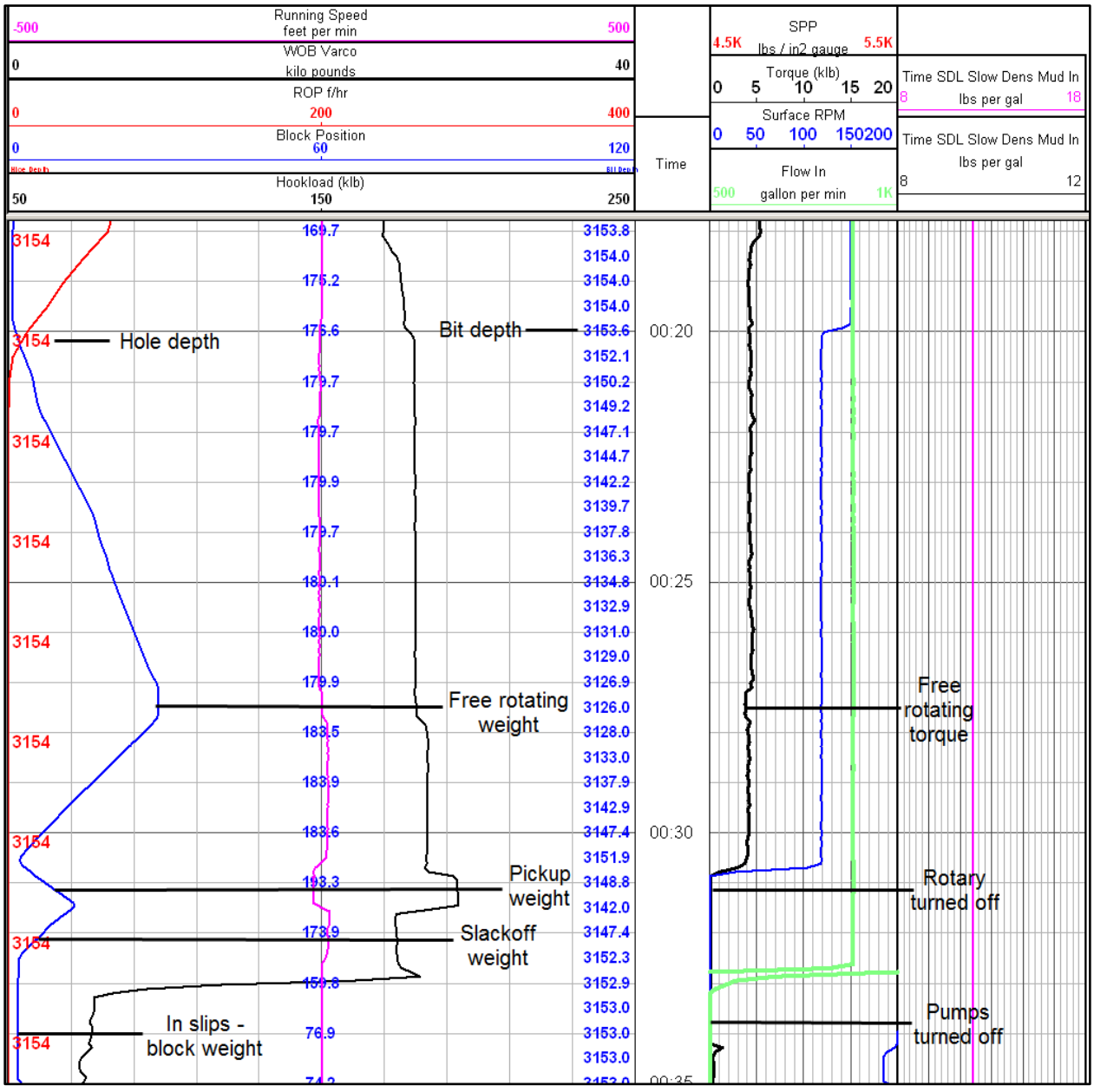

Figure 4.7 – Real-time plot for a drilling operation

4.3 Well A Sections

4.3.1.1 Run 100 - Drilling the 12 ¼" x 12 ¾" Tophole Section

This section was drilled with a 12 ¼" Mill Tooth Tricone bit and Halliburton's Geo-Pilot rotary steerable assembly. A 12 ¾" underreamer was used for hole enlargement. Detailed string information can be found in Appendix D. The hole section is from 2525 ft to 5232 ft, and the entire section is open hole. The mud used was 12.0 ppg WARP OBM, and the inclination of the section ranges from 20˚ to 45˚. The real-time plot for the run was examined and readings for actual loads taken. The connection procedure was followed for most points. The most questionable readings were left out. Block weight is 74 klb according to the real-time plot.

Different hook load discrepancies were tested, and -12% gave the best match with the real-time data. 12% of the weight is subtracted from the drillstring in String Editor in Wellplan. Figure 4.8 shows the drag hook load chart before applying the hook load sensor discrepancy. Figure 4.9 shows the drag hook load chart after applying the discrepancy and with the adjusted friction factors in Table 4.1.

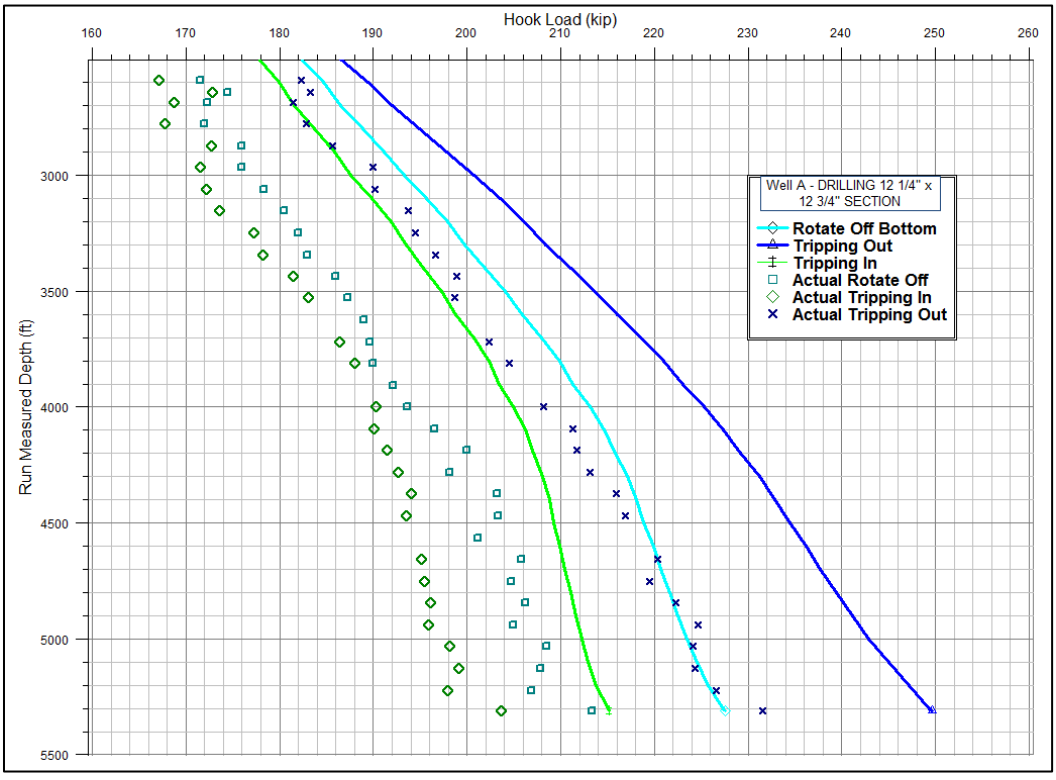

Figure 4. 8 – Run 100: Drag Hook Load Chart with no hook load discrepancy

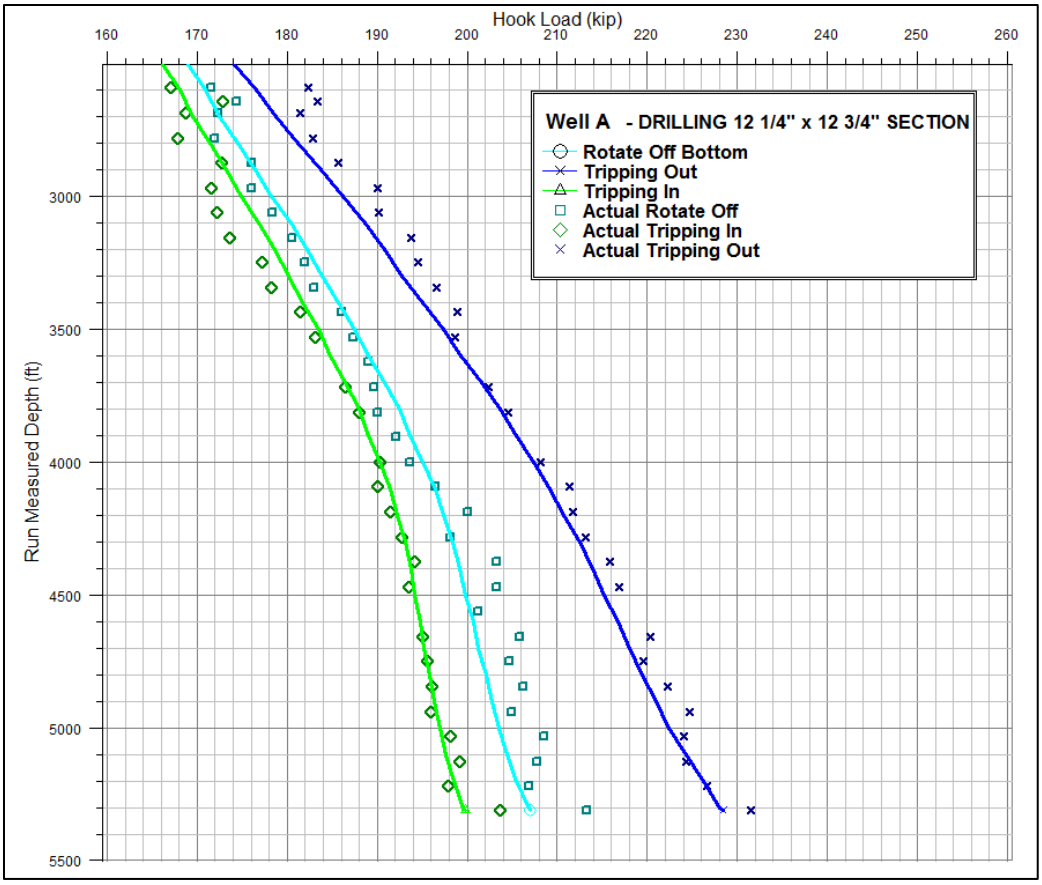

Figure 4.9 – Run 100: Drag Hook Load Chart with a hook load discrepancy of -12%

For tripping out, the simulated line should be a hint to the left of the real-time points. For tripping in, the simulated line should be a hint to the right of the real-time points. Figure 4.9 shows that the simulations for trip in and trip out match up quite well. However, the interval from 2600 ft to 3500 ft shows a hint more drag than the rest of the run. For a drilling run, the points of greatest interest are the rotate off-bottom points. It is ideal to have this simulated line pass in the middle or through the real-time points. For the interval from 4186 ft to TD the simulated rotating of bottom line is below the real-time points. The cause of this is most likely that the quality of the real-time readings is poorer for this interval. The connection procedure was poorly followed for this interval, making it hard to get good readings from the real-time plot. Figure 4.10 shows the torque chart for the 100 run. Because the friction factors for rotating off-bottom will not change the simulated line in the drag charts, the friction factors for rotating off-bottom must be found from adjustments made in the torque chart.

The different friction factors in Table 4.1 are like hook load sensor discrepancies also found by trial and error method, and adjusted until one that will match most points is found. The casing of the main well goes to 2500 ft. The sidetrack, Well A, kicks off at 2525 ft and has open hole to the TD of the 100 run.

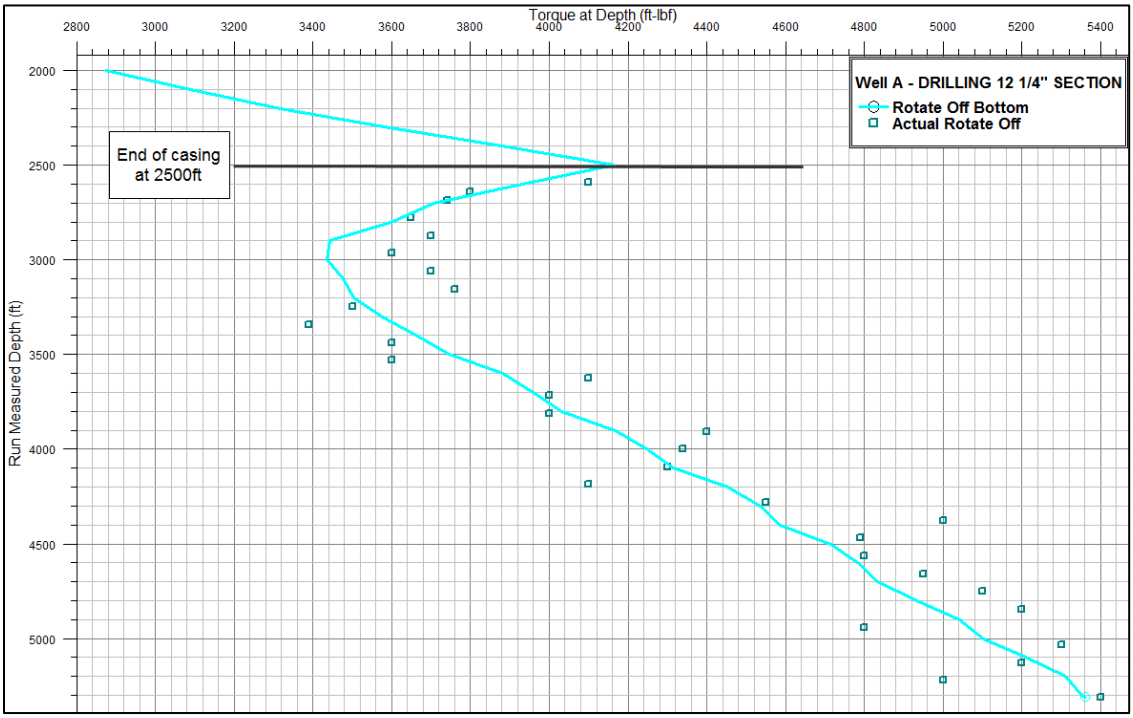

Figure 4.10 – Run 100: Torque Chart with a hook load discrepancy of -12%

The friction factors found for Run 100:

Friction Factors – 100 Run					
Trip Out - Casing	Trip Out - Open hole	Trip In - Casing	Trip In - Open hole	Rotate Off-Bottom - Casing	Rotate Off-Bottom - Open hole
0.11	0.16	0.06	0.05	0.31	0.05

Table 4.1 – Run 100: Friction factors

Vibrations:

During the run any vibration seen was met with attempts to mitigate. No prolonged vibrations were encountered, and on the surface after POOH the BHA components were inspected and found to have no damage. The MWD download also confirmed that no severe vibrations were present.

4.3.2.1 Run 200 - Drilling the 10 ¾" Casing While Drilling Tophole Section

This section was drilled with a 12 ¼" Baker Hughes EZCase Tricone bit. Detailed string information can be found in appendix D. The length of the run is 5310 ft to 5710 ft. The 10 ¾" casing was cemented with casing shoe at 5714 ft. The mud used is still WARP OBM, but it was weighted up to 12.2 ppg before the run. The inclination ranges from 45˚ to 44˚. The real-time plot gave usable hook load readings. The block weight is 80 klb according to the real-time plot. Figure 4.11 shows the drag hook load chart after applying hook load sensor discrepancy and with the adjusted friction factors in Table 4.2 The discrepancy was found to be -4%.

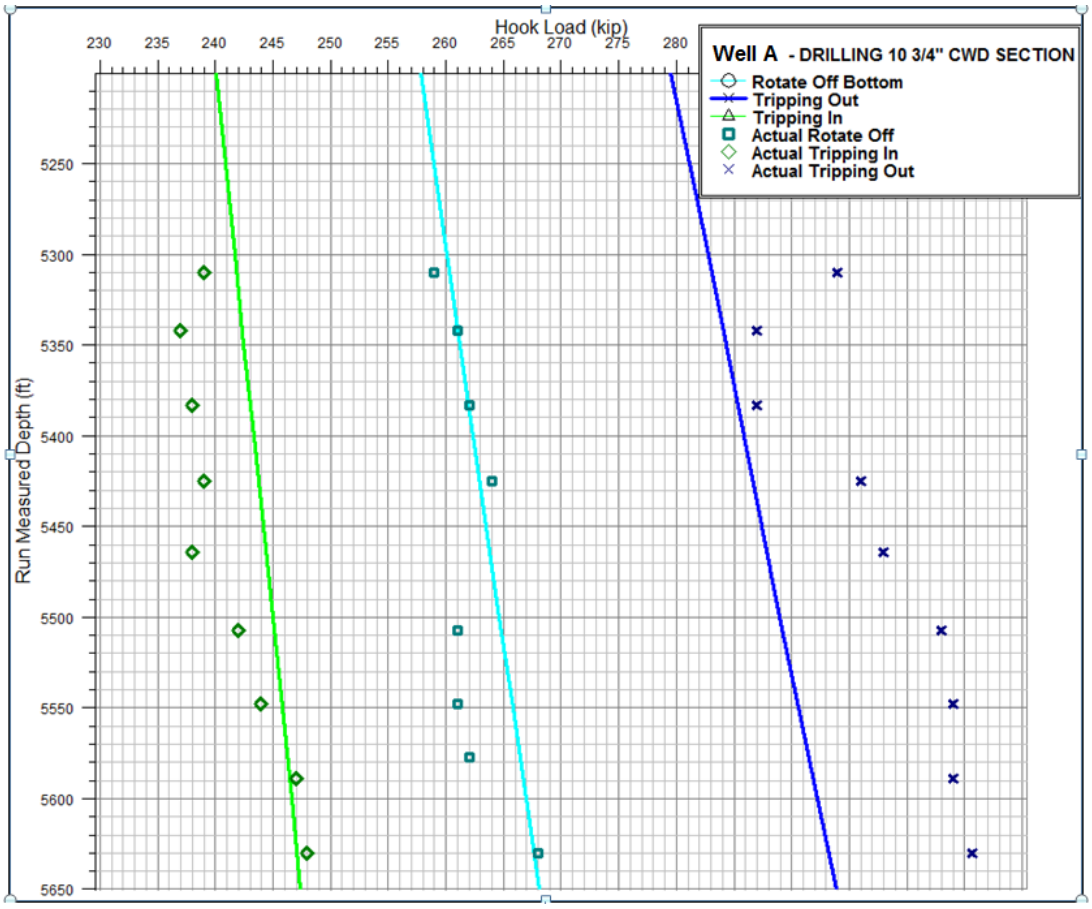

Figure 4. 11 – Run 200: Drag Hook Load Chart with a hook load discrepancy of -4%

Casing while drilling runs are usually special cases and the discrepancy found in other runs will not match for CWD. In order to apply WOB when casing drilling, a so-called "pump-off" effect has to be overcome. In CWD there is an extremely tight annulus and there will be more hydrodynamic viscous drag. The hook load sensor discrepancies and friction factors found for CWD runs are not compared with the other runs due to the pump-off effect. For instance, the

rotate off-bottom friction factor inside casing is high for this run. But casing drilling is still included in the post-run analysis and the run information is inserted in the Friction Factor Table. Casing drilling is a relatively new technology and over time it might be possible to find a trend by comparing runs.

Friction Factors – 200 Run					
Trip Out - Casing	Trip Out - Open hole	Trip In - Casing	Trip In - Open hole	Rotate Off-Bottom - Casing	Rotate Off-Bottom - Open hole
0.16	0.16	0.15	0.15	0.39	0.11

Table 4.2 – Run 200: Friction factors

4.3.3.1 Run 300 - Drilling the 9 ½" x 10 ¼" Overburden Section

This run was drilled with a 9 ½" Baker Hughes PDC bit and Halliburton's Geo-Pilot rotary steerable assembly. A 10 ¼" underreamer was used for hole enlargement. Detailed string information can be found in Appendix D. The length of the run is from 5310 ft to 5913 ft, with cased hole to 5714 ft and open hole for the rest of the length. The well was displaced to 14.4 ppg WARP OBM before tripping in. The inclination of the run ranges from 40˚ to 44˚. Because the length of the run where there was drilling of new formation is from 5714 ft to 5913 ft, there were only a couple of readings to be obtained from the real-time plot. The block weight for the run was 75 klb according to the real-time plot.

The run encountered several stringers at the following depths: 5732 ft, 5831 ft, 5842 ft, 5881 ft, 5901 ft and 5912 ft. The stringer at 5901 ft took 5 ½ hours to drill, and when the bit reached the stringer at 5912 ft ROP dropped. No progress was made and the string was tripped to examine the bit. At surface the bit was severely worn and undergauged. Figure 4.12 shows the drag hook load chart for the run. The same discrepancy as found in run 100 is applied.

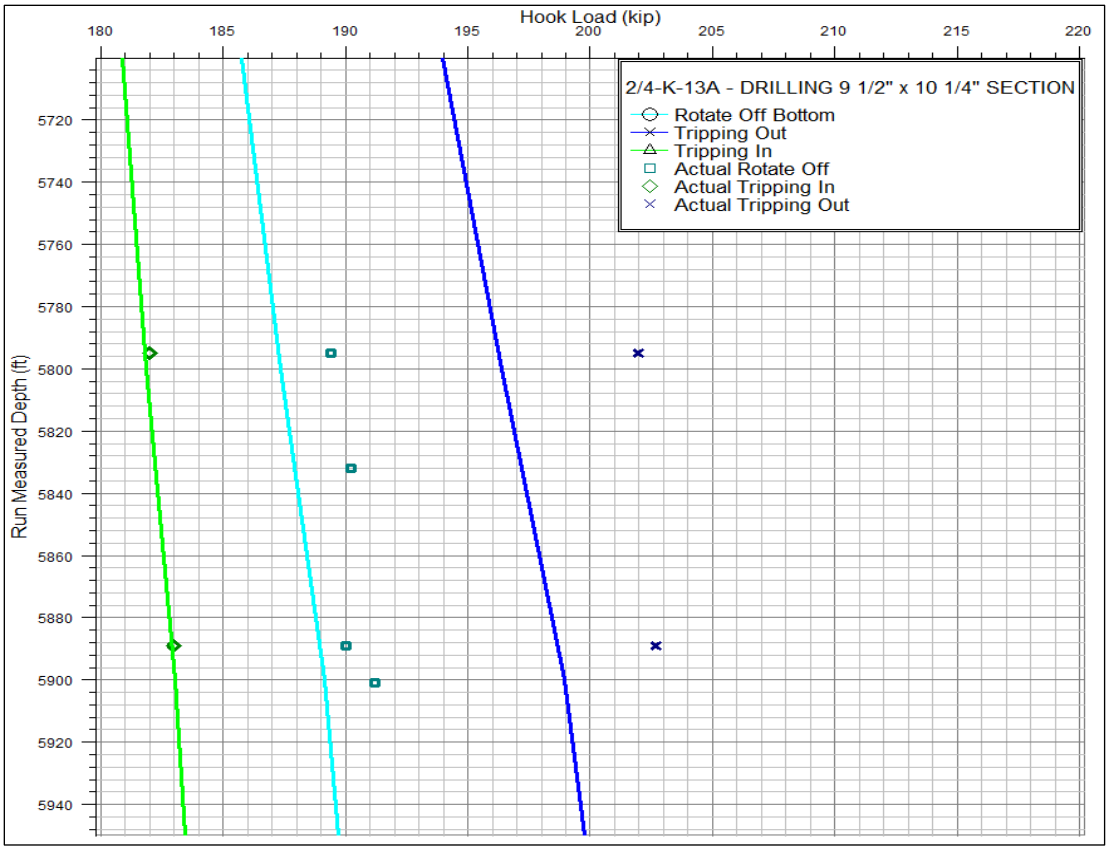

Figure 4.12 – Run 300: Drag Hook Load Chart with a hook load discrepancy of -12%

The friction factors for this run were disregarded and changed to the friction factors found in the 400 run. A run length of 203 feet with 2-5 real-time readings is not enough to get reliable friction factors. In addition to this the connection procedure was poorly followed, and rotate off-bottom time was low. This is also why the discrepancy of -12% found in run 100 was used for this run. Run 100 had higher quality readings. The run had no reliable readings for rotating off-bottom torque values, and it was therefore not possible to generate a torque chart.

Friction Factors – 300 Run					
Trip Out - Casing	Trip Out - Open hole	Trip In - Casing	Trip In - Open hole	Rotate Off-Bottom - Casing	Rotate Off-Bottom - Open hole
0.08	0.18	0.05	0.15	0.17	0.07

Table 4.3 – Run 300: Friction factors

Vibrations:

Stick-slip was high at times when drilling stringers. This was the overburden run that had the most vibrations, but the BHA components were still in good condition after POOH.

4.3.4.1 Run 400 - Drilling the 9 ½" x 10 ¼" Overburden Section

This run was drilled with a 9 ½" Halliburton PDC bit and Halliburton's Geo-Pilot rotary steerable assembly. A 10 ¼" underreamer was used for hole enlargement. Detailed string information can be found in Appendix D. The length of the run is from 5913 ft to 7142 ft, with open hole the entire length. The mud used is WARP OBM, and the mud density ranges from 14.4 ppg to 14.8 ppg. The inclination ranges from 39˚ to 44˚. The real-time plot for the run was examined and readings for actual loads taken. The block weight was 73 klb according to the real-time plot.

The DDR indicated that a slip-and-cut had been performed before this run, and a new hook load sensor discrepancy had to be found. A hook load sensor discrepancy of -8% gave the best result for this run. However, run 700 would later prove to have significantly more quality readings and the discrepancy of this run was chosen. This discrepancy was -7%. The discrepancy of runs 400, 500 and 600 was then changed to -7%.

During this run was where the first gas problems were seen. The well had to be shut in due to increased flow returns. Stringers were encountered in this run as well, but they were not as dense as the previous run. At 7076 ft the well was shut in and gas was circulated out. The mud system was weighted up to 16.6 ppg before drilling was continued. After a packoff at 7110 ft, the progression of the drilling slowed down. At 7142 ft it was decided to POOH and inspect the bit. The mud system was weighted up to 14.8 ppg before tripping out, because gas levels in the well were high. At surface the bit was damaged and the under reamer cutters were severly chipped and broken. Figure 4.13 shows the drag hook load chart for the run.

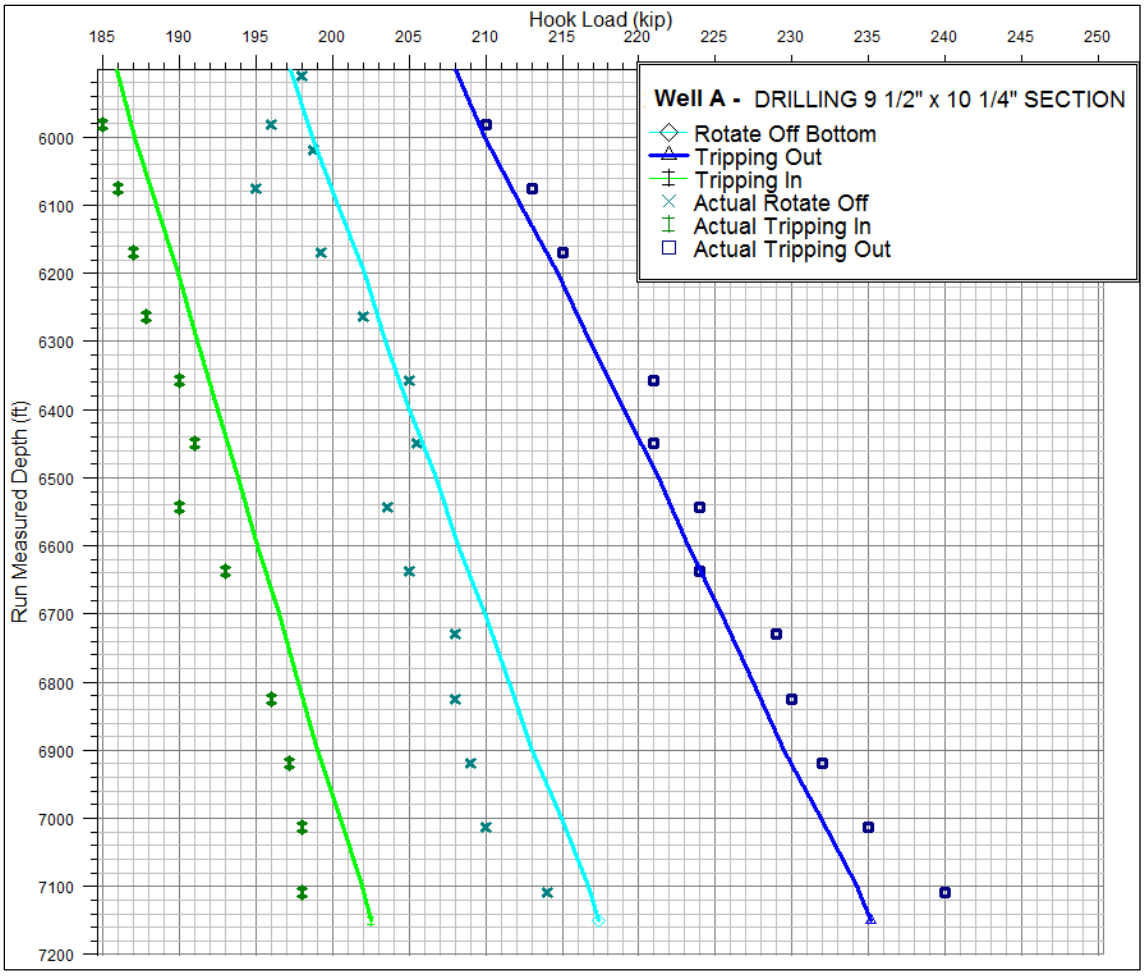

Figure 4.13 – Run 400: Drag Hook Load Chart with a hook load discrepancy of -7%

The simulations matched well with the applied discrepancy and the friction factors in Table 4.4.

Friction Factors – 400 Run					
Trip Out - Casing	Trip Out - Open hole	Trip In - Casing	Trip In - Open hole	Rotate Off-Bottom - Casing	Rotate Off-Bottom - Open hole
0.08	0.18	0.05	0.15	0.17	0.07

Table 4.4 – Run 400: Friction factors

Vibrations:

Drillstring vibrations were not an issue during this run.

4.3.5.1 Run 500 - Drilling the 9 ½" x 10 ¼" Overburden Section

This run was drilled with a 9 ½" Halliburton PDC bit and Halliburton's Geo-Pilot rotary steerable assembly. A 10 ¼" underreamer was used for hole enlargement. Detailed string information can be found in Appendix D. The length of the run is from 7142 ft to 7189 ft, and it is open hole. The mud used was 14.8 ppg WARP OBM, and the inclination of the run was 39°. The block weight was 73 klb according to the real-time plot.

The drillstring was washed and reamed into hole due to some minor restrictions in the open hole section. At 7188 ft a stringer was encountered, and drilling slowed down. After breaking through the stringer, gas influx in the well became a problem at 7189 ft. Several days were used trying to get the gas levels in the well down. Attempts to wash or ream down to TD were met with pack off tendencies and torque spikes. A heavy pill was circulated downhole and the string was tripped out.

The length of the drilling run was only 42 ft, so it was not possible to take any useful real-time readings for generating a torque and drag hook load chart for the drilling operation.

4.3.5.2 Run 500B - POOH From 7189 ft

Even though it was not possible to produce a torque and drag hook load chart for the drilling operation of the 500 run, the POOH operation for this run provided many quality readings. The drag hook load chart is shown in Figure 4.14.

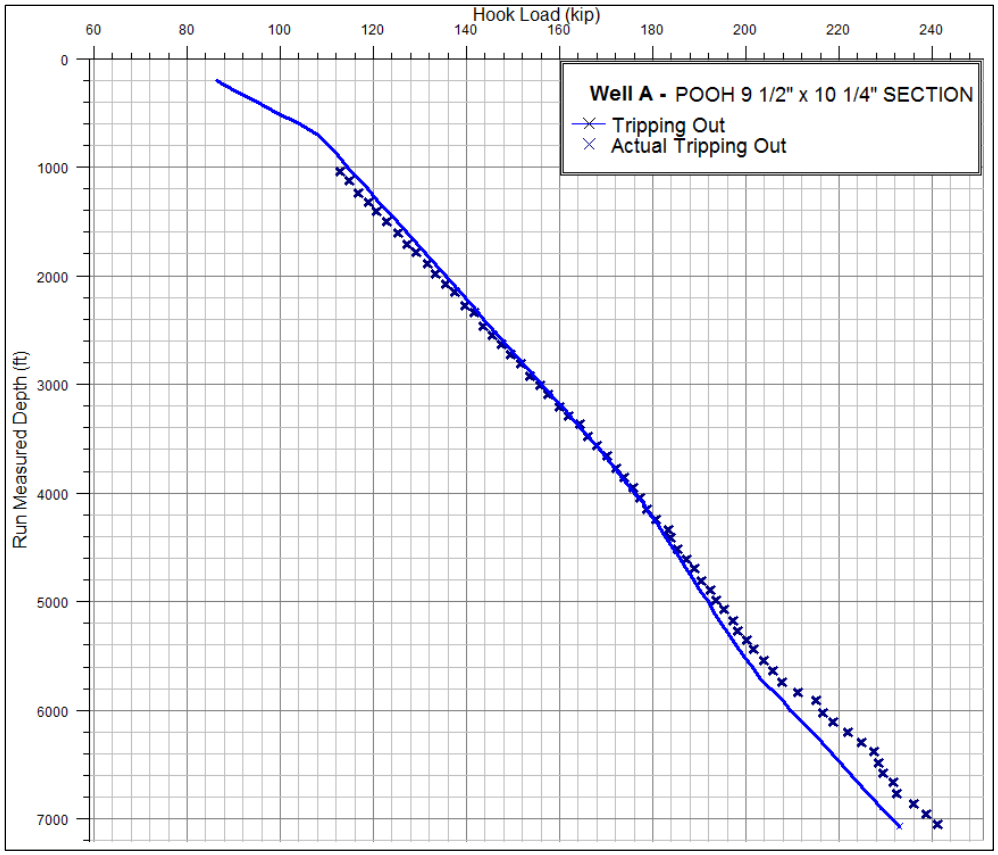

Figure 4.14 – Run 500B: Drag Hook Load Chart with a hook load discrepancy of -7%

The chart shows that there was some drag from TD to 5000 ft. Poor hole conditions are the probable cause of the drag, because the start of the open hole interval is at 5714 ft. From 2500 ft the real-time readings start drifting under the simulated line. This is common for tripping out readings. The reason is that as the string becomes shorter and lighter, the readings get more imprecise. Readings above 2000 – 3000 ft are for this reason usually neglected when doing an analysis. This is also why the 500 run is the first run where a trip-out chart has been presented in this field case. The previous runs are not of sufficient length to give a good representation of drag when tripping out.

Friction Factors – 500B Run	
Trip Out - Casing	Trip Out - Open hole
0.08	0.18

Table 4.5 – Run 500B: Friction factors

4.3.6.1 Run 600 - Drilling the 9 ½" Overburden Section

This run was drilled with a 9 ½" Baker Hughes Roller Cone bit and a simple rotary BHA. Complete string information can be found in Appendix D. The assembly had no MWD components and the goal was to drill past the problem zone of the previous run and then drill ahead blind. Because of the gas level in the well and the mud weight required, there was insufficient margin to drill more than 201 ft. The run length was from 7189 ft to 7390 ft. The mud used was 14.9 ppg WARP OBM, and the inclination of the run was 39˚. During drilling, the string kept torqueing up and had packoff tendencies much like the previous run. The decision was made to plug and abandon this section. Before pulling the drillstring out of hole, a cement plug was set through the BHA. This drilling run was like the previous drilling run too short for generating a useful torque and drag hook load chart. The mud weight was weighted up to 15.9 ppg before POOH.

4.3.6.2 Run 600B - Tripping Out From Section TD

Like the 500B run, the 600B run also gave good real-time trip-out readings for generating a drag hook load chart. Figure 4.15 shows the drag hook load chart for the run.

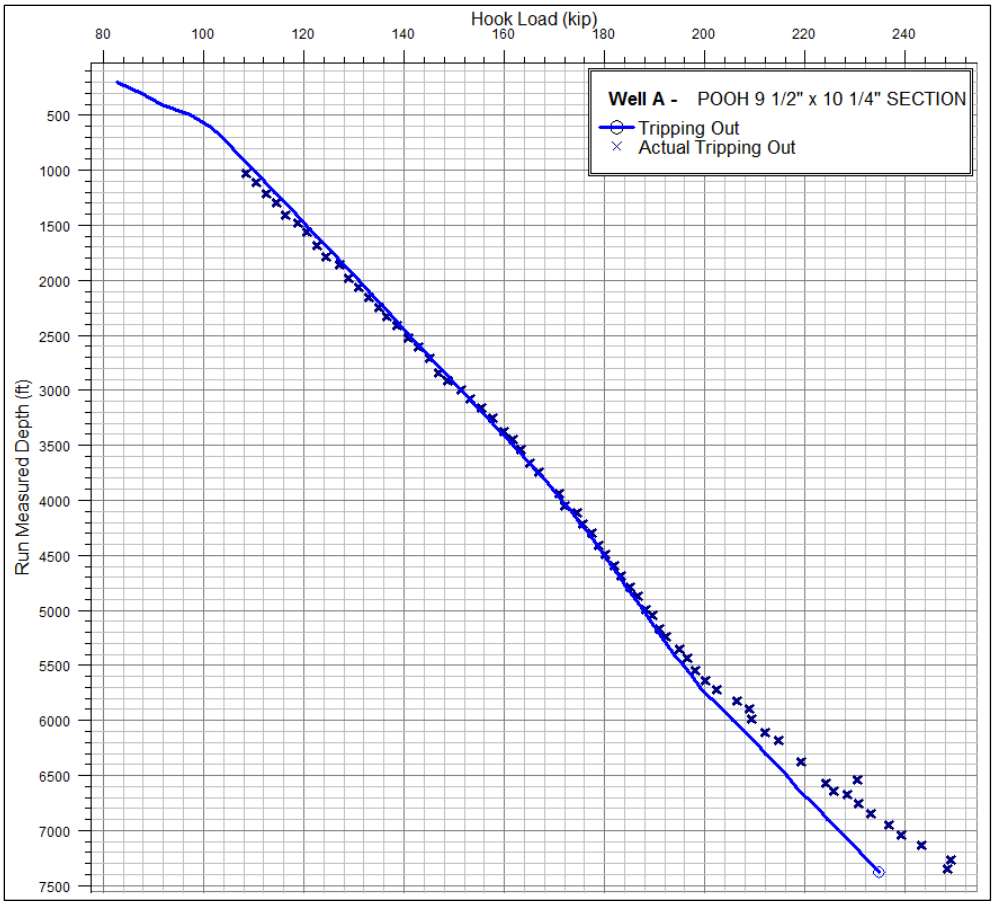

Figure 4.15 – Run 600B: Drag Hook Load Chart with a hook load discrepancy of -7%

The chart is similar to that of run 500B. These two trip-out operations support the friction factor found for tripping out inside casing. This trip-out also indicates drag in the lower part. A number of reasons are the probable cause of this drag for 500B and 600B. It is the start of the open hole section and the interval that has the largest inclination of the well. Inclination and the casing shoe impact the effect of the hole cleaning. Increased drag close to TD is a signature of poor hole cleaning. This interval is also in the Miocene formation, which is known to be a troublesome formation at times.

Friction Factors – 600B Run	
Trip Out - Casing	Trip Out - Open hole
0.08	0.18

Table 4.6 – Run 600B: Friction factors

4.3.6.3 Run 650 - Cement Plug

It was decided to set cement plugs back to the casing shoe because of the gas levels in the well. This was done with a dedicated cement string. After setting the cement plugs, the technical sidetrack A T2 was drilled out of the cement plug in the 10 ¾" casing shoe.

4.4 Well A T2 Sidetrack Sections

4.4.1.1 Run 700 - Drilling the 9 ½" x 10 ¼" Overburden Section

This section was drilled with a 9 ½" Halliburton Long Gauge PDC bit and Halliburton's Geo-Pilot rotary steerable assembly. A 10 ¼" underreamer was used for hole enlargement. Detailed string information can be found in Appendix D. The run was drilled from 5702 ft to 11715 ft, and the entire length is open hole. The mud used was 14.5 ppg WARP OBM, and the inclination of the run ranges from 31˚ to 45˚. The connection procedure was followed for most of the real-time points taken. The block weight was 73 klb according to the real-time plot.

A major problem zone was encountered at 5895 ft leading to the string packing off and a stuck pipe incident. The string was worked free with up to 100 klb over pull. The run also had stringers at 5905 ft, 5921 ft, 6179 ft, 7359 ft, 7992 ft, 8042 ft, 8337 ft and 8854 ft. But none of these caused significant problems. After sidetracking, the gas levels in the well were under control.

Runs 400, 500 and 600 supported a hook load sensor discrepancy of -8%. The 700 run had good real-time readings for the entire run length, and the data quality was significantly higher than the previous runs. A discrepancy of -7% was the best fit for this run, and so the discrepancy of runs 400, 500 and 600 was changed to -7%. Figure 4.16 shows the drag hook load chart for the run.

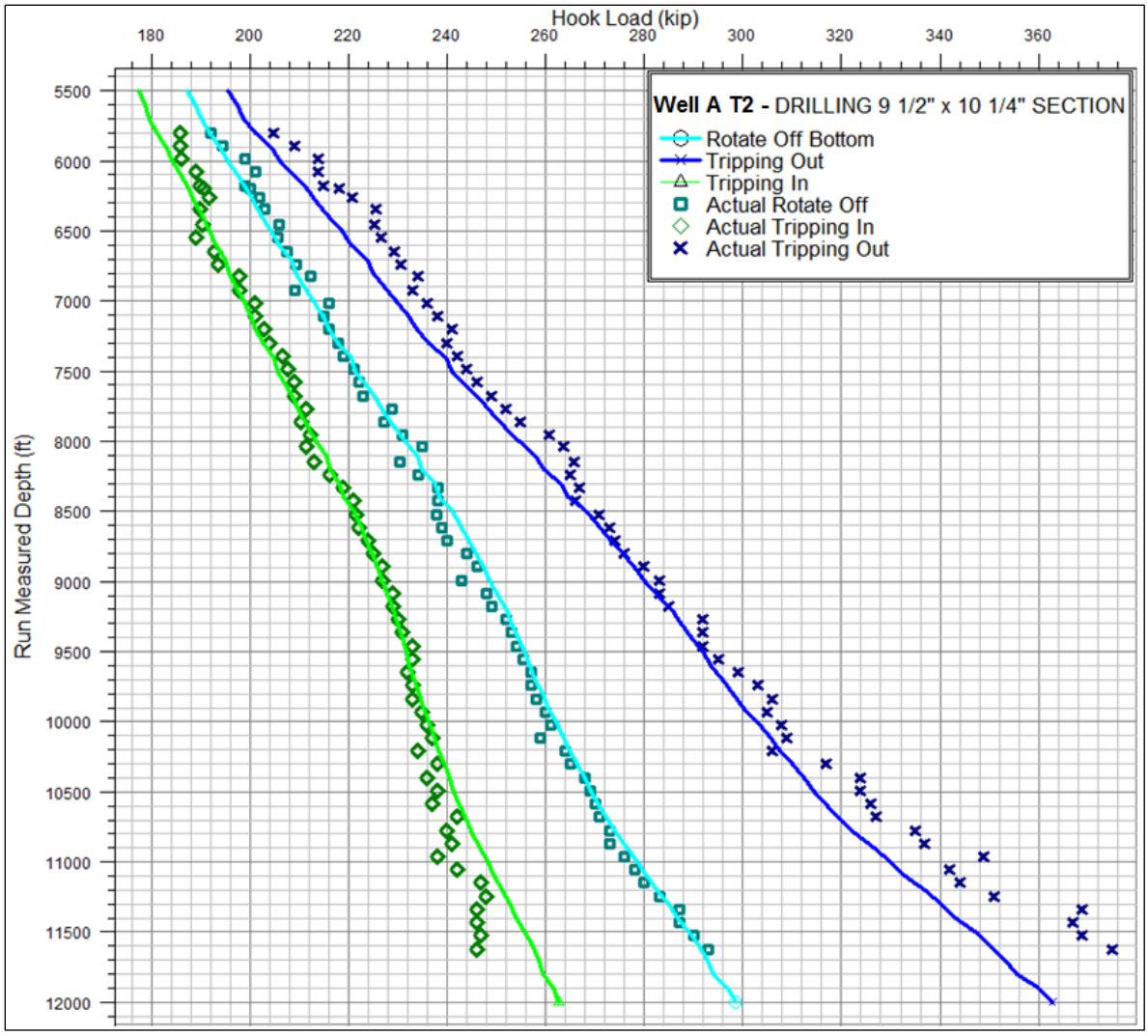

Figure 4.16 – Run 700: Drag Hook Load Chart with a hook load discrepancy of -7%

Some drag is seen for tripping in and tripping out in the lower part of the section. This is as previously mentioned, a classic drag signature of poor hole cleaning.

Figure 4.17 shows the torque chart for the rotating off-bottom readings of the drilling run. The torque readings for this run were of varying quality.

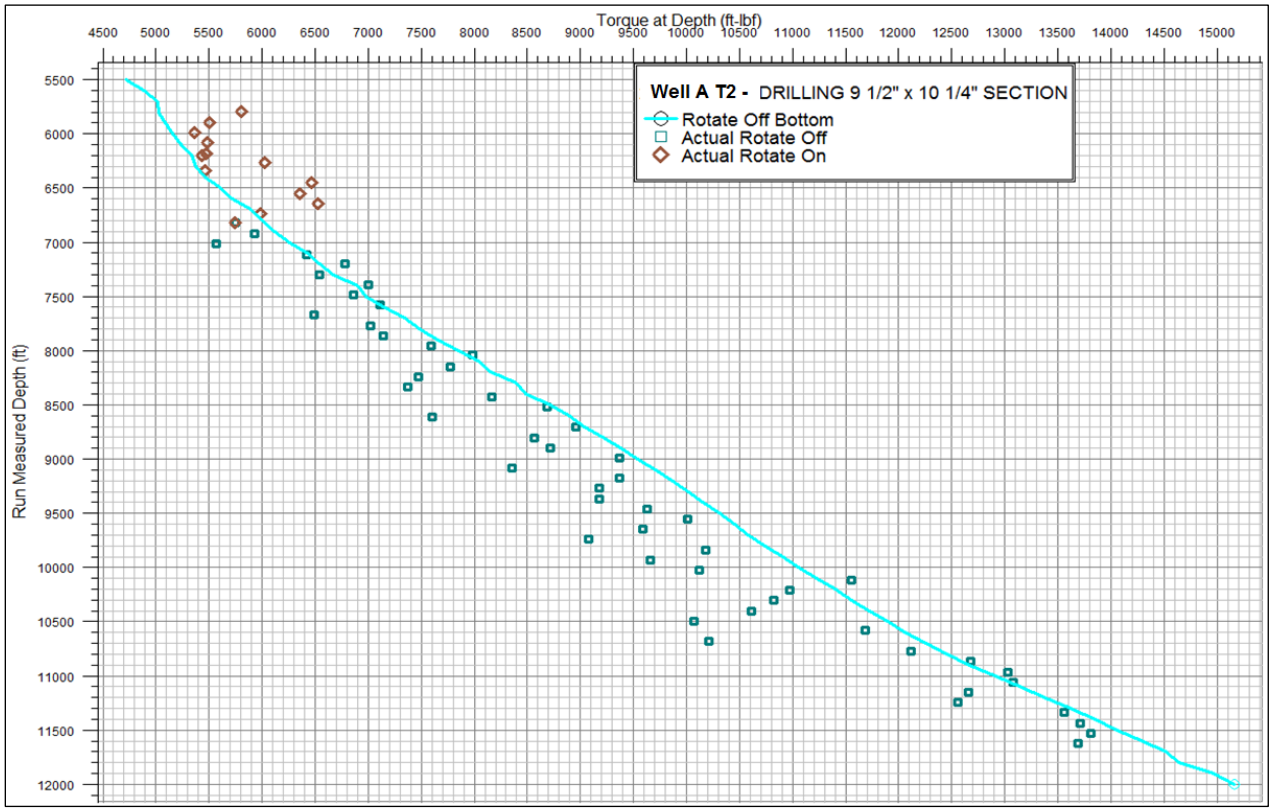

Figure 4.17 – Run 700: Torque Chart with a hook load discrepancy of -7%

Friction Factors – 700 Run					
Trip Out - Casing	Trip Out - Open hole	Trip In - Casing	Trip In - Open hole	Rotate Off-Bottom - Casing	Rotate Off-Bottom - Open hole
0.08	0.18	0.11	0.08	0.17	0.07

Table 4.7 – Run 700: Friction factors

Vibrations:

The run had some stick-slip vibrations, but no serious vibration issues.

4.4.1.1 Run 700B - Tripping Out From Section TD

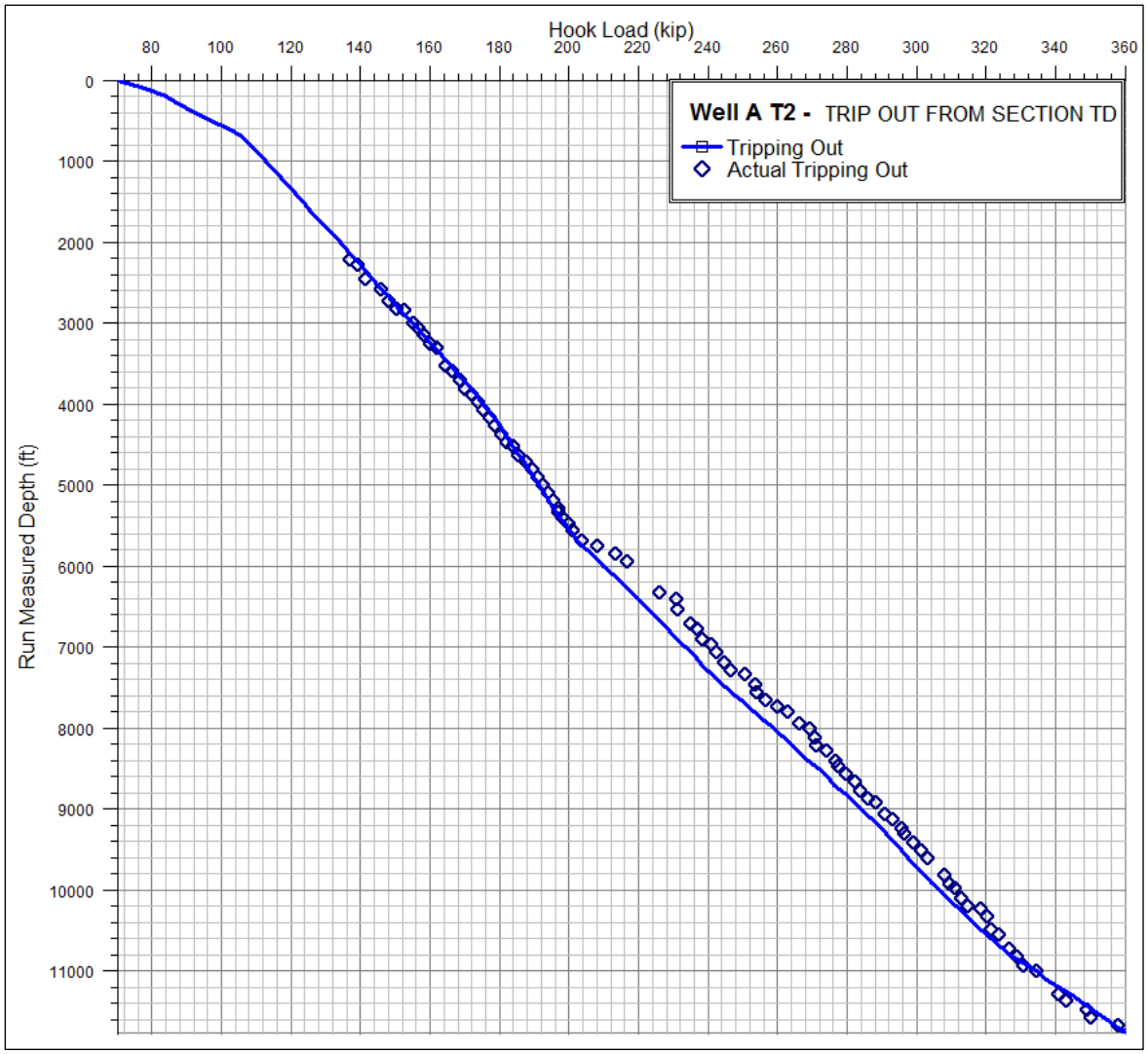

Figure 4.18 – Run 700B: Drag Hook Load Chart with a hook load discrepancy of -7%

For this trip out operation there is no increase in drag near TD as seen in 500B and 600B. The hole cleaning after the drilling run seems to have been better for this case. However, there is increased drag in the interval 5800 ft – 10500 ft. From the 700 drilling run, it is known that there were frequent stringers from 5800 ft to 8600 ft. In addition, the interval with increased drag in the 500B and 600B runs was from 5500 ft to 7500 ft. Run 500B and 600B do not have the same wellpath as 700B, because Well A was plugged and sidetracked at 5752 ft. It is still a good indication that the formation of these intervals is troublesome, and is the cause of the excess drag rather than poor hole cleaning. This is as previously mentioned, in the Miocene formation.

4.4.2 Run 740 - Running the 7 ¾" Liner With Bow-Spring Centralizers

The 7 ¾" liner was run with one Weatherford S1S+ Bow-Spring Centralizer per joint. Bow-spring centralizers are presented in detail in Appendix E. When doing Wellplan simulations against real-time hook load readings, bow-spring centralizers must be inserted a standoff devices in the parameters tab. Without standoff devices it will be difficult to get the simulations to match, and the friction factors found will not be realistic. The centralizers exert a running force of 422 lb/ft inside the 10 ¾" casing and 150 lb/ft inside the 10 ¼" open hole section. The starting force of the centralizers inside the casing is 568 lb/ft. This is the force needed to get the string moving from a static position. When running casing or liner with bow-spring centralizers this will be the critical force to analyze with regards to buckling and yielding. Wellplan does not simulate the starting force. In order to simulate this, the starting force must manually be inserted into the running force column seen in Figure 4.19. Then a torque and drag effective tension graph and hook load chart with buckling and yield limits can be generated. These can be found in Appendix D for the 740 liner run. For this liner run there was not a significant difference between starting force and running force. The simulations for the two gave almost the same lines and both starting force and running force were well inside the buckling and yield limits. In other cases the starting force can be as much as double the running force. In these cases it can be crucial to simulate for starting force to avoid buckling or yielding.

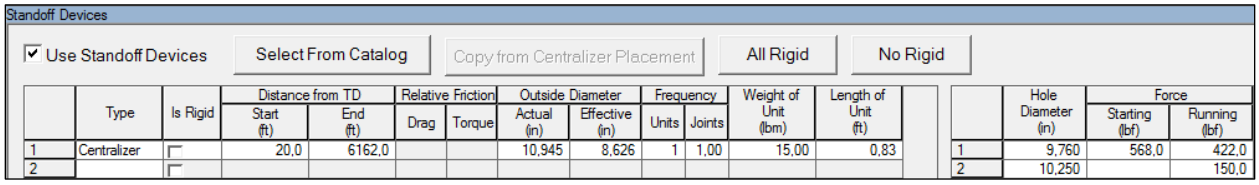
Standoff Devices

Use Standoff Devices | Select From Catalog | Copy from Centralizer Placement | All Rigid | No Rigid

	Type	Is Rigid	Distance from TD		Relative Friction		Outside Diameter		Frequency		Weight of Unit (lbm)	Length of Unit (ft)
			Start (ft)	End (ft)	Drag	Torque	Actual (in)	Effective (in)	Units	Joints		
1	Centralizer	☐	20,0	6162,0			10,945	8,626	1	1,00	15,00	0,83
2		☐										

	Hole Diameter (in)	Force	
		Starting (lbf)	Running (lbf)
1	9,760	568,0	422,0
2	10,250		150,0

Figure 4.19 – Standoff devices for the 740 run

The mud used for this run was 14.5 ppg WARP OBM. The 7 ¾" liner was run to 6192 ft, and a 5 ½" drillpipe was then run to 11712 ft. Different pipe handling systems were used. This gave a block weight of 74 klb for the 7 ¾" liner and 69 klb for 5 ½" drillpipe. The simulations and real-time hook load readings are shown in Figure 4.20.

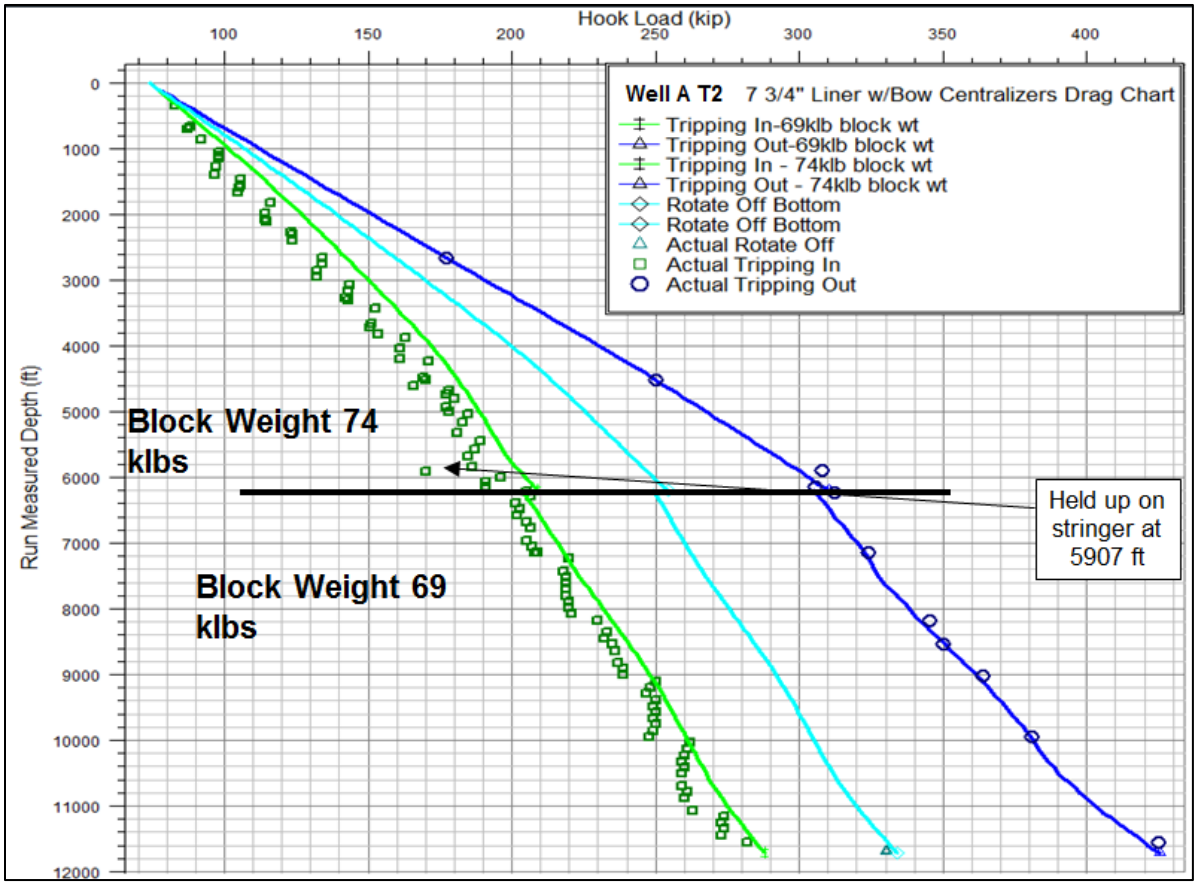

Figure 4.20 – Run 740: Drag Hook Load Chart with a hook load discrepancy of -7%

The simulations and hook load readings match well. The run had some problems with stringers and tight spots. Especially a stringer at 5907 ft is quite noticeable on the hook load readings. This stringer caused the most amount of trouble time. It was passed by pumping with 45 gpm, 80-100 psi, rotating 10 rpm and 10-15 klb/ft torque. Other tight spots were at 5962 ft, 6117 ft, 6185 ft and from 11619 ft to 11715 ft.

Friction Factors – 740 Run	
Trip In - Casing	Trip In - Open hole
0.12	0.08

Table 4.8 – Run 740: Friction factors

4.4.3.1 Run 800 - Drilling the 6 ½" Reservoir Section

This section was drilled with a 6 ½" Baker Hughes Tricone Insert Bit and Halliburton's Geo-Pilot rotary steerable assembly. Detailed string information can be found in Appendix D. The length of the hole section is from 11715 ft to 12940 ft, and the entire section is open hole. The mud used at the start of the section was 13.0 ppg WARP OBM, and the mud weight was increased to 13.2 ppg while drilling from 12063 ft to 12157 ft. Standard connection procedure used. A slip-and-cut operation was performed before the 800 run. Tried with the previous hook load sensor discrepancy of -7%, and it matched well. Applied -6% and -8% also to see if one would fit better, but -7% was the best choice.

Figure 4.21 shows the torque and drag hook load chart for the 800 drilling run. There are two simulated lines, one frozen with 13.0 ppg mud weight and one frozen with 13.2 ppg mud weight.

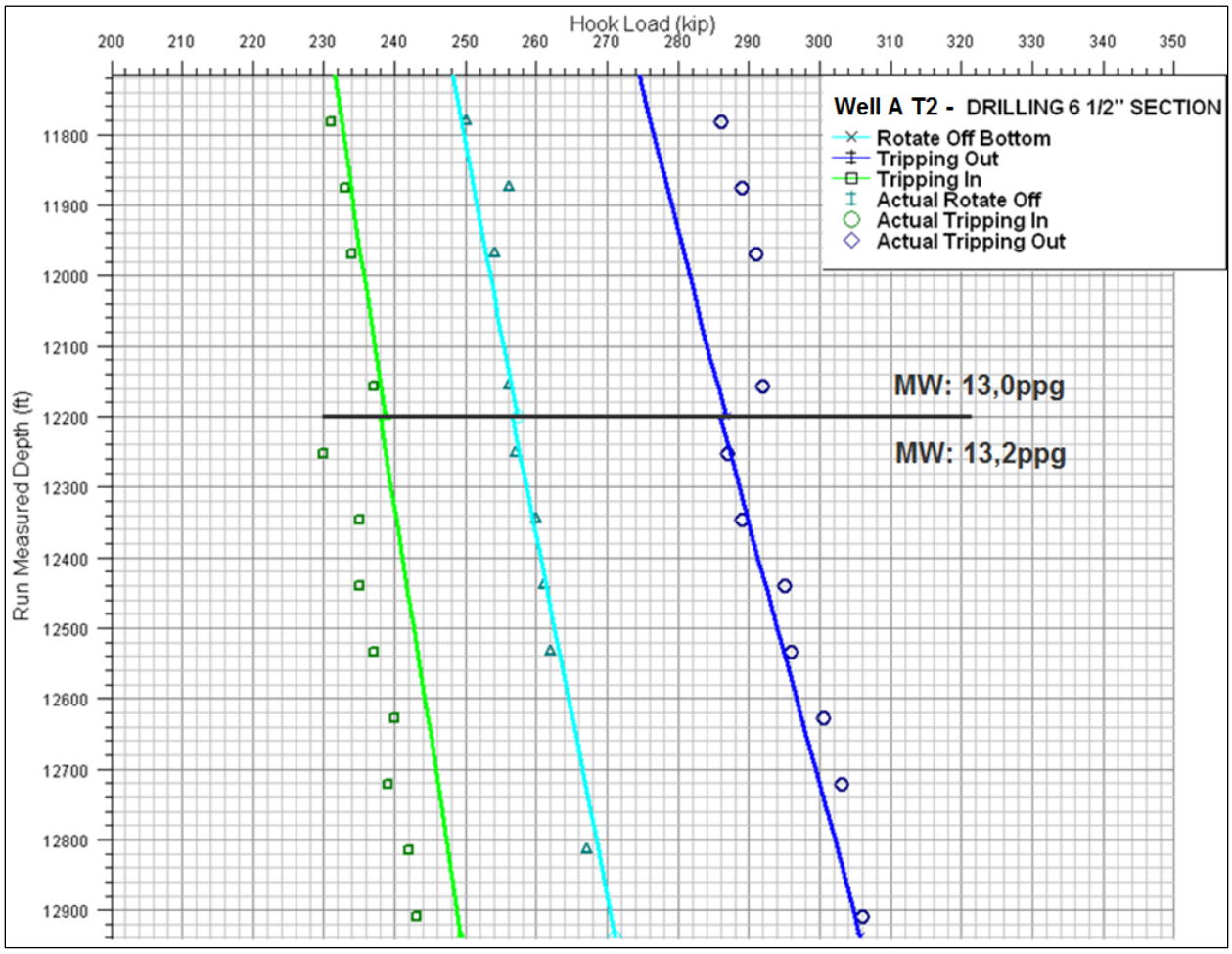

Figure 4.21 – Run 800: Drag Hook Load Chart with a hook load discrepancy of -7%

At 12234 ft there was observed loss of return flow and an increase in torque (from 8 to 12 klb/ft) according to the DDR. A lost circulation material (LCM) pill was pumped and the assembly was pulled back to 11000 ft. This wiper trip had no notable drag. A drag chart of the wiper trip for the run can be found in Appendix D. Figure 4.22 shows the torque chart for the rotating off-bottom readings of the drilling run.

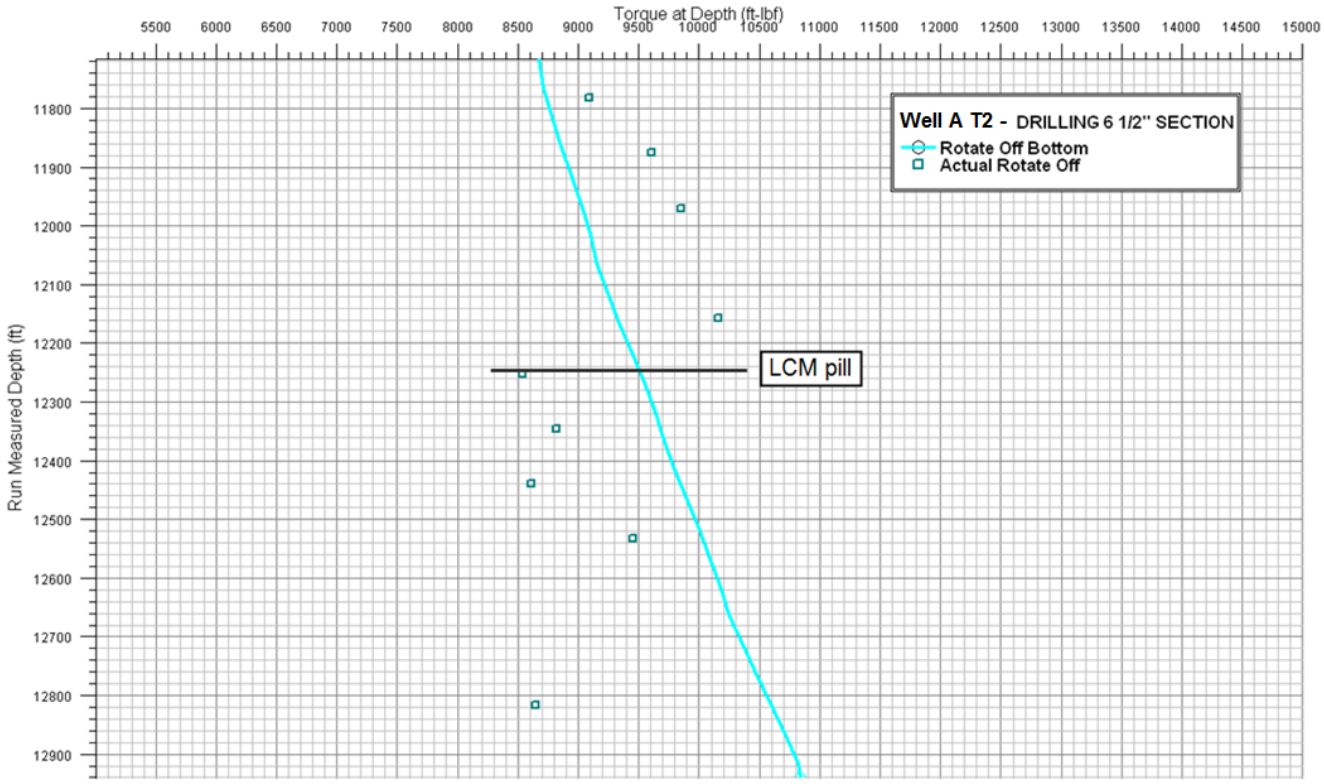

Figure 4.22 – Run 800: Torque Chart with a hook load discrepancy of -7%

There is a clear decrease in torque after the LCM pill has been pumped. Nothing is noted in the records of a friction reducing pill also being pumped. But this might be the case considering the cutback in torque below this point. The thing that is clear is that the friction has been reduced. Whether this one done as a side effect of the LCM pill or by an additional friction reducing pill is difficult to say based on the available data. The friction factors for the run are shown in Table 4.9.

Friction Factors – 800 Run					
Trip Out - Casing	Trip Out - Open hole	Trip In - Casing	Trip In - Open hole	Rotate Off-Bottom - Casing	Rotate Off-Bottom - Open hole
0.09	0.15	0.07	0.15	0.13	0.05

Table 4.9 – Run 800: Friction factors

Vibrations:

Constant high stick-slip levels were observed initially with the RPM kept at 80 until the roller reamer was below the liner shoe at 11912 ft. Despite increasing the RPM to 140, the stick-slip levels remained high with occasional peaks. It was decided to limit the RPM to 120. After a connection at around 12250 ft, the stick-slip vibration levels were greatly reduced. After POOH there was no damage to the BHA components.

4.4.3.1 Run 800B - Tripping Out From Section TD

The well was circulated clean before the interval from TD to 11682 ft was back reamed with a flow of 255 gpm, running speed of 10 ft/m and rotation of 120 rpm. After back reaming the well was circulated clean again and the string was tripped out from TD. Figure 4.23 shows the drag hook load chart for tripping out from the 6 ½" section TD. The pink line and the associated real-time points are for the reaming operation, and the blue line and associated real-time points are for tripping.

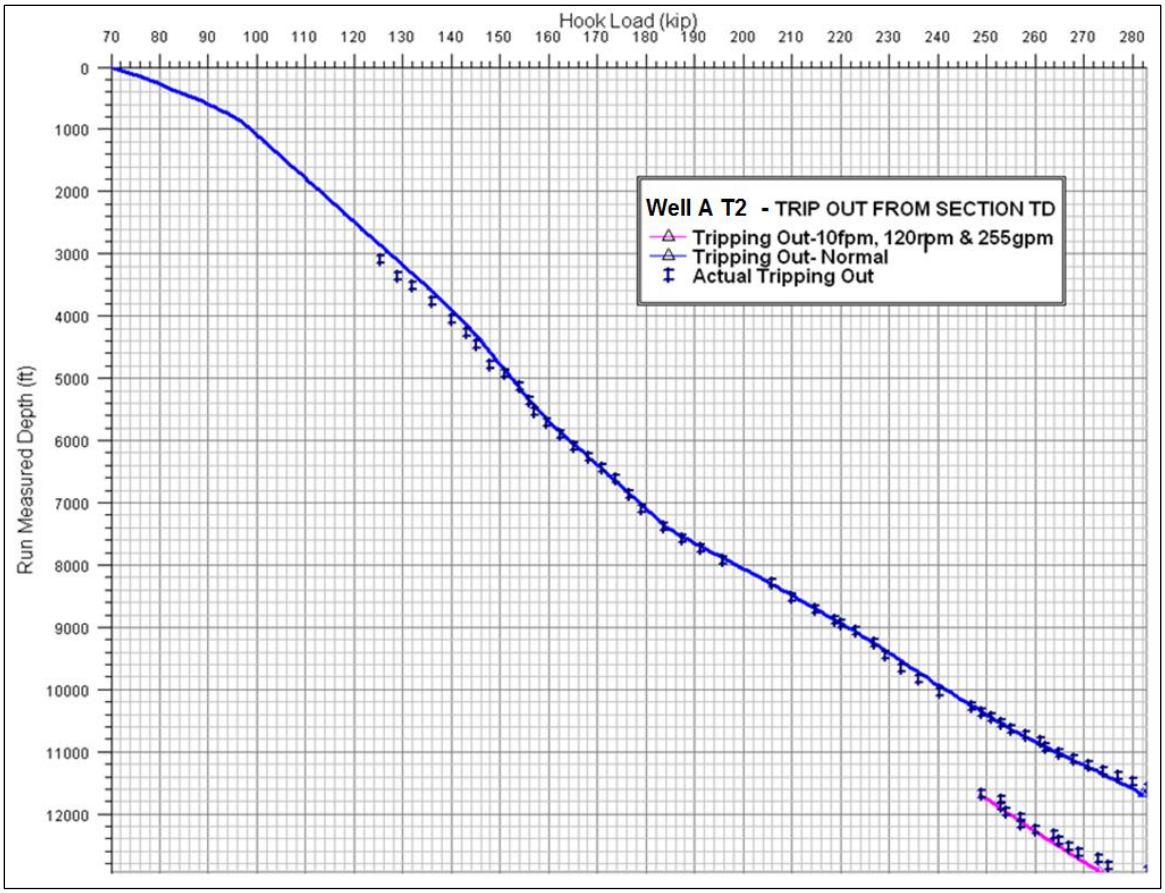

Figure 4.23 – Run 800B: Drag Hook Load Chart with a discrepancy of -7%

The same discrepancy and friction factors found in the drilling run are applied. For this tripping run the simulations match the real-time data perfectly.

Friction Factors – 800B Run	
Trip Out - Casing	Trip Out - Open hole
0.09	0.15

Table 4.10 – Run 800B: Friction factors

4.4.2 Run 840 - Running the 5” Liner With Spiraglider Centralizers

The 5” liner was run with two Weatherford ST HD Spiraglider Centralizers per joint. Spiraglider centralizers are presented in detail in Appendix E. When doing Wellplan simulations against real-time hook load readings, spiraglider centralizers do not need to be inserted as standoff devices in the parameters tab. The reason is that spiragliders are rigid with a fixed OD, and will have the same running force inside casing as in open hole. The centralizers are however still inserted, in order for the well to contain all elements in the Wellplan file. These files are used as historic data and can be consulted in the planning of future wells. The spiraglider gives a friction reduction effect, but a study to quantify this effect has not been done by the service company’s drilling optimization engineers. The relative friction for the centralizer is therefore set to 1.0 for both torque and drag, and the effect of the spiragliders is instead seen as a reduction, or in some cases increase, in the friction factor for the runs they are used.

Standoff Devices

☑ Use Standoff Devices | Select From Catalog | Copy from Centralizer Placement | All Rigid | No Rigid

	Type	Is Rigid	Distance from TD		Relative Friction		Outside Diameter		Frequency		Weight of Unit (lbm)	Length of Unit (ft)
			Start (ft)	End (ft)	Drag	Torque	Actual (in)	Effective (in)	Units	Joints		
1	Centralizer	☑	0,0	1850,0	1,00	1,00	6,250	6,250	2	1,00	10,00	0,83
2		☐										

Figure 4.24 – Standoff devices for the 840 run

The mud used for the run was 13.2 ppg WARP OBM, and the inclination range was 0˚ to 45˚. Figure 4.25 shows the drag hook load chart for the simulations and measurements for the liner running operation.

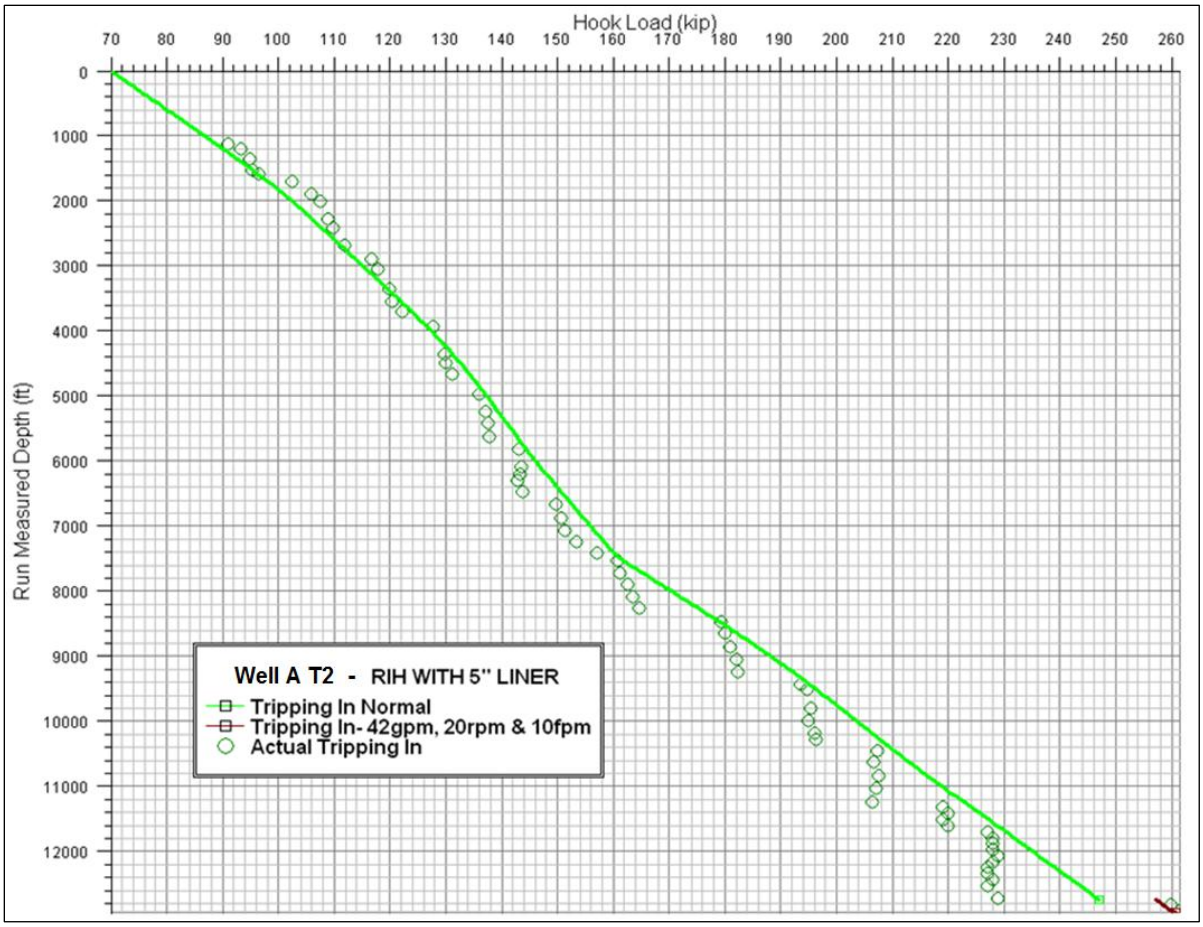

Figure 4.25 – Run 840: Drag Hook Load Chart with discrepancy of -7%

The friction factors for the RIH operation are shown in Table 4.11.

Friction Factors – 840 Run	
Trip In - Casing	Trip In - Open hole
0.06	0.10

Table 4.11 – Run 840: Friction factors

4.5 Historical Hook Load Sensor Discrepancy

The hook load discrepancy for each run is noted in the Friction Factor Table. By taking the discrepancy of every drilling run completed from the Field Case Rig since 2009, a historical bar chart can be made. This is shown in Figure 4.26 The majority of the hook load discrepancies were -8%. Only two of the discrepancies are on the plus side. The discrepancies found in the field case study presented in this thesis are the eight discrepancies from 2013. A clear trend can be seen in the bar chart, and for the next well to be drilled from this rig a hook load discrepancy from -7% to -12% can be expected.

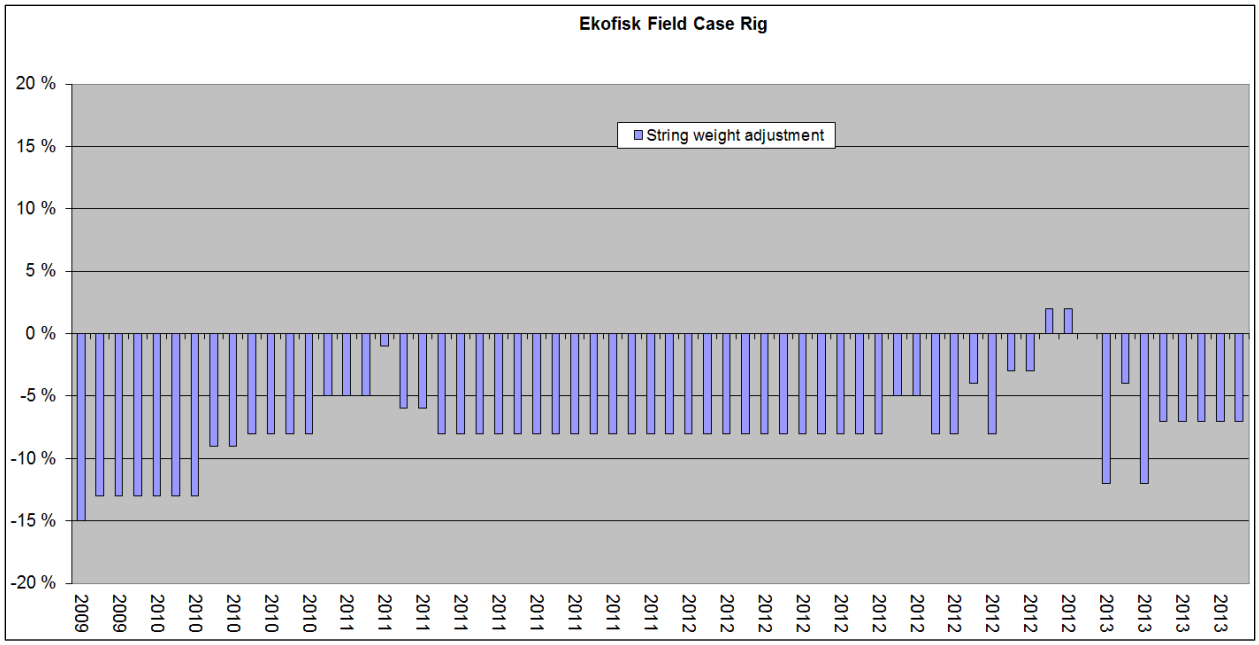

Figure 4.26 – Historic hook load sensor discrepancies for the Field Case Rig

The hook load sensor discrepancy issues of the rigs used by the operator have been a focus area for many years, as there were clear indications that the models used had calibration issues. After the drilling optimization engineers started mapping the discrepancies in 2009, they raised the question of the hook load sensor discrepancies in 2011. The hook load sensor of the rig with the largest discrepancies was taken to shore in 2012 and tested in the shipyard. The tests confirmed that the sensor deviated with increasing load to a maximum of -16% discrepancy. The historic hook load discrepancies of this Example Rig are presented in Figure 4.27. After the test the sensor was recalibrated, indicated with a red line in the figure, and the discrepancies began to deviate on the plus side.

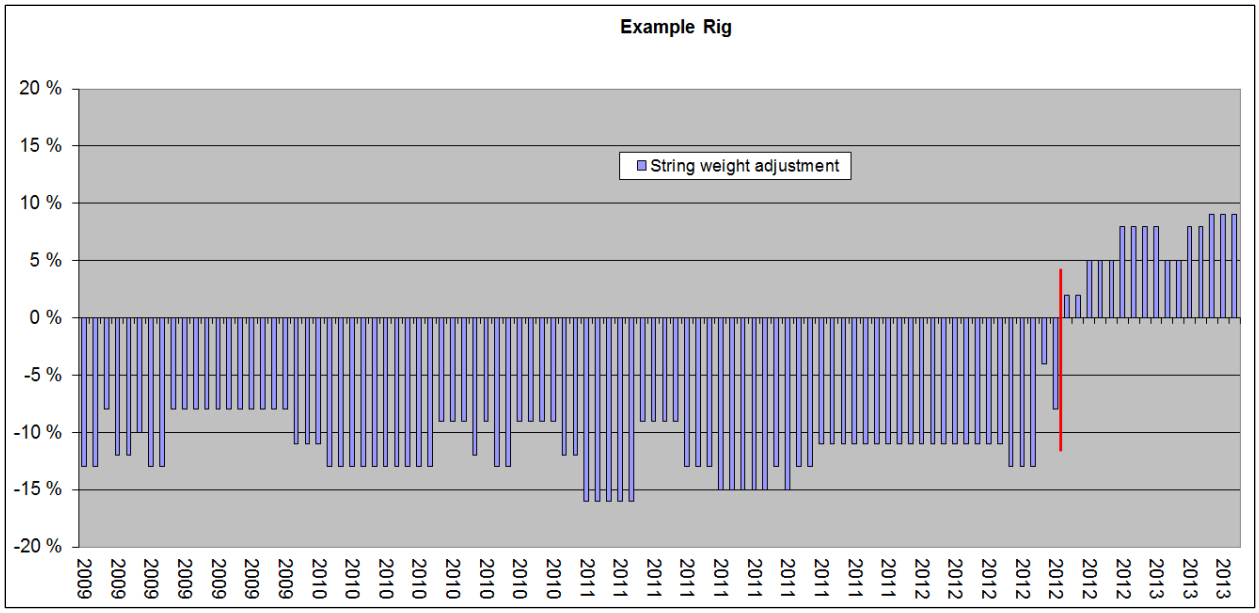

Figure 4.27 – Historic hook load discrepancies for the Example Rig

4.6 Historical Friction Factors

According to Johancsik et al. (1984): "It is believed that friction coefficients will depend largely on mud type and whether a hole is predominantly cased or open. Thus, friction coefficients from a number of similar wells must be compared to verify useful values for prediction use. This requires collection of a significant amount of field data for statistical comparison." [5]

The Friction Factor Table contains information from every run of every well drilled from the Field Case Rig as well as the other of the operator's rigs since 2009. By comparing the friction factors for cased and open hole for pick-up, slack-off and rotate off-bottom from the different wells, it is possible to see if there is correlation from well to well.

5 Discussion

A post-run analysis is like a puzzle, in which every run provides the engineer with various pieces of information. After going thoroughly through all the runs, it is possible to present a detailed overview of the well at hand. However, in order to rely on the results of the analysis there has to be a systematic approach for the discrepancies used and the friction factors found. It is easy to get the simulated lines to match with the real-time data for a single run. It is far more difficult to find discrepancies and friction factors that will give good results for an entire hole section of 2-6 runs.

A post-run analysis is a back and forth process, something that was seen in the field case. An analysis of a run can be completed and all the values and parameters seem to match well, then a following run can have data that does not match up. If this run has a greater number of quality readings, then this run must be chosen as the benchmark and the previous runs analyzed again. In the work of this thesis there were several times where the discrepancies and friction factors found in previous runs had to be changed after obtaining new information.

5.1 Torque and Drag

The torque and drag found in the field case was mainly a result of poor hole cleaning near TD and around the casing shoe at the beginning of open hole sections. In addition there was observed drag in intervals of the Miocene formation. This formation is known to have caused some torque and drag issues for several wells in the field. The torque and drag present for this well was not severe, and did not cause any problems during the operations. The deviations for measured drag compared with simulated drag was typically 5-15 klb more. The things that caused trouble time for this well was the stringers encountered on some of the runs.

The results from several years of post-run analysis have provided many important learning points and new knowledge on torque and drag modeling. Sheave friction was for long a major problem for one of the rigs when modeling. The friction in the sheaves would lead to the simulations not matching the real-time data. Once the sheave efficiency was found by doing post-run analysis of wells drilled from this rig, the modeling went a lot smoother. In some of the last days of the work of this thesis, the first well drilled after the drilling optimization engineers had completed the post-run analysis for that rig. The simulations they had done in planning matched perfectly with

the real-time data. The directional drillers responsible for the well were very impressed with the modeling done. This is a clear indication that a post-run analysis is a valuable tool.

5.2 Buckling and Tensile Limit Window

All operations for this well were above buckling limits and below tensile limits. No buckling or yielding was an issue during the drilling process. The wells drilled with the service company's drilling procedures rarely have these types of issues, mainly because of experience and excellent well planning along with detailed real-time monitoring.

5.3 Data Issues

The real-time hook load readings are often of questionable quality, and in some cases they have not been taken at all during a run. When doing a post-run analysis it is necessary to quality check existing readings or take new readings from a real-time hook load plot to ensure the data quality. As stated previously in the thesis, an analysis of bad data will not be of much use.

A more systematic approach to taking these readings in real-time would save a significant amount of time in the post-run analysis. In the work of thesis the amount of hours spent taking readings from real-time hook load plots was noted. After the last run was analyzed the amount had exceeded 40 hours. It is safe to assume that an experienced engineer will need less time than a student to take the necessary readings. However, if approximately half the time is spent taking these readings, this still this amounts to 2-3 full workdays. If the readings were taken properly in real-time, there would be no need for some of the best drilling optimization engineers in the industry to spend hours taking readings from plots for each post-run analysis. This would free up a lot of time for them to focus on other issues.

5.4 Hookload Discrepancy Issues

Finding the hook load discrepancies is another time consuming part of a post-run analysis. This can be removed by routinely calibrating the hook load sensors on the rigs. Then the actual free rotating hook loads would match the theoretical free rotating hook loads and there would be no need for a discrepancy.

Removing the discrepancy would also remove the confusion when comparing the modeling to other engineering software or companies which have not compensated for hook load discrepancies.

Something that could make the analysis more precise is to subtract or add the discrepancy on every single string component. The common practice is to apply the discrepancy on drillpipes, heavyweight drillpipes and drill collars. These are the longest elements of a string, and the ones that will make the biggest impact when corrected for discrepancy. The difference for additional corrections to the other components is usually minimal, and this was confirmed by doing it on a run in the field case. Applying discrepancy to every component would make a post-run analysis even more time consuming than it already is, and would not add any notable value. For this reason, it is not done by the service company's engineers. But arguably, correcting for discrepancy for each component would be the most correct way to do it.

A problem with the hook load sensor discrepancy is that because the exact discrepancy is not known in the planning phase, it is difficult to compare the planning simulations and the post-run simulations. Because of the discrepancy the differences will be so significant that this comparison is left out of the post-run analysis completely.

5.5 Model Calibration

Three calibration models by IRIS have been reviewed. Automatic real-time calibration of computer models is something that would greatly enhance the drilling process.

5.6 The Friction Factor Table

The Friction Factor Table is a spreadsheet of final friction factors gathered from post-run analysis stored in a historical database for use in planning future wells. It is currently five years in the making and besides friction factors it also contains the following information for every run: Bit and BHA records, vibration data, hook load sensor discrepancies, mud weight, mud system, run depths, drilling-reaming-and-circulating hours, sheave friction correction, inclination range, and additional run information. Filters can be applied for effectively locating the required information.

5.7 Vibration Issues

The field case well had some drilling vibrations, but no severe vibrations that damaged the BHA components were seen. Stick-slip was high in the runs through dense formation with stringers and in the reservoir section. Stick-slip vibrations are common in the reservoir sections drilled on the operator's field.

The Johancsik and Aadnoy 3-D torque and drag models have been presented in this thesis. None of these models include drilling vibrations. Vibrations are very complex to model, and the modeling done rarely matches reality. Accordingly, not much time is spent on vibration modeling during well planning in the industry. There is software that will calculate critical parameters and the critical time intervals for vibrations, but extensive modeling in the planning phase is not done. Instead, a plan is made for RPM, fluid flow and other parameters before drilling starts. Any vibration during drilling is mitigated real-time in accordance with the mitigation guidelines. Standard mitigation guidelines can be found in Appendix B.

6 Conclusion

The following conclusions have been found in this thesis:

- A post-run analysis is a valuable tool for evaluating drilling problems, finding friction factors, evaluating drillstring vibrations and finding hook load sensor discrepancies. The lessons learned are captured and transferred to the planning and drilling of future wells in a continuous drilling optimization loop.
- Real-time data is essential for calibrating the models. If a better system for taking real-time measurements during the operations was implemented, time would not have to be spent on securing data quality in a post-run analysis.
- Proper model calibration is necessary to determine correct friction factors as well as simulating correct loads. Hook load sensor discrepancies could be minimized by introducing a common hook load sensor calibration procedure on the rigs. Models could also be corrected in real-time by automatic model calibration methods as developed by IRIS.
- Because of hook load sensor discrepancies, there will be little value in comparing the simulated well planning to actual results. The differences are too large.
- The Friction Factor Table made by the service company's drilling optimization engineers is highly qualified for prediction and planning use.

References

1. Halliburton. 2012. Torque Drag Analysis (Using the Torque Drag Analysis Module). In WELLPLAN™ Software Release 5000.1.10 Training Manual. © 2013 Halliburton. All Rights Reserved.
2. Lohne, H.P., Gravdal, J.E., Dvergsnes, E.W., Nygaard, G., and Vefring, E.H. 2008. Automatic Calibration of Real-Time Computer Models in Intelligent Drilling Control Systems - Results From a North Sea Field Trial. IPTC 12707, Proc., International Petroleum Technology Conference, Kuala Lumpur, Malaysia 3-5 December.
3. Gravdal, J.E., Lorentzen, R.J., Fjelde, K.K., and Vefring, E.H. 2010. Tuning of Computer Model Parameters in Managed-Pressure Drilling Applications Using an Unscented-Kalman-Filter Technique. September SPE Journal: 856-866. SPE- 97028-PA.
4. Cayeux, E., Daireaux, B., Dvergsnes, E.W., Sælevik, G., and Zidan, M. 2012. An Early Warning System for Identifying Drilling Problems: An Example From a Problematic Drill-Out Cement Operation in the North-Sea. Paper IADC/SPE 150942 presented at the IADC/SPE Drilling Conference and Exhibition, San Diego, California, 6-8 March, 2012.
5. Johancsik, C.A., Friesen, D.B. and Dawson, R. 1984. Torque and Drag in Directional Wells – Prediction and Measurement. Journal of Petroleum Technology **36** (6): 987-992. SPE-11380-PA.
6. Aadnoy, B.S., Fazaelizadeh, M. and Hareland, G. 2010. A 3D Analytical Model for Wellbore Friction. Journal of Canadian Petroleum Technology **49** (10): 25-36. SPE-141515-PA.
7. Halliburton. Products and Services – Baroid – Technical Challenges – Drilling Fluids Challenges – Torque and Drag. http://www.halliburton.com/ps/default.aspx?pageid=5676&navid=2979 (accessed 14 January 2013)
8. Mirhaj, S.A., Fazaelizadeh, M., Kaarstad, E. and Aadnoy, B.S. 2010. New Aspects of Torque-and-Drag Modeling in Extended-Reach Wells. Paper SPE 135719 presented at the SPE Annual Technical Conference and Exhibition, Florence, Italy, 19-22 September.
9. Mirhaj, S.A., Kaarstad, E. and Aadnoy, B.S. 2010. Minimizing Friction in Shallow Horizontal Wells. Paper IADC/SPE 135812 presented at the IADC/SPE Asia Pacific

Drilling Technology Conference and Exhibition, Ho Chi Minh City, Vietnam, 1-3 November.

10. Mitchell, R.F. and Samuel, R. 2009. How Good Is the Torque/Drag Model? SPE Drilling & Completion **24** (1): 62-71. SPE-105068-PA.
11. Mason, C.J. and Chen, D.C.K. 2007. Step Changes Needed To Modernize T&D Software. Paper SPE/IADC 104609 presented at the SPE/IADC Drilling Conference, Amsterdam, The Netherlands, 20-22 February.
12. Bellarby, J. 2009. Well Completion Design, volume 56. Amsterdam, The Netherlands: Elsevier.
13. Aadnoy, B.S. 2006. Mechanics of Drilling. Aachen, Germany: Shaker Verlag.
14. Samuel, R. 2010. Friction Factors: What are They for Torque, Drag, Vibration, Bottom Hole Assembly and Transient Surge/Swab Analyses? Paper IADC/SPE 128059 presented at the IADC/SPE Drilling Conference and Exhibition, New Orleans, Louisiana, USA, 2-4 February.
15. Maidla, E.E., and Wojtanowicz, A.K. 1987. Field Comparison of 2-D and 3-D Methods for the Borehole Friction Evaluation in Directional Wells. Paper SPE 16663 presented at the 62nd Annual Technical Conference and Exhibition of SPE, Dallas, Texas, 27-30 September.
16. Belayneh, M. 2006. A Review of Buckling in Oil Wells. Aachen, Germany: Shaker Verlag.
17. He, X., Halsey, G.W., and Kyllingstad, Å. 1995. Interaction between Torque and Helical Buckling in Drilling. Paper SPE 30521 presented at the SPE Annual Technical Conference & Exhibition, Dallas, U.S.A, 22-25 October.
18. Kyllingstad, A. 1995. Buckling of tubular strings in curved wells. Journal of Petroleum Science and Engineering **12**: 209-218.
19. Dawson, R. and Paslay, P.R. 1984. Drill Pipe Buckling in Inclined Holes. SPE Journal of Petroleum Technology **36** (10): 1734-1738. SPE-11167-PA.
20. Samuel, R. and Kumar, A. 2012. Effective Force and True Force: What are They? Paper IADC/SPE 151407 presented at the IADC/SPE Drilling Conference and Exhibition, San Diego, USA, 6-8 March.

21. Luke, G.R. and Jukvam-Wold, H.C. 1993. Determination of True Hook Load Line Tension Under Dynamic Conditions. SPE Drilling & Completion **8** (4): 259-264. SPE-23859-PA.
22. Schlumberger Oilfield Glossary – search "drawworks" http://www.glossary.oilfield.slb.com/en/Terms.aspx?LookIn=term%20name&filter=drawworks (accessed 20 March 2013)
23. Drilling Today 2013. Rotary Drilling. http://dthrotarydrilling.com/News/3-Feb-2010/ROTARY_DRILLING.html (accessed 20 March 2013)
24. Adnoy, B.S., Cooper, I., Miska, S.Z., Mitchell, R.F., and Payne, M.L. 2009. Advanced Drilling and Well Technology, 544 – 554. Richardson, Texas: SPE.
25. Adnoy, B.S., Cooper, I., Miska, S.Z., Mitchell, R.F., and Payne, M.L. 2009. Advanced Drilling and Well Technology, 117 – 128. Richardson, Texas: SPE.
26. Halliburton. 2012. Vibration Sensors and Vibration Mitigation Guidelines. http://www.halliburton.com/premium/ss/contents/Brochures/web/H05514_ADT_Brochure.pdf (downloaded 15 January 2013)
27. Santos, H., Plàcido, J.C.R., and Wolter, C. 1999. Consequences and Relevance of Drillstring Vibration on Wellbore Stability. Paper SPE/IADC 52820 presented at the SPE/IADC Drilling Conference, Amsterdam, Holland, 9-11 March.
28. Mathis, W. and Thonhauser, G. 2007. Mastering Real-Time Data Quality Control – How To Measure and Manage the Quality of (Rig) Sensor Data. Paper SPE/IADC 107567 presented at the SPE/IADC Middle East Drilling Technology Conference & Exhibition, Cairo, Egypt, 22-24 October.
29. Nybø, R., Frøyen, J., Lauvsnes, A.D., Korsvold, T. and Choate, M. 2012. The Overlooked Drilling Hazard: Decision Making From Bad Data. Paper SPE 150306 presented at the SPE Intelligent Energy International, Utrecht, The Netherlands, 27-29 March.
30. Schumberger oilfield glossary, search slip-and-cut. http://www.glossary.oilfield.slb.com/en/Terms.aspx?LookIn=term%20name&filter=cut+slip (accessed 25 May 2013)

31. Chen, D.C-K. 2004. New Drilling Optimization Technologies Make Drilling More Efficient. Proc., Canadian International Petroleum Conference, Calgary, Canada, 8-10 June.
32. Herbert, M., Solbakk, T. and Rørvik, H. 2010. Moving to the Next Level of Integrated Operations in Drilling. Paper SPE 128755 presented at the SPE Intelligent Energy Conference and Exhibition, Utrecht, The Netherlands, 23-25 March.
33. Akinniranye, G., Weber, A., Elsweisy, H., Palacio, J., Poedjono, and Goobie, R. 2007. Implementation of a Shock and Vibration Mitigation Process: Achieving Real-Time Solutions and Savings. Paper SPE/IADC 107903 presented at the SPE/IADC Middle East Drilling Technology Conference & Exhibition, Cairo, Egypt, 22-24 October.
34. Liu, G. and Weber, L. 2012. Centralizer Selection and Placement Optimization. Paper SPE 150345 presented at the SPE Deepwater Drilling and Completions Conference, Galveston, Texas, 20-21 June.
35. Weatherford. 2010. Cementing Products Brochure: Bow-Spring Centralizer Sub, http://www.weatherford.com/weatherford/groups/web/documents/weatherfordcorp/WFT000459.pdf (downloaded 23 April 2013)
36. Weatherford. 2009. Mechanical Cementing Products, http://www.weatherford.com/weatherford/groups/web/documents/weatherfordcorp/WFT017530.pdf (downloaded 5 May 2013)
37. Weatherford. 2013. Cementing Products: SpiraGlider Centralizer System, http://www.weatherford.com/dn/WFT085643 (downloaded 5 May 2013)

Appendixes

Appendix A: Aadnoy's Simple Geometry Torque and Drag Models

A.1 Inclination Dependent Torque and Drag

A.1.1 Inclined Straight Sections

Figure A.1 shows the free body diagram of a mass element on an inclined plane and an inclined drillstring. The force required to pull a drillstring along an inclined plane is [13]:

$$F = mg\cos\alpha + \mu mg\sin\alpha \tag{a.1}$$

For lowering of a drillstring, the friction will act opposite in the direction of motion, giving a top force of [8]:

$$F = mg\cos\alpha - \mu mg\sin\alpha \tag{a.2}$$

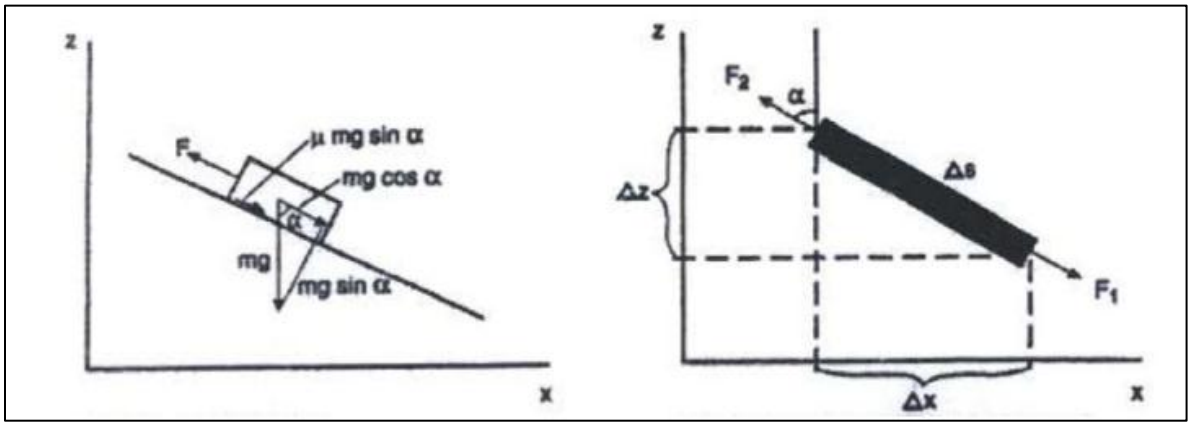

Figure A.1 – Forces on an inclined object (left) and Geometry and forces for a straight inclined hole (right) [13]

This is a Coulomb friction model. When the drillstring is stationary, an increase or decrease in the load will lead to upward or downward movement of the drillstring. A drillstring with weight $mg = w\Delta s$ and inclination α, will have axial weight and drag force in a straight inclined section as follows (Fig. A.1) [13]:

$$F = F_1 + w\Delta s(\cos\alpha \pm \mu\sin\alpha) \tag{a.3}$$

The plus sign defines pulling out of hole, and the minus sign defines running into hole. The first term inside the bracket defines the weight of the pipe and the second term defines the additional friction force required to move the pipe. The change in force when the motion starts either upward or downward is found by subtracting the weight from the forces defined above. Where the weight is [13]:

$w\Delta s \cos \alpha$

The rotating friction, the torque, follows the same principle. The applied torque is equal to the normal moment ($w\Delta sr$) multiplied by the friction factor μ. Giving torque as:

$$T = \mu w \Delta sr \sin \alpha \tag{a.4}$$

It is important that the unit mass of the drillpipe or the weight is corrected for buoyancy. The buoyancy factor is given as:

$$\beta = 1 - \frac{\rho_{mud}}{\rho_{pipe}} \tag{a.5}$$

And the buoyed unit mass must be:

$$w = \beta w_{drill\ pipe} \tag{a.6}$$

A.1.2 Curved Sections

A.1.2.1 Drop Off Bends

In the following, equations to calculate the drag forces when a drillstring is run or pulled through a bend will be derived. Figure A.2 shows the forces acting when a pipe is pulled through a drop-off section. A few parameters need to be defined before doing the actual analysis. A normal force N results between the drillstring and the hole because of the bend. A frictional force Q resists the motion of pulling the string. The weight of the drillstring will be the unit weight w multiplied with the length of the differential element, $wRd\alpha$. Using an x, z reference system, the weight can be decomposed into the following components:

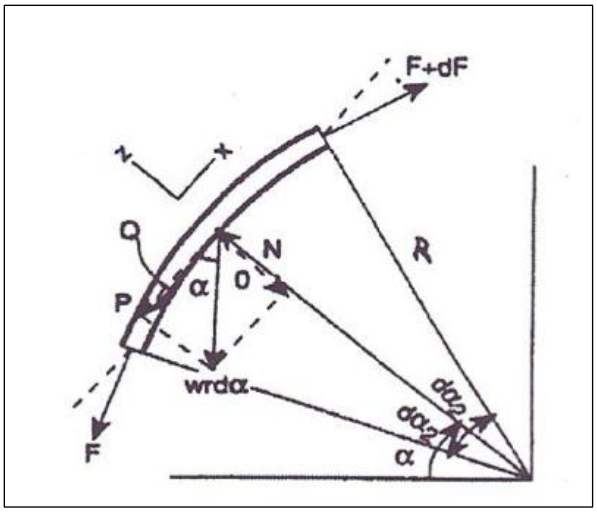

Figure A.2 – Drag forces in a drop-off bend [13]

Pulling out of the hole:

Performing force balance in the x and z direction, the equation for the tension in the drillstring becomes [13]:

$$dF = \{\mu F + wR(\mu \sin\alpha + \cos\alpha)\}d\alpha \qquad \text{(a.7)}$$

Integrating Eq. a.7, the final solution for the additional force through the bend is given by:

$$F_2 = F_1 e^{\mu(\alpha 2 - \alpha 1)} + \frac{wR}{1+\mu^2}\begin{Bmatrix}(1-\mu^2)(\sin\alpha_2 - e^{\mu(\alpha_2-\alpha_1)}\sin\alpha_1) \\ (-2\mu)(\cos\alpha_2 - e^{\mu(\alpha_2-\alpha_1)}\cos\alpha_1)\end{Bmatrix} \qquad \text{(a.8)}$$

Here F_1 is the tension at the bottom and F_2 is the tension at the top of the bend.

The equation above is valid for pulling the drillstring upwards.

Running into the hole:

When the drillstring is run into the hole, the forces $F\ and\ F + dF$ interchange places in figure A.2, and the friction force Q changes direction. Resulting in the differential equation [13]:

$$dF = \{\mu F + wR\{\mu \sin\alpha - \cos\alpha\}\, da\} \qquad \text{(a.9)}$$

This gives the solution:

$$F_2 = \{F_1 e^{\mu(\alpha_2 - \alpha_1)} + wR\{\sin\alpha^2 - e^{\mu(\alpha_2 - \alpha_1)} \sin\alpha_1\} \quad \text{(a.10)}$$

Note that the forces have been redefined for this case. F_2 is always referring to the force in the top of the string.

The frictional torque is equal to the normal force multiplied with the pipe radius, integrated over the length of the bend, $ds = rd\alpha$. The tension in the pipe for a static position is:

$$F = F_1 - wR(\sin\alpha - \sin\alpha_1) \quad \text{(a.11)}$$

The general expression for the torque becomes:

$$T = \int \mu r N \quad \text{(a.12)}$$

And integrating the equation above, the resulting torque for drop off bends becomes:

$$T = \mu r\{F_1 + wR\sin\alpha_1\}(a_2 - a_1) - 2\mu r wR(\cos\alpha_2 - \cos\alpha_1) \quad \text{(a.13)}$$

A.1.2.2 Buildup Bends

Figure A.3 shows the forces in a build-up section. The basic definitions remain the same as for the previous case.

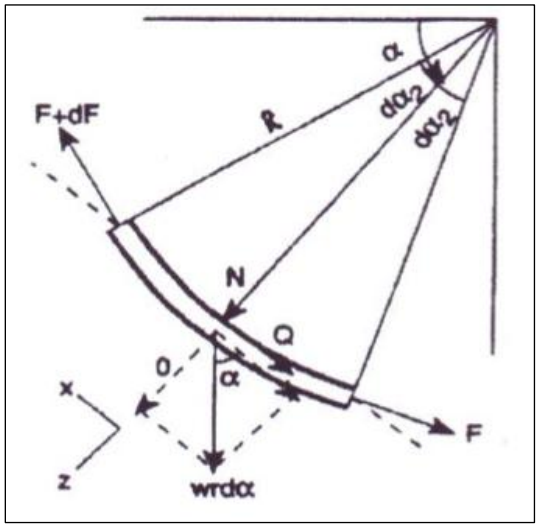

Figure A.3 – Drag forces in a build-up bend [13]

Repeating the previous analysis, it can be shown that the pull force is now defined by:

$$dF = \{\mu F - wR(\mu \sin\alpha + \cos\alpha)\}d\alpha \qquad \text{(a.14)}$$

$$F_2 = F_1 e^{-\mu(a_1 - a_2)} - wR\{\sin\alpha_2 - e^{-\mu(a_2 - a_1)} \sin\alpha_1\} \qquad \text{(a.15)}$$

Finally, for the case of lowering the pipe through the buildup bends gives: $dF = Q - P$

$$dF = \{\mu F - wR(\mu \sin\alpha + \cos\mu)\}\, d\alpha \qquad \text{(a.16)}$$

Which solved again with F_2 defining the top force becomes:

$$F_2 = F_1 e^{-\mu(a_1 - a_2)} - \frac{wR}{1+\mu^2}\begin{cases}(1-\mu^2)(\sin\alpha_2 - e^{\mu(a_1 - a_2)} \sin\alpha_1) \\ -2\mu(cos\alpha_2 - e^{\mu(a_1 - a_2)} \cos\alpha_1)\end{cases} \qquad \text{(a.17)}$$

Repeating the process for buildup bends, the torque becomes:

$$T = \mu r\{(F_1 + wR\sin\alpha_1)|a_2 - a_1|\} + 2\mu wRr(\cos\alpha_2 - \cos\alpha_1) \qquad \text{(a.18)}$$

Appendix B: Reviewed Vibration

B.1 Vibration Mechanisms

The following mechanisms are written based on information presented in Halliburton ADT Vibration Brochure [26]:

B.1.1 Stick-Slip – Torsional Vibrations

Frictional torque on bit and BHA causes the drillstring to periodically twist up and then spin free. Variations in downhole RPM can be as large as 3 to 15 times the average surface RPM. Stick-slip is the main cause of torsional vibrations, and usually occurs:

- In hard formations or salt
- In deep wells
- In wells with large inclination angle
- When using aggressive PDC bits combined with high WOB

Consequences of stick-slip are:

- Fluctuations in the surface torque readings greater than 15 % of average
- PDC bit damage
- Reduction in ROP
- Connection over-torque
- Back-off and drillstring twist-offs
- Mud pulse telemetry interferences
- Stabilizer- and bit gauge fatigue

B.1.2 Bit Bounce – Axial Vibrations

Large variations in WOB cause the bit to repeatedly lift off-bottom and then drop, impacting the formation. Bit bounce is connected to the axial stiffness of the drillstring and the mass of the BHA. It usually occurs when drilling hard formations with tricone bit. Consequences of bit bounce are:

- Damage to bit and BHA, which could lead to failure of downhole tools
- Low ROP
- Triggers lateral BHA vibrations when severe
- Damage to drillstring from axial and lateral shocks induced by string flexing

- Damage to hoisting equipment in shallow wells
- Fluctuations in hook load weight

B.1.3 Bit Whirl – Lateral Vibrations

Occurs when the bit has cut a hole larger than its own diameter, causing the bit to *walk* around the hole producing unusual bottomhole patterns. The bit is not rotating around its natural geometric center. PDC bit-wellbore gearing resulting from excessive side-cutting forces causes this. When the BHA is whirling, it continuously impacts the wellbore. Consequences of bit whirl are:

- Damage to bit cutting structure
- Damage to stabilizer and tool joint
- Creation of ledges in the borehole
- The overgauged hole can cause BHA whirl

B.1.4 BHA Whirl – Lateral Vibrations

This is a vibration mechanism similar to bit whirl. In BHA whirl the BHA has an eccentric rotation about a point that is not its geometric center. This leads to the BHA rolling around the wellbore as it rotates. Consequences of BHA whirl are:

- High shock and vibrations in the BHA
- Main cause of BHA and downhole tool failure
- Repeated flexing of drill collars causes increased fatigue rates of these components
- High bending stresses damages drill collar connections
- Lateral shocks will cause downhole electronic failure

B.1.5 Torsional Resonance

This is “drill collar torsional resonance” to be more specific. This mechanism is a natural torsional frequency of the drill collar which is being excited. This specific type of vibration usually occurs when drilling with PDC bits in very hard formations. Consequences of torsional resonance are:

- Most damaging at higher rotational speeds: Higher amplitude resonance at harmonics of the drill collar’s natural frequency are possible
- Can lead to a backwards turning of the bit and cutter damage

- Damage to downhole electronics

B.1.6 Parametric Resonance

Bit/formation interaction causes axial excitations that induce severe lateral vibrations. Axial fluctuations at a specific frequency causes lateral deflections of the drillstring through small lateral displacements already present. The small bends which exist in the wellbore will be magnified due to the wave traveling through them. Parametric resonance is typically encountered in interbedded formations or undergauge holes, and consequences are:

- Accelerated drillstring failure
- Creates the opportunity for borehole enlargement which can lead to poor directional control
- Can lead to whirl and other mechanisms of vibration

B.1.7 Bit Chatter

When the individual teeth on the PDC bit lose their shearing cutting action, each blade or each individual cutter is impacted on the formation. This creates a high frequency resonance of the bit and BHA. Bit chatter usually occurs when drilling with PDC bits in high compressive strength rocks, and consequences are:

- Bit cutter impact damage
- High frequency vibrations cause failure of electronic equipment due to vibration of electronic components and solder joint
- A bit dysfunction can lead to bit whirl

B.1.8 Modal Coupling

Vibration occurring in axial, torsional and lateral direction simultaneously creates axial and torsional oscillations and large shocks along the BHA. This is the most severe of the vibration mechanisms, and is usually a result from failing to control one of the previously mentioned mechanisms. This allows it to become severe enough to initiate one or more of the other mechanisms simultaneously. Modal coupling usually occurs in environments where stick-slip, whirl or bit bounce is likely, and consequences are:

- MWD component failures (motor, M/LWD tool etc.)
- Localized tool joint and/or stabilizer wear

- Washout or twist-offs from connection fatigue cracks
- Increased average torque

B.2 Vibration Mitigation

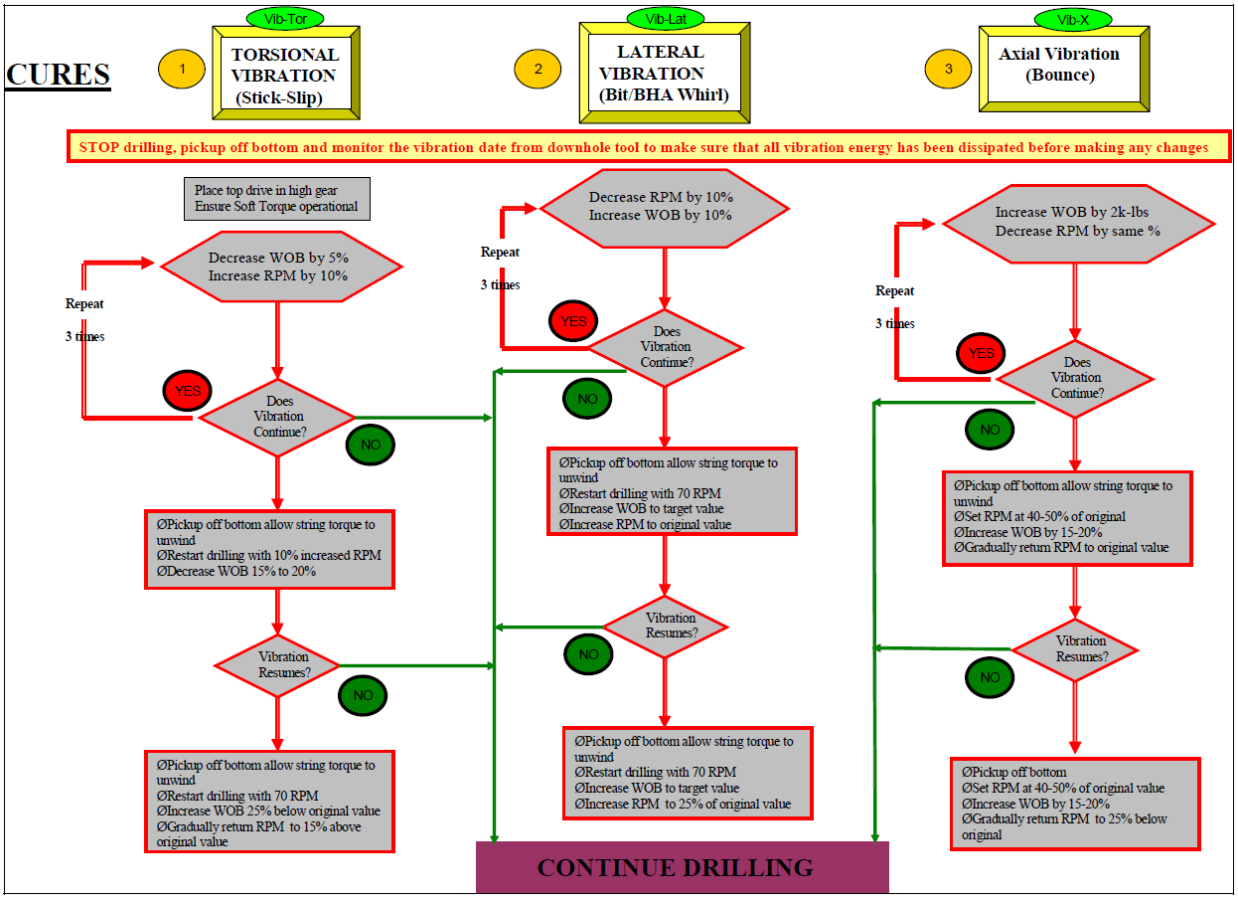

Figure B.1 – Standard drillstring vibration mitigating actions [33]

Appendix C: Connection Procedure

The operator uses this standard procedure for all connections.

The pumps are ON for all these measurements

- Driller drills off weight at stand down
- Back-reaming is to be at the discretion of the DD (directional considerations)
- Back-ream pulling up at a consistent speed, and according to DD-approved back-reaming RPM and DD-approved interval
- At the top of DD's back-ream interval, stop and rotate freely at 120 RPM for 30 seconds
- Record the free rotating weight and free rotating torque
- Then, continue by reaming down at back-reaming RPM
- Pull up at a consistent speed to DD-approved interval without rotary
- Record pickup weight
- Work back down at consistent speed
- Record slackoff weight
- Lower pipe into slips and turn pumps off
- Perform connection
- After connection, turn rotary on before bringing up pumps (To minimize the ECD effect by breaking gels through rotary before pumping)
- If back-reaming is required, keep rotary steerable in undeflected position, it's always rotary first

Appendix D: Post-Run Analysis

All charts and drillstring information are adjusted for the discrepancy percentage found in the analysis. This has been subtracted from drillpipes, heavyweight drillpipes and drill collars of notable length.

D.1 The 12 ¼" x 12 ¾" Tophole Section

Run 100

Hole Section Editor

Hole Name: 12 3/4" Hole Section — Import Hole Section

Hole Section Depth (MD): 5310,0 ft — Additional Columns

	Section Type	Measured Depth (ft)	Length (ft)	Tapered?	Shoe Measured Depth (ft)	ID (in)	Drift (in)	Effective Hole Diameter (in)	Friction Factor	Linear Capacity (bbl/ft)	Excess (%)	Item Description	Manufacturer	Model
1	Riser	62,0	62,00			13,625				0,1803		Riser		
2	Casing	2500,0	2438,00		2500,0	12,347	12,259	12,415		0,1481		13 3/8 in, 68 ppf, K-55,		
3	Open Hole	5310,0	2810,00			12,750		12,750		0,1579	0,00			
4														

String Editor

String Initialization — String Name: Well A _0100_Drillstring - 12% — String (MD): 5310,0 ft — Specify: Top to Bottom — Import String

Library — Export — Import

	Section Type	Length (ft)	Measured Depth (ft)	OD (in)	ID (in)	Weight (ppf)	Item Description
1	Drill Pipe	4500,25	4500,2	5,500	4,778	25,80	Drill Pipe, 5,500 in, 25,80 ppf, S-135, FHDSTJ
2	Heavy Weight	365,21	4865,5	5,500	3,500	49,33	Heavy Weight Drill Pipe, 5,50Heavy Weight Drill Pipe 24000, 5.5 in, 56.06 pp
3	Drill Collar	3,61	4869,1	8,000	3,750	150,17	X-Over Sub
4	Drill Collar	61,14	4930,2	8,250	2,812	141,06	Drill Collar 8.25 in, 8.25 x 2.8125 in, 6 5/8 REG
5	Jar	33,28	4963,5	8,250	3,000	147,22	8 Megaton Energizer
6	Drill Collar	91,33	5054,8	8,250	2,812	132,00	8 1/4 X 2.8125 - 150# Drill Collar
7	Jar	29,62	5084,4	8,250	3,000	147,22	8 Megaton Jar
8	Drill Collar	60,88	5145,3	8,250	2,812	141,06	Drill Collar 8.25 in, 8.25 x 2.8125 in, 6 5/8 REG
9	Stabilizer	6,00	5151,3	8,000	2,813	156,00	Integral Blade Stabiliser
10	Drill Collar	30,27	5181,6	8,250	2,812	132,00	8 1/4 X 2.8125 - 150# Drill Collar
11	Drill Collar	3,03	5184,6	8,250	3,000	156,00	Float Sub (Non ported flapper)
12	Underreamer	13,39	5198,0	10,000	2,800	246,68	Underreamer, 10,000 in, 246,68 ppf, V-150, 3 1/2 Reg. Pin
13	Drill Collar	7,59	5205,6	8,000	2,375	132,00	Drill Collar, 8,000 in, 132,00 ppf, S,
14	MWD	10,17	5215,8	8,150	4,000	145,20	8 P4M HOC
15	MWD	7,84	5223,6	8,000	2,375	133,30	8 HCIM HF
16	MWD	4,37	5228,0	8,000	2,375	133,80	8 PWD HF
17	MWD	5,08	5233,1	8,000	2,375	136,50	8 DGR HF
18	Stabilizer	3,87	5236,9	8,000	2,375	382,51	Inline Stabilizer (ILS)
19	MWD	12,18	5249,1	8,000	2,375	143,90	8 EWR-P4 HF
20	MWD	1,85	5251,0	8,000	3,250	151,60	8 P-P XOVER (H/C)
21	Drill Collar	25,58	5276,5	8,000	3,500	129,70	Evader Gyro MWD
22	Drill Collar	9,20	5285,7	6,750	3,500	105,60	Geo-Pilot 9600 Flex Collar
23	Stabilizer	3,17	5288,9	9,625	2,375	156,45	Geo-Pilot 9600_0
24	Stabilizer	4,89	5293,8	9,625	2,375	156,45	Geo-Pilot 9600_1
25	Drill Collar	13,65	5307,4	9,625	2,375	137,68	Drill Collar, 9,625 in, 137,68 ppf, S,
26	Bit	2,56	5310,0	12,250		235,00	Tricone

Figure D.1 Run 100: Hole section and drillstring information w/-12% discrepancy

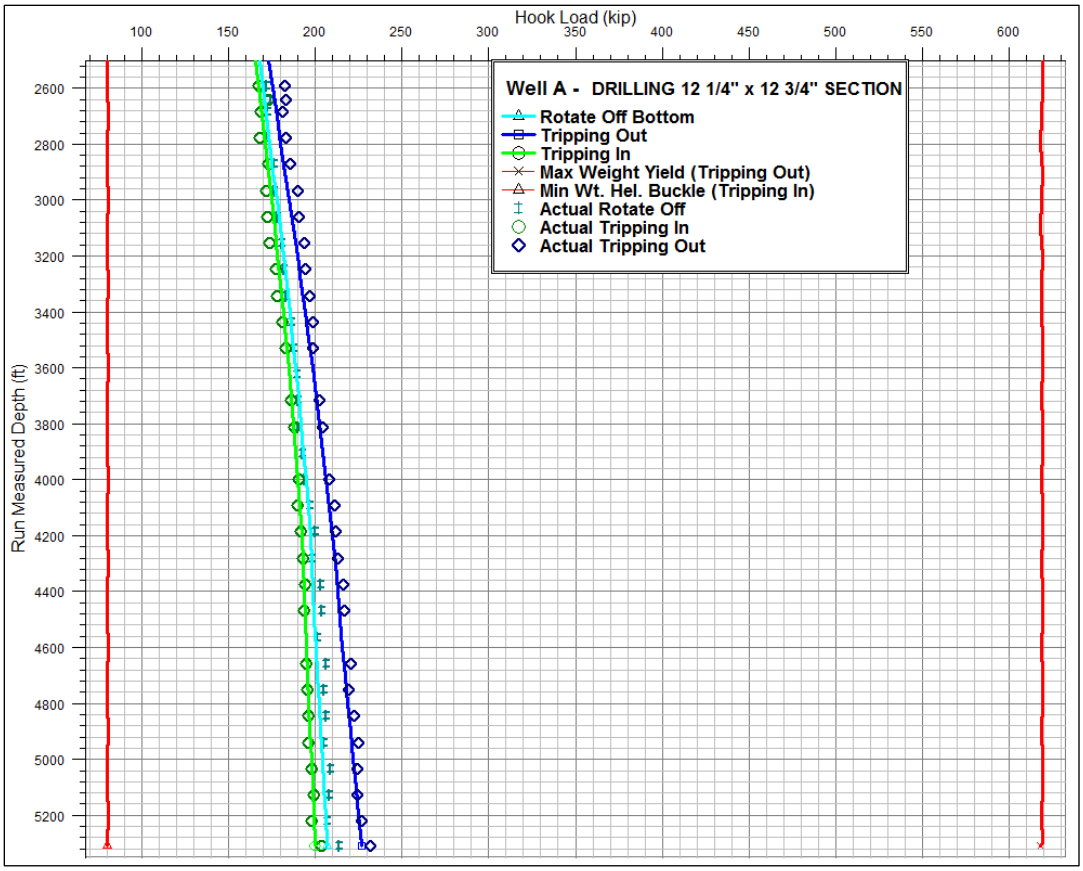

Figure D.2 – Run 100: Drag Hook Load Chart with buckling and yield limits w/-12% discrepancy

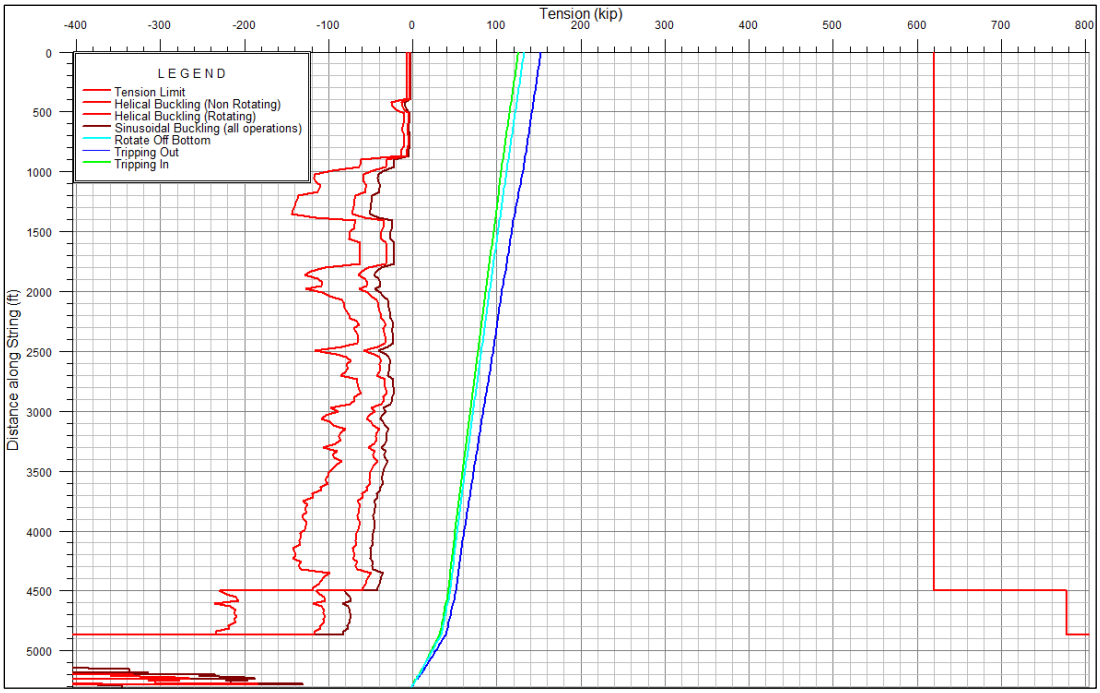

Figure D.3 – Run 100: Effective Tension Graph w/-12% discrepancy

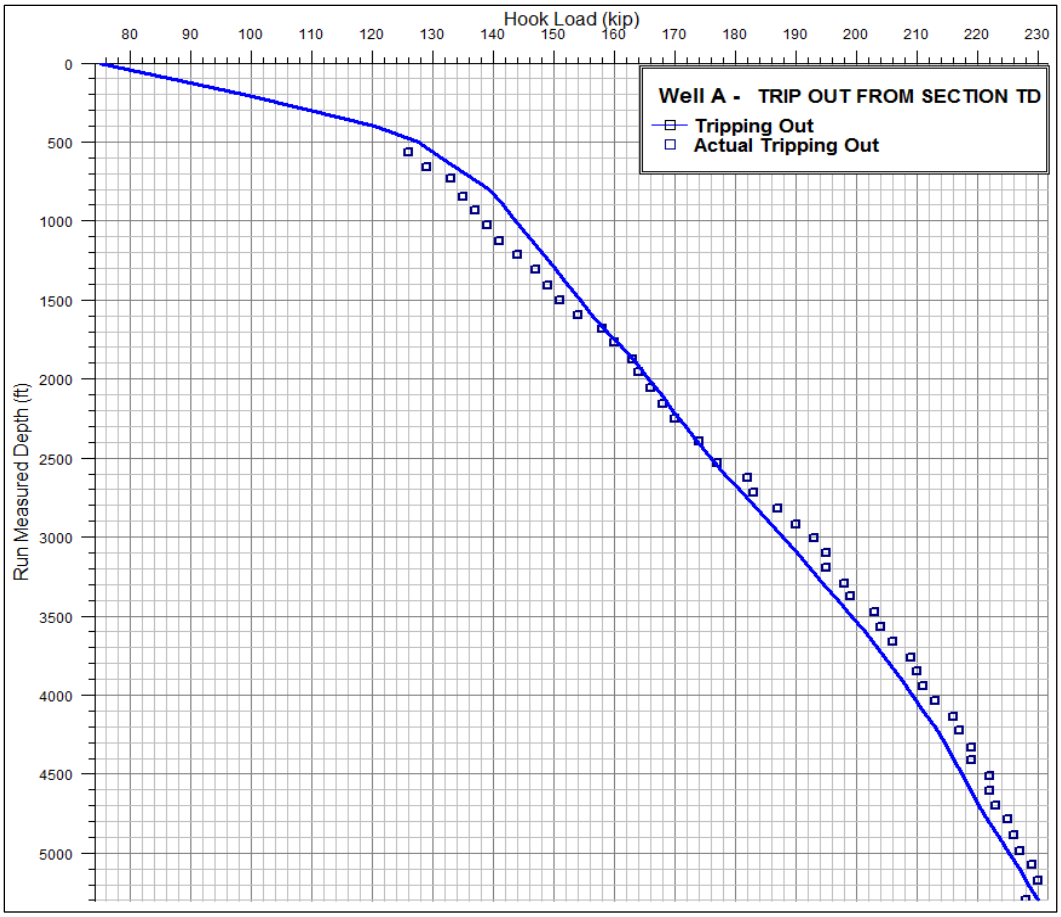

Figure D.4 – Run 100B: POOH from section TD

Run 200

-4% discrepancy is subtracted from drill collars of notable length.

String Editor

String Initialization

String Name: Well A _0200_Drillstring_InSite -4%

String (MD): 5728,0 ft Specify: Top to Bottom Import String

Library: Export, Import

	Section Type	Length (ft)	Measured Depth (ft)	OD (in)	ID (in)	Weight (ppf)	Item Description
1	Drill Collar	5607,05	5607,0	10,750	9,824	50,88	Drill Collar, 10,750 in, 50,88 ppf, S,
2	Drill Collar	20,15	5627,2	10,250	6,500	168,13	Pupjoint
3	Sub	3,00	5630,2	10,250	2,810	260,00	Float Sub, 10,250 in, 260,00 ppf, 4145H MOD, 4 1/2 REG
4	Drill Collar	15,09	5645,3	10,250	6,500	168,13	Pup joint
5	Drill Collar	77,60	5722,9	10,750	9,824	38,90	10 3/4 X 10.05 - 38.9# Casing
6	Drill Collar	4,17	5727,1	10,000	3,500	234,87	Wearsox
7	Bit	0,94	5728,0	12,250		235,00	EZcase bit

Figure D. 5 – Run 200: Drillstring information w/-4% discrepancy

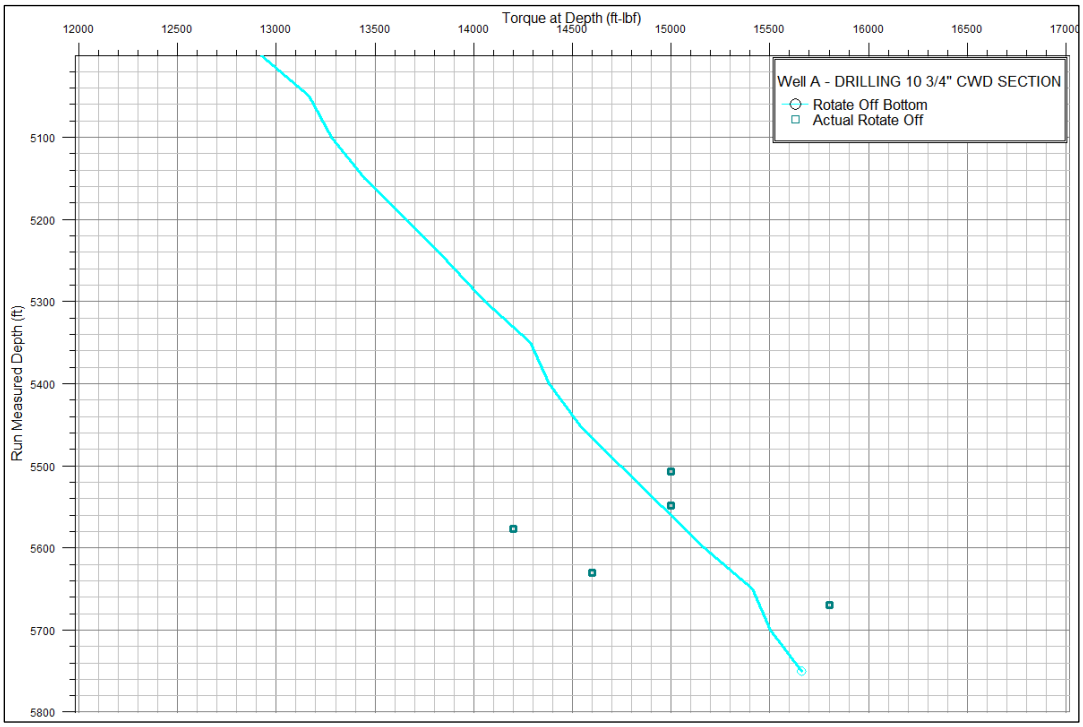

Figure D.6 – Run 200: Torque Chart w/-4% discrepancy

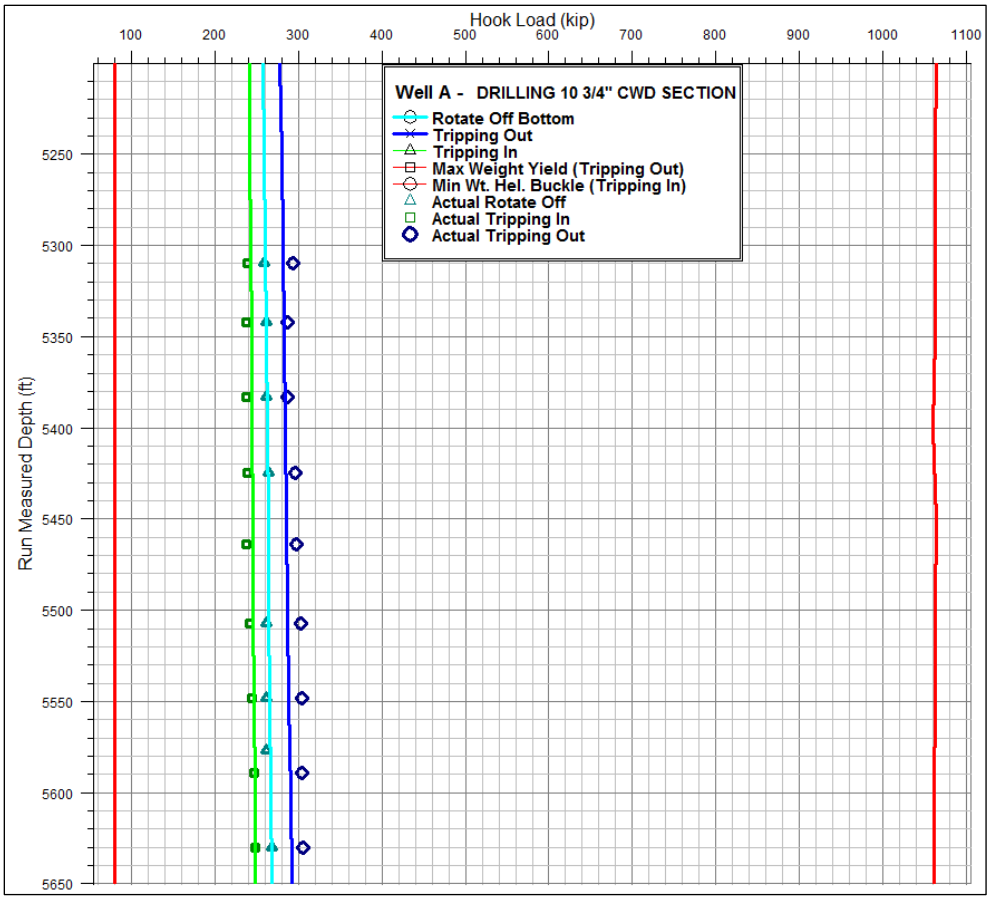

Figure D.7 – Run 200: Drag Hook Load Chart with buckling and yield limits w/-4% discrepancy

Figure D.8 – Run 200: Effective Tension Graph w/-12% discrepancy

D.2 The 9 ½" x 10 ¼" Overburden Section

The drillstring has the same components for runs 300, 400, 500 and 700, except for the bit type and of course the drillpipe length. For run 300 a Baker Hughes PDC bit is used and for run 700 a Halliburton Long Gauge PDC bit is used. For the two remaining runs a Halliburton PDC bit is used. -7% discrepancy is subtracted from drillpipes, drill collars and heavyweights of notable length.

String Editor

String Initialization — String Name: **Well A** - 9 1/2" x 10 1/4" Geopilot w/PDC -7% — String (MD): 11643,0 ft — Specify: Top to Bottom — Import String — Library: Export, Import

	Section Type	Length (ft)	Measured Depth (ft)	OD (in)	ID (in)	Weight (ppf)	Item Description
1	Drill Pipe	10918,80	10918,8	5,500	4,778	27,25	Drill Pipe, 5,500 in, 27,25 ppf, S-135, FHDSTJ
2	Drill Collar	3,00	10921,8	7,250	3,500	35,00	Drift Catcher Sub
3	Heavy Weight	152,00	11073,8	5,500	3,500	52,13	Heavy Weight Drill Pipe, 5.500 in, 52.13 ppf, 1340 MOD, 5 1/2 FH DSTJ
4	Drill Collar	3,50	11077,3	6,500	3,000	89,00	X-Over Sub
5	Jar	34,00	11111,3	6,500	2,750	92,85	Accelerator
6	Drill Collar	3,50	11114,8	6,500	3,000	89,00	X-Over Sub
7	Heavy Weight	122,00	11236,8	5,500	3,500	52,13	Heavy Weight Drill Pipe, 5.500 in, 52.13 ppf, 1340 MOD, 5 1/2 FH DSTJ
8	Drill Collar	3,50	11240,3	6,500	3,000	89,00	X-Over Sub
9	Jar	31,00	11271,3	6,500	3,000	89,00	Jar
10	Sub	3,50	11274,8	7,125	3,000	88,00	Cross Over sub
11	Heavy Weight	214,00	11488,8	5,500	3,500	52,13	Heavy Weight Drill Pipe, 5.500 in, 52.13 ppf, 1340 MOD, 5 1/2 FH DSTJ
12	Sub	3,50	11492,3	7,125	3,000	88,00	X-Over Sub
13	Stabilizer	6,38	11498,7	6,750	2,813	100,77	9.375 Integral Blade
14	Drill Collar	30,50	11529,2	6,750	2,812	100,16	Drill Collar 6.75 all in, 6.75 x 2.8125 in, NC50
15	Drill Collar	3,00	11532,2	6,750	3,000	97,86	Float Sub
16	Underreamer	13,50	11545,7	8,375	2,250	114,30	XR800 UnderReamer
17	Drill Collar	7,00	11552,7	7,250	2,250	95,00	Roller Reamer
18	MWD	7,50	11560,2	6,750	1,920	112,09	Downhole Screen
19	MWD	10,00	11570,2	6,900	3,250	103,60	6 3/4 HOC
20	MWD	7,60	11577,8	6,750	1,905	96,30	6 3/4 PWD w/AC conversion Sub
21	MWD	24,53	11602,3	6,750	1,920	109,40	6 3/4 ADR Collar/ HCIM
22	MWD	4,55	11606,9	6,750	1,920	97,80	6 3/4 DGR Collar
23	Stabilizer	1,95	11608,8	6,750	1,920	112,09	Inline Stabilizer (ILS) PXP
24	Drill Collar	9,19	11618,0	5,000	1,713	76,00	Geo-Pilot 7600 Flex Collar
25	Stabilizer	11,70	11629,7	7,625	1,490	113,00	Geo-Pilot 7600_0
26	Drill Collar	11,52	11641,2	7,625	1,490	113,00	Geo-Pilot 7600_1
27	Bit	1,78	11643,0	9,500		105,00	PDC - HDBS_SFG65R

Figure D.9 – Run 300, 400, 500 and 700 w/-7% discrepancy

Hole Section Editor

Hole Name: 10 1/4" Hole Section — Import Hole Section

Hole Section Depth (MD): 11643,0 ft — ☑ Additional Columns

	Section Type	Measured Depth (ft)	Length (ft)	Tapered?	Shoe Measured Depth (ft)	ID (in)	Drift (in)	Effective Hole Diameter (in)	Friction Factor	Linear Capacity (bbl/ft)	Excess (%)	Item Description
1	Riser	62,0	62,00	☐		13,625				0,1803		Riser
2	Casing	5714,0	5652,00	☐	5714,0	9,760	9,625	9,760		0,0925		10 3/4 in, 55,5 ppf, TN110SS,
3	Open Hole	11643,0	5929,00	☐		10,250		10,250		0,1021	0,00	

Figure D.10 – Overburden hole section

Run 300

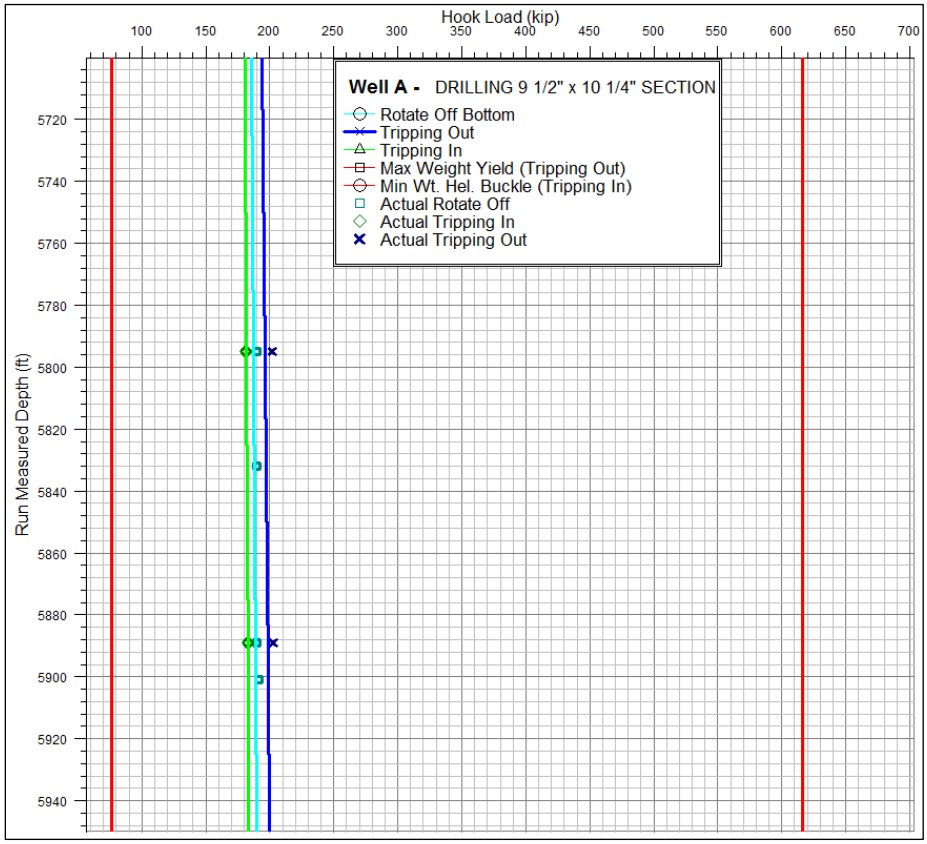

Figure D.11 – Run 300: Drag Hook Load Chart with buckling and yield limits w/-7% discrepancy

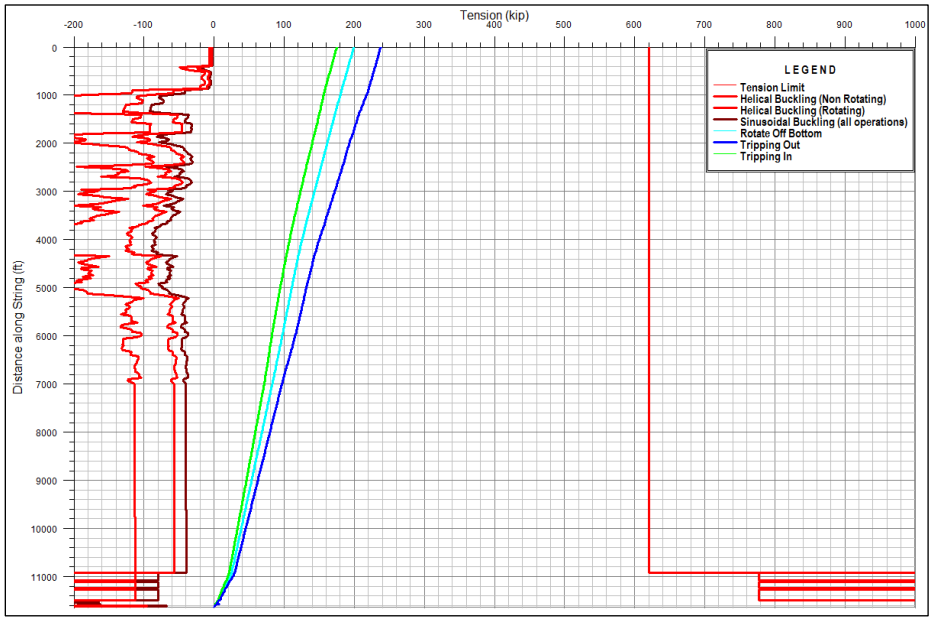

Figure D.12 – Run 300: Effective Tension Graph w/-7% discrepancy

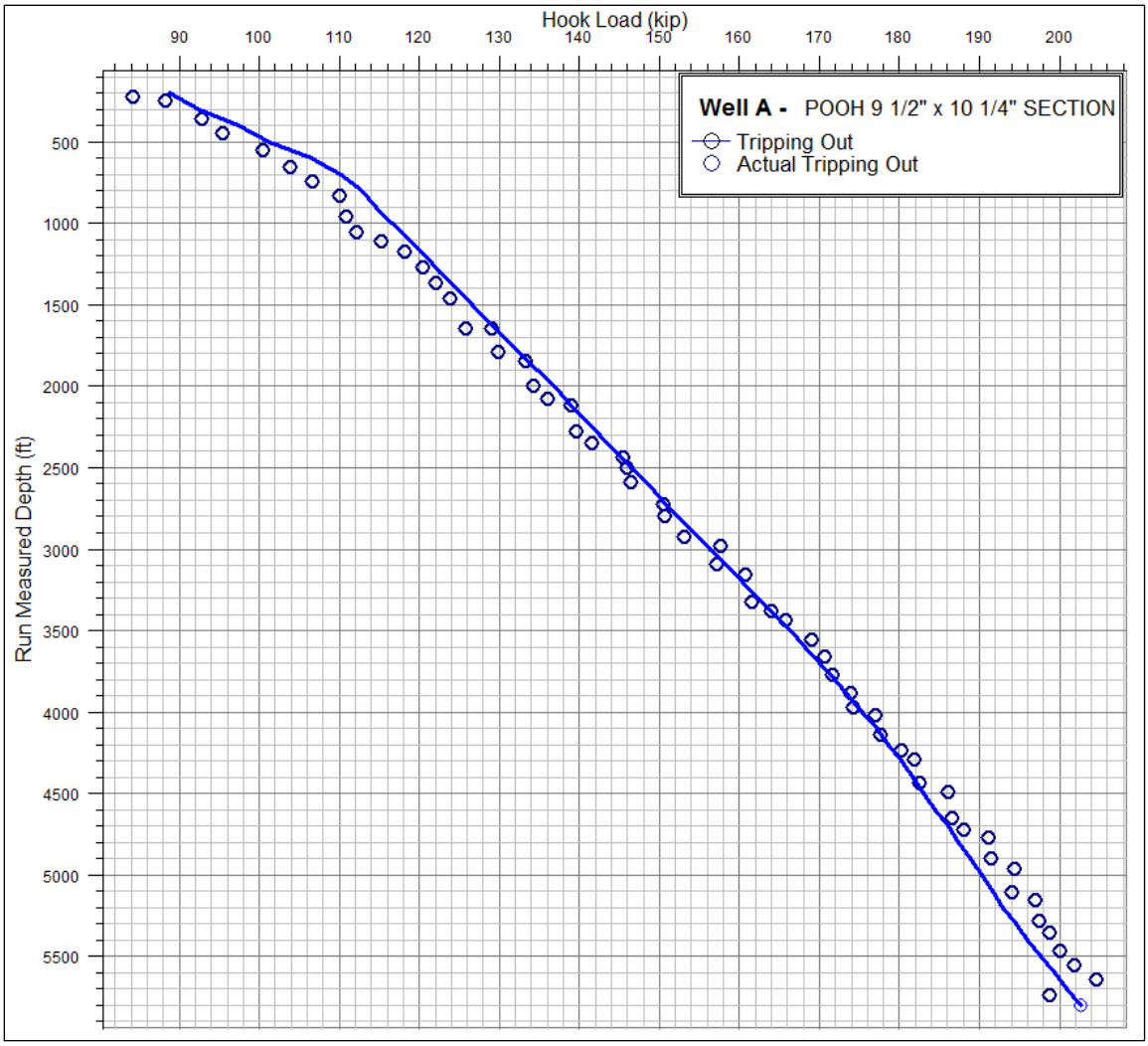

Figure D.13 – Run 300: POOH w/-7% discrepancy

Run 400

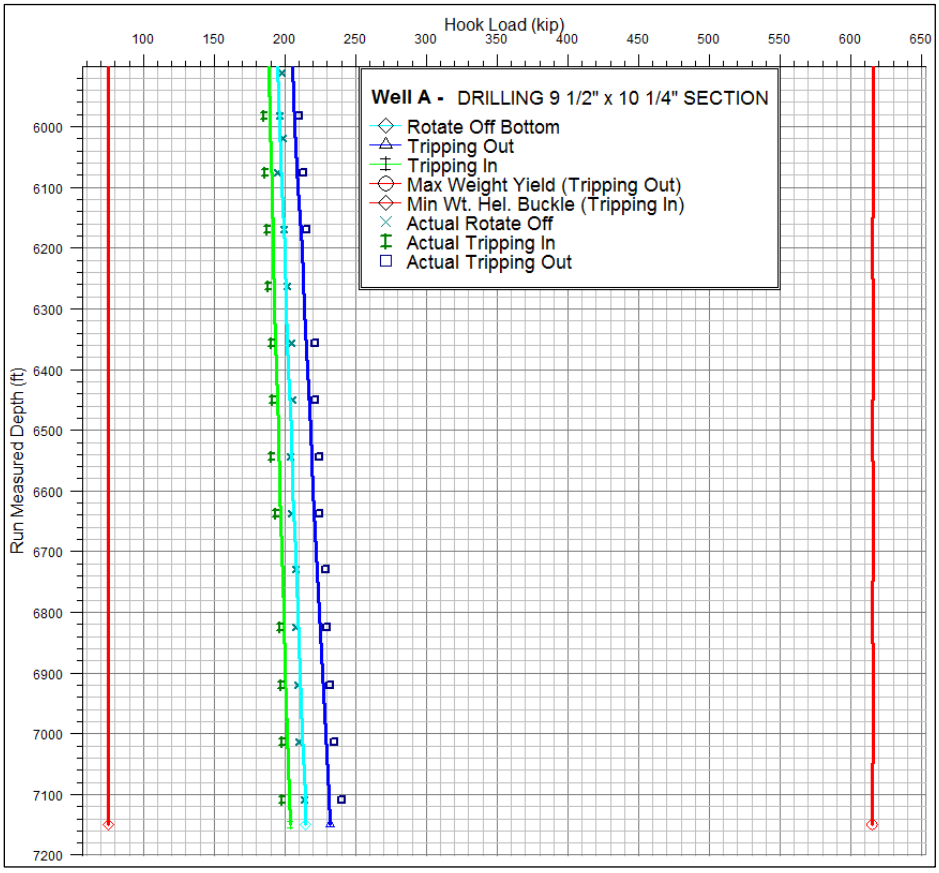

Figure D.14 – Run 400: Drag Hook Load Chart with buckling and yield limits w/-7% discrepancy

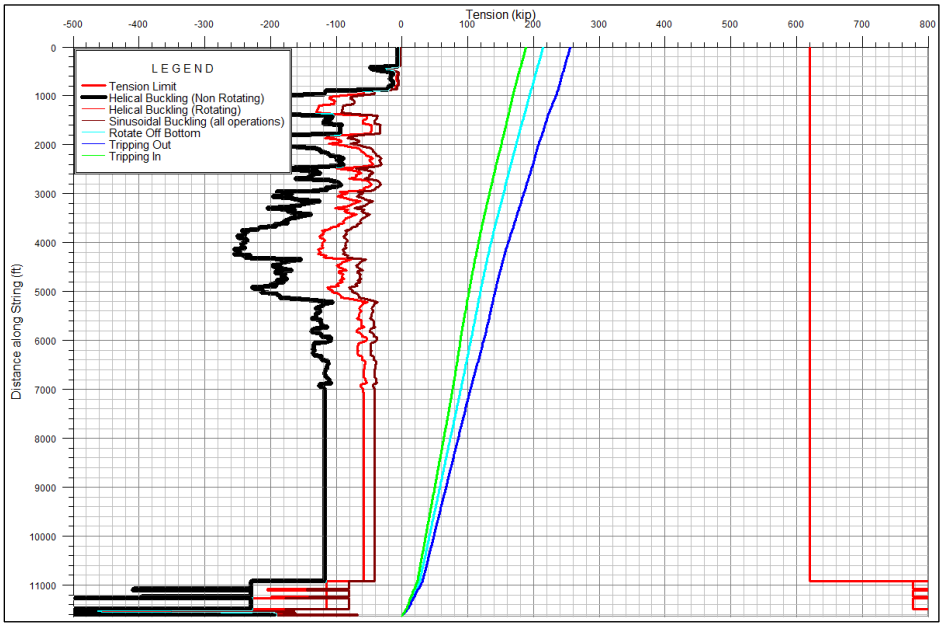

Figure D.15 – Run 400: Effective Tension Graph w/-7% discrepancy

Run 500

Same string information as in Figure D.9.

Run 600

This string had a tricone bit and did not have MWD components. -7% discrepancy substracted from drillpipe, heavyweights and drill collars of notable length.

String Editor

String Initialization

String Name: **Well A -** 0600_Drillstring - 7%

String (MD): 11643,0 ft Specify: Top to Bottom Import String

Library: Export, Import

	Section Type	Length (ft)	Measured Depth (ft)	OD (in)	ID (in)	Weight (ppf)	Item Description
1	Drill Pipe	11020,16	11020,2	5,500	4,778	27,25	Drill Pipe, 5,500 in, 27,25 ppf, S-135, FHDSTJ
2	Heavy Weight	154,27	11174,4	5,500	3,500	52,13	Heavy Weight Drill Pipe, 5,500 in, 52,13 ppf, 1340_MOD, 5 1/2 FH DSTJ
3	Drill Collar	4,05	11178,5	7,000	2,000	120,45	X-Over Sub
4	Jar	36,92	11215,4	6,625	2,560	99,94	6.1/2 Megaton Energizer
5	Drill Collar	2,62	11218,0	7,000	2,600	113,06	X-Over Sub
6	Heavy Weight	120,15	11338,2	5,500	3,500	52,13	Heavy Weight Drill Pipe, 5,500 in, 52,13 ppf, 1340_MOD, 5 1/2 FH DSTJ
7	Drill Collar	3,78	11342,0	7,000	2,500	114,43	X-Over Sub
8	Jar	30,40	11372,4	6,625	2,560	99,94	6.1/2 Megaton Jar
9	Drill Collar	3,51	11375,9	7,000	3,000	107,07	X-Over Sub
10	Heavy Weight	212,00	11587,9	5,500	3,500	52,13	Heavy Weight Drill Pipe, 5,500 in, 52,13 ppf, 1340_MOD, 5 1/2 FH DSTJ
11	Drill Collar	3,39	11591,3	6,000	2,700	76,85	X-Over Sub
12	Stabilizer	6,65	11597,9	6,750	3,000	97,86	Stabilizer
13	Drill Collar	30,74	11628,6	6,750	2,812	100,50	6 3/4 X 2.8125 - 100.5# Drill Collar
14	Drill Collar	2,38	11631,0	6,625	2,875	95,36	Float Sub
15	Stabilizer	7,14	11638,2	6,562	2,875	93,13	Stabilizer
16	Drill Collar	4,01	11642,2	6,562	3,000	91,17	X-Over Sub
17	Bit	0,83	11643,0	9,500		114,43	Tricone - MX-C09 Insert

Figure D.16 – Run 600: Drillstring information w/-7% discrepancy

Run 700

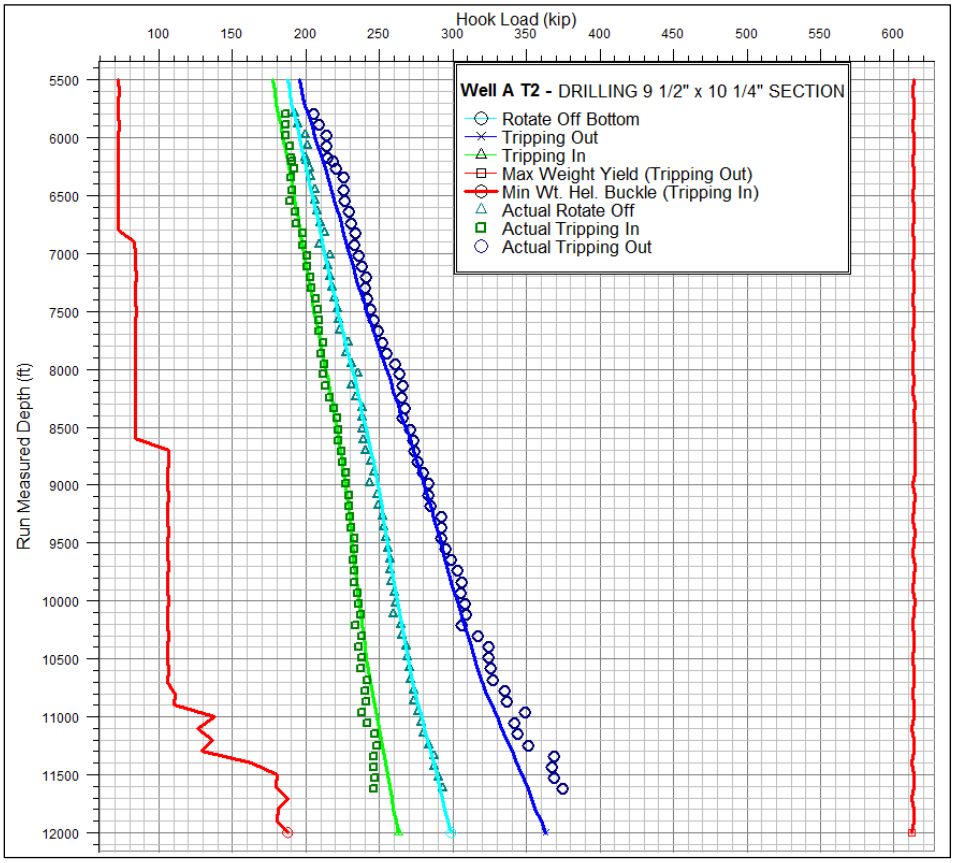

Figure D.17 – Run 700: Drag Hook Load Chart with buckling and yield limits w/-7% discrepancy

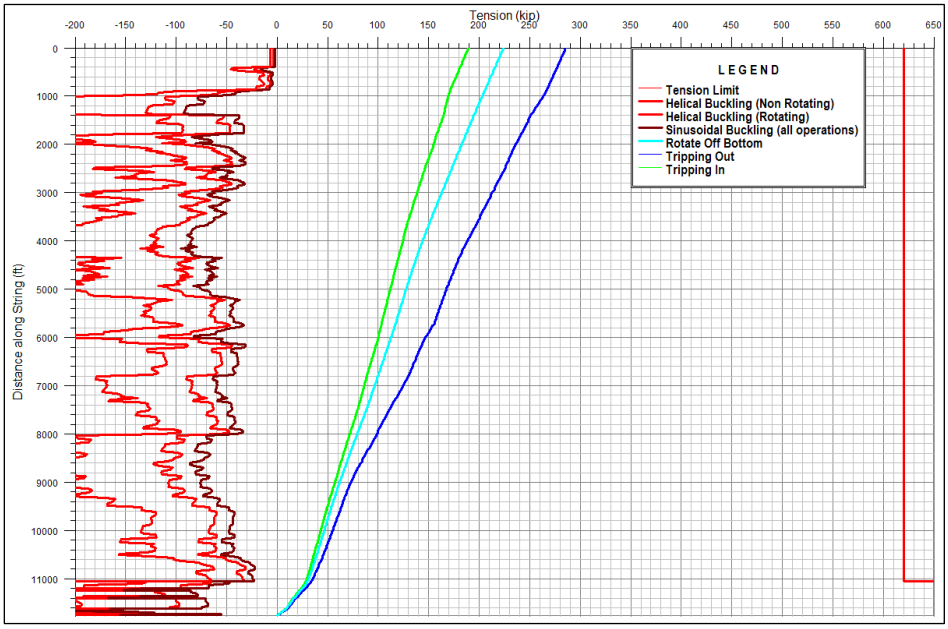

Figure D.18 – Run 700: Effective Tension Graph w/-7% discrepancy

Run 740

Torque Drag Effective Tension Graph with starting force of 568 lb/ft and running force of 422 lb/ft.

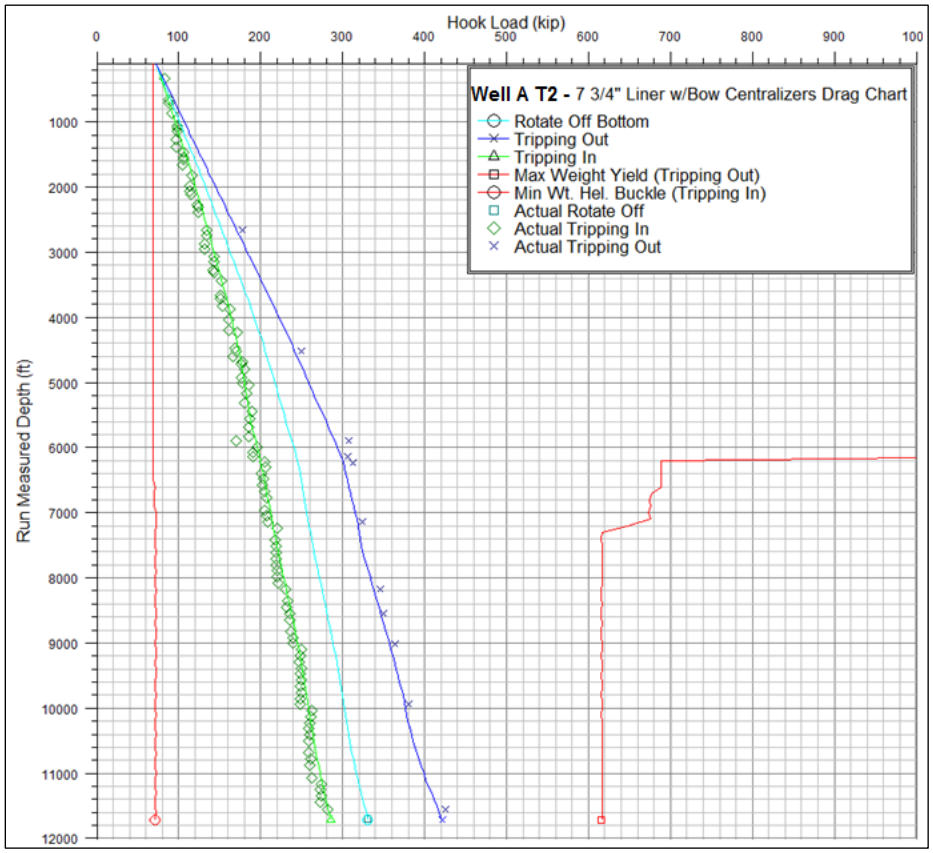

Figure D.19 – Run 740: Drag Hook Load Chart with buckling and yield limits w/-7% discrepancy

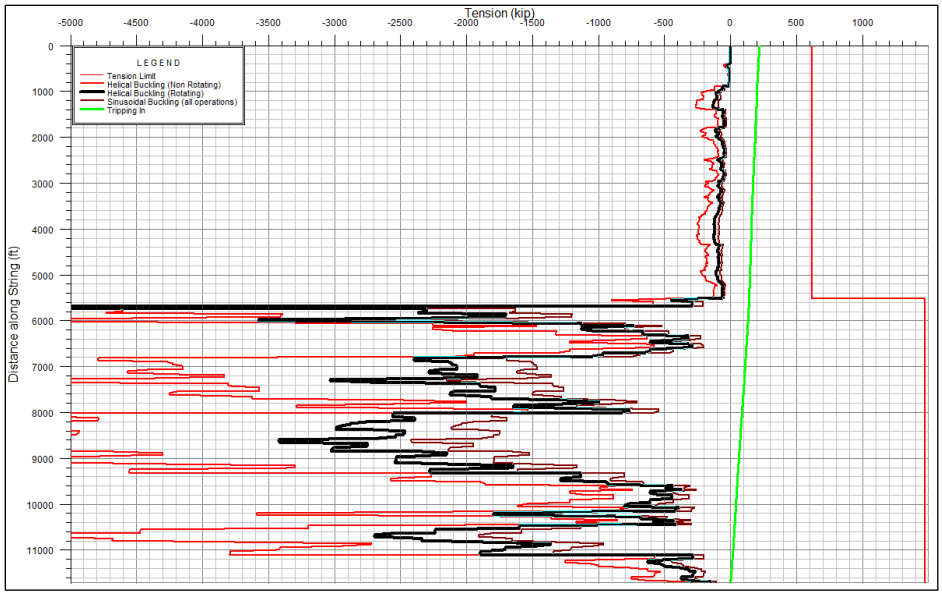

Figure D.20 – Run 740: Effective Tension Graph w/-7% discrepancy

D.3 The 6 ½" Reservoir Section

Run 800

Hole Section Editor

Hole Name: 6 1/2" Hole Section — Import Hole Section

Hole Section Depth (MD): 12940,0 ft — ☑ Additional Columns

	Section Type	Measured Depth (ft)	Length (ft)	Tapered?	Shoe Measured Depth (ft)	ID (in)	Drift (in)	Effective Hole Diameter (in)	Friction Factor	Linear Capacity (bbl/ft)	Excess (%)	Item Description
1	Riser	62,0	62,00	☐		13,625				0,1803		Riser
2	Casing	5525,0	5463,00	☐	5714,0	9,760	9,625	9,760		0,0925		10 3/4 in, 55,5 ppf, TN110SS,
3	Casing	11715,0	6190,00	☐	11715,0	6,560	6,500	6,560		0,0418		7 3/4 in, 46,1 ppf, TN110SS,
4	Open Hole	12940,0	1225,00	☐		6,500		6,500		0,0410	0,00	

Figure D.21 – Run 800: 6 ½" Hole Section

-7% discrepancy is subtracted from drillpipes, drill collars and heavyweights of notable length:

String Editor

String Initialization

String Name: **Well A -** 0800_Drillstring-7%

String (MD): 12940,0 ft Specify: Top to Bottom Import String

Library: Export, Import

	Section Type	Length (ft)	Measured Depth (ft)	OD (in)	ID (in)	Weight (ppf)	Item Description
1	Drill Pipe	5491,28	5491,3	5,500	4,778	27,25	Drill Pipe, 5,500 in, 27,25 ppf, S-135, FHDSTJ
2	Drill Collar	4,00	5495,3	5,000	3,000	45,00	X-Over Sub
3	Drill Pipe	6590,00	12085,3	4,000	3,240	17,97	Drill Pipe, 4,000 in, 17,97 ppf, S-135, NC40 DSTJ
4	Drill Collar	3,00	12088,3	5,375	2,563	59,75	Drift Catcher Sub
5	Heavy Weight	282,00	12370,3	4,000	2,250	31,20	Heavy Weight Drill Pipe, 4,000 in, 31,20 ppf, 4145H_MOD, VAM EIS NC 40
6	Drill Collar	3,00	12373,3	5,000	2,500	50,19	X-Over Sub
7	Jar	35,00	12408,3	4,750	2,250	47,00	Accelerator
8	Drill Collar	92,00	12500,3	4,750	2,250	39,72	Drill Collar, 4.750 in, 39.72 ppf, DC, NC38 DSTJ
9	Jar	30,18	12530,5	4,750	2,250	46,84	Jar
10	Drill Collar	215,00	12745,5	4,750	2,250	39,72	Drill Collar, 4.750 in, 39.72 ppf, 4145H MOD, NC38 DSTJ
11	Stabilizer	5,91	12751,4	4,750	1,500	54,37	Rollar Reamer
12	Drill Collar	9,76	12761,1	4,750	2,250	46,84	Pony Collar
13	Sub	3,00	12764,1	4,750	2,250	46,90	Float Sub
14	MWD	6,50	12770,6	4,750	1,250	56,21	Downhole Screen
15	MWD	26,42	12797,1	4,750	1,250	45,70	BAT Collar
16	MWD	11,23	12808,3	4,750	2,812	46,10	4 3/4 SHORT HOC
17	Stabilizer	3,59	12811,9	4,750	1,250	56,21	Inline Stabilizer (ILS)
18	MWD	17,34	12829,2	4,750	1,250	49,60	4 3/4 GEO-TAP_0
19	Stabilizer	6,62	12835,8	4,750	1,250	49,60	4 3/4 GEO-TAP_1
20	MWD	11,10	12846,9	4,750	1,250	50,50	4 3/4 CTN Collar
21	MWD	6,98	12853,9	4,750	1,250	45,50	4 3/4 ALD Collar 175C_0
22	Stabilizer	7,33	12861,2	4,750	1,250	45,50	4 3/4 ALD Collar 175C_1
23	MWD	27,27	12888,5	4,750	1,250	53,70	4 3/4 ADR Collar
24	MWD	9,26	12897,8	4,750	1,250	47,00	4 3/4 GM Collar
25	Stabilizer	3,58	12901,3	4,750	1,250	56,21	ILS
26	MWD	9,19	12910,5	4,750	2,610	47,00	4 3/4 DM Collar
27	Drill Collar	11,55	12922,1	4,750	2,250	44,00	Geo-Pilot Flex Collar
28	Stabilizer	16,36	12938,5	5,250	3,120	52,94	Geo-Pilot 5200
29	Bit	1,55	12940,0	6,500		48,00	Tri-Cone Bit, 0.641 in²

Figure D.22 – Run 800: Drillstring information w/-7% discrepancy

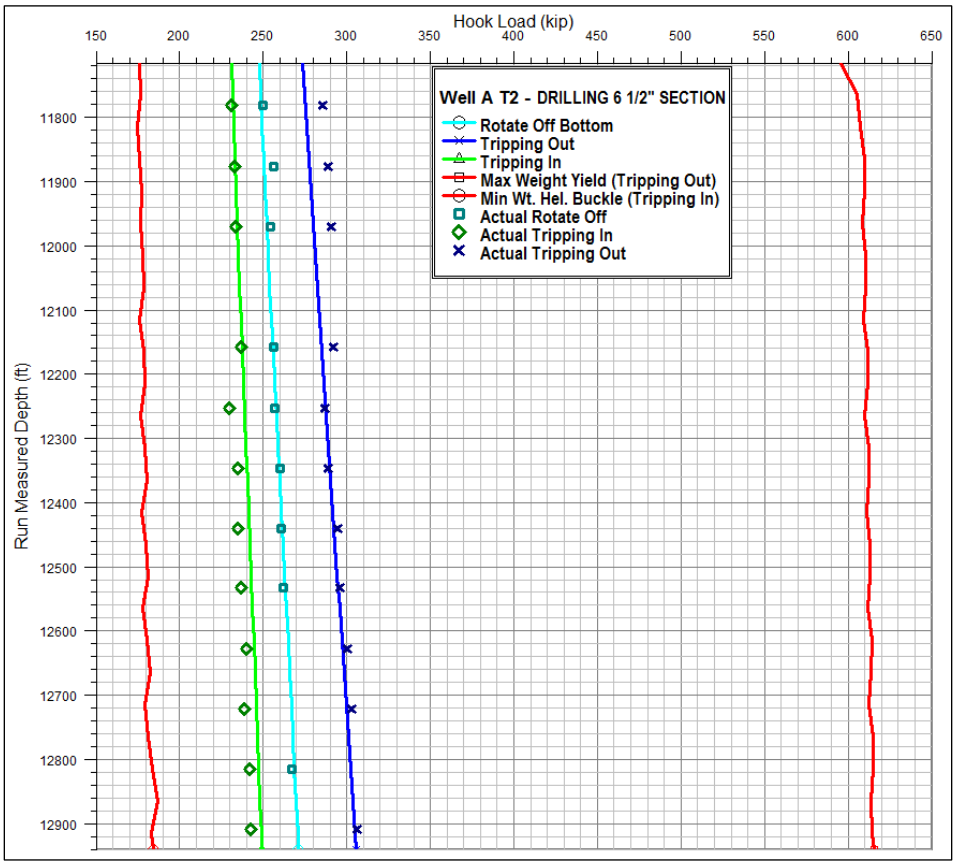

Figure D. 23 – Run 800: Drag Hook Load Chart with buckling and yield limits w/-7% discrepancy

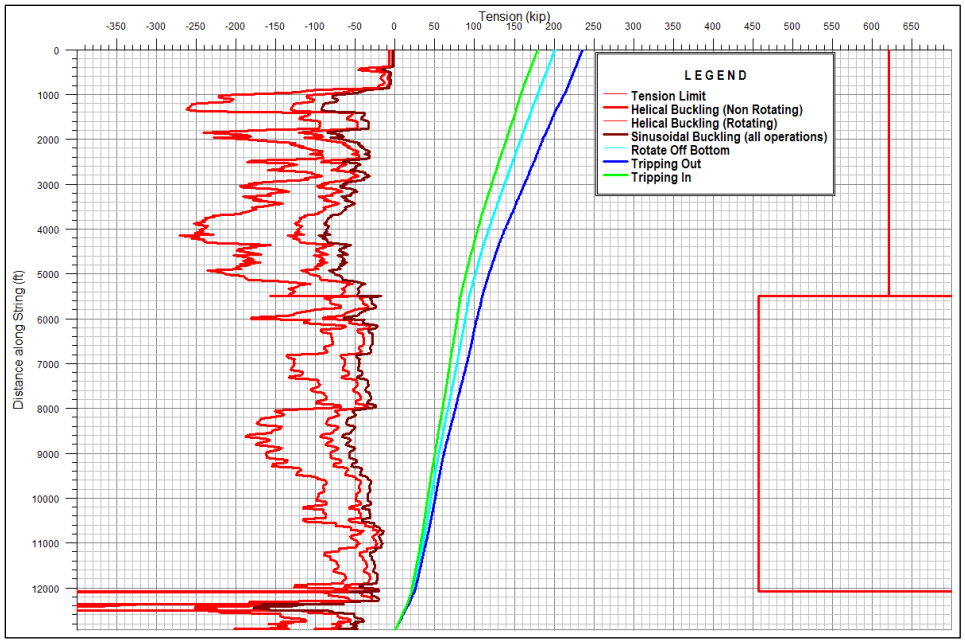

Figure D.24 – Run 800: Effective Tension Chart w/-7% discrepancy

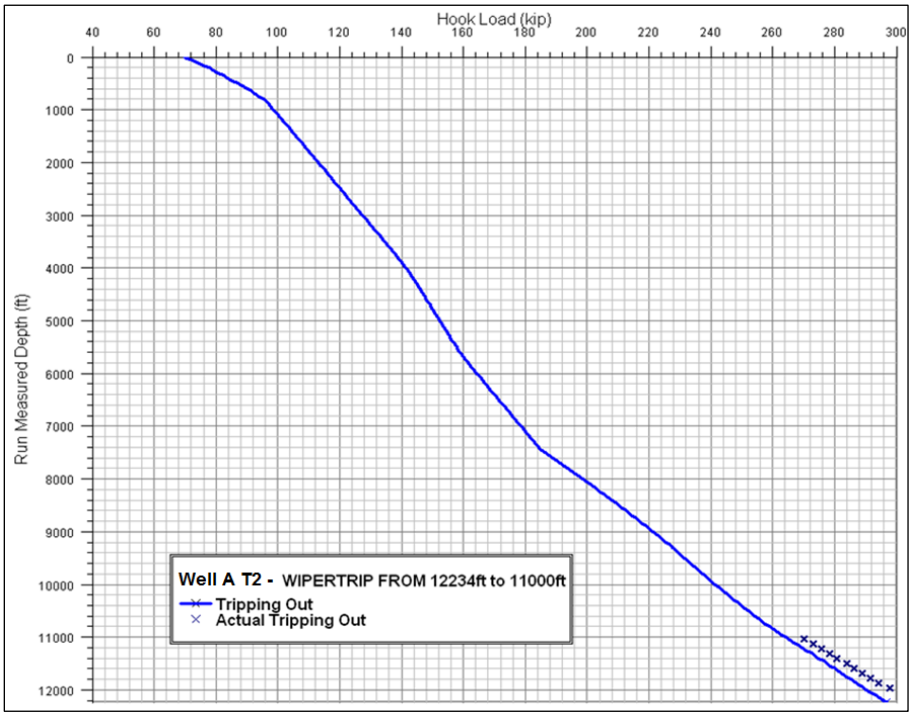

Figure D.25 – Run 800: Wiper trip w/-7% discrepancy

Run 840

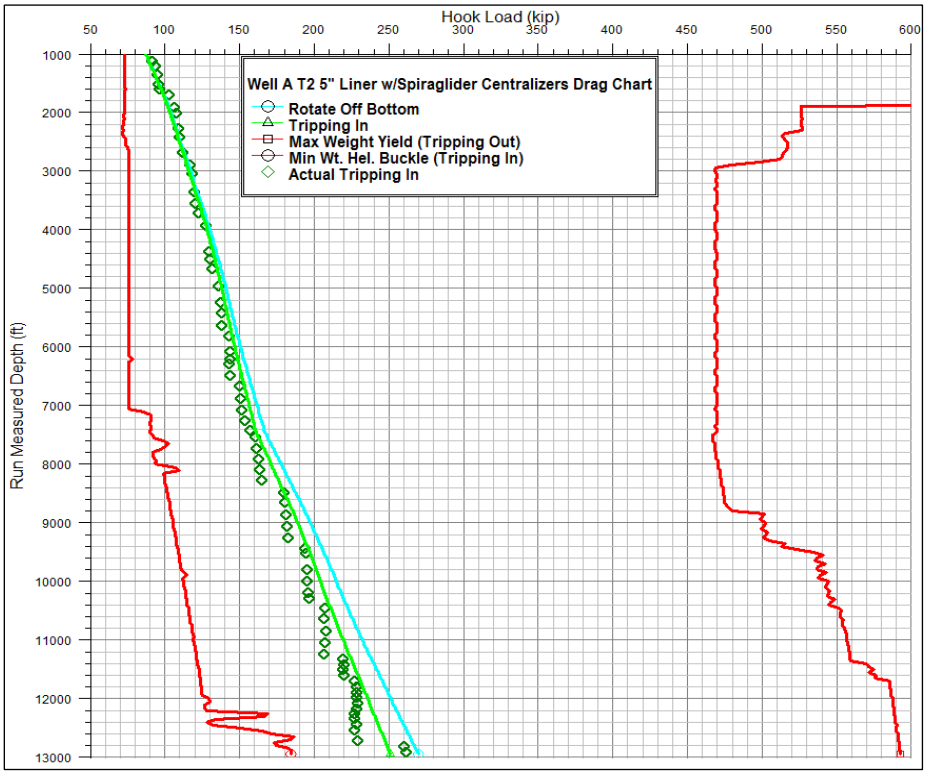

Figure D.26 – Run 840: Drag Hook Load Chart with buckling and yield limits w/-7% discrepancy

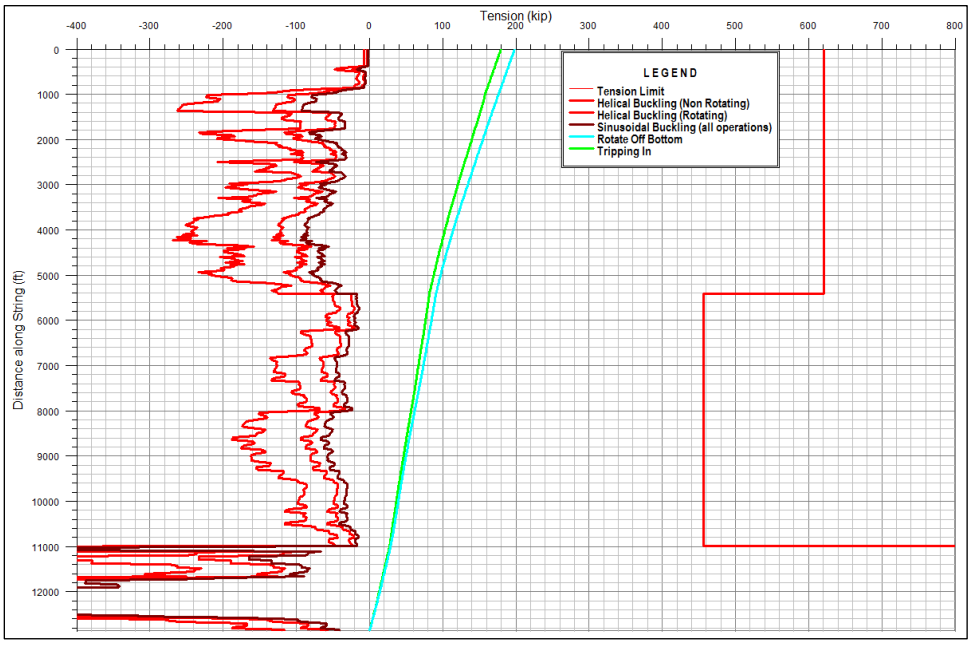

Figure D.27 – Run 840: Effective Tension Graph w/-7% discrepancy

D.4 Survey Data

MD (ft)	INC (°)	AZ (°)	TVD (ft)	DLS (°/100ft)
0	0	0	0	0
423	0	0	423	0
500	0,46	261,56	500	0,6
600	0,43	268,7	600	0,06
700	0,5	278,94	700	0,11
800	0,45	275,43	800	0,06
900	0,56	261,34	900	0,17
1000	1,85	209,64	1000	1,57
1100	4,5	182,45	1099,8	2,98
1200	7,09	175,74	1199,3	2,67
1300	10,39	173,06	1298,1	3,32
1400	13,72	172,48	1395,9	3,33
1500	14,2	169,35	1492,9	0,89
1600	14,93	166,34	1589,7	1,05
1700	14,96	169,56	1686,3	0,83
1800	15	172,8	1783	0,84
1825	15,34	174,35	1807,1	2,12
1850	15,78	175,87	1831,2	2,4
1875	16,31	177,95	1855,2	3,13
1900	16,61	180,31	1879,2	2,93
1925	16,86	182,21	1903,1	2,41
1950	17,27	183,37	1927	2,13
1975	17,63	184,51	1950,9	1,99
2000	18,26	185,71	1974,6	2,92
2025	18,74	186,41	1998,3	2,12
2050	19,14	186,94	2022	1,74
2075	19,47	187,43	2045,6	1,47
2100	19,68	187,27	2069,1	0,87
2125	19,86	187,54	2092,7	0,81
2150	20,08	187,8	2116,2	0,95
2175	20,19	187,99	2139,6	0,51
2200	20,39	188,06	2163,1	0,81
2225	20,46	188	2186,5	0,29
2250	20,57	188,07	2209,9	0,45
2275	20,59	188,03	2233,3	0,1
2300	20,53	188,13	2256,7	0,28
2325	20,48	188,1	2280,2	0,2
2350	20,61	188,16	2303,6	0,53
2375	20,55	188,06	2327	0,28
2400	20,52	188,21	2350,4	0,24
2425	20,47	188,15	2373,8	0,22
2450	20,42	188,29	2397,2	0,28
2475	20,48	188,35	2420,7	0,25
2500	20,8	187,52	2444	1,73

2525	21,28	186,4	2467,4	2,5
2550	21,52	185,89	2490,7	1,21
2575	21,65	185,17	2513,9	1,18
2600	21,63	184,27	2537,1	1,33
2625	21,53	183,02	2560,4	1,88
2650	21,51	181,79	2583,6	1,81
2675	21,4	180,56	2606,9	1,85
2700	21,34	179,23	2630,2	1,95
2725	21,27	177,63	2653,5	2,34
2750	21,1	176,56	2676,8	1,69
2775	20,99	175,74	2700,1	1,26
2800	21,06	175,58	2723,5	0,36
2825	21,02	175,66	2746,8	0,2
2850	20,95	176,21	2770,1	0,84
2875	20,76	177,05	2793,5	1,42
2900	20,68	178,14	2816,9	1,58
2925	20,6	178,99	2840,3	1,24
2950	20,5	180,15	2863,7	1,68
2975	20,35	181,56	2887,1	2,06
3000	20,36	183,5	2910,6	2,7
3025	20,32	185,1	2934	2,23
3050	20,55	186,5	2957,4	2,16
3075	20,95	187,65	2980,8	2,28
3100	21,4	188,43	3004,1	2,12
3125	21,75	188,58	3027,4	1,42
3150	22,09	188,64	3050,6	1,36
3175	22,25	188,5	3073,7	0,67
3200	22,46	188,09	3096,8	1,05
3225	22,65	187,29	3119,9	1,44
3250	22,7	185,99	3143	2,01
3275	22,69	184,77	3166,1	1,88
3300	22,7	183,29	3189,1	2,28
3325	22,78	181,48	3212,2	2,82
3350	22,8	180,18	3235,2	2,02
3375	22,91	178,89	3258,3	2,05
3400	22,96	177,41	3281,3	2,32
3425	23,11	176,33	3304,3	1,79
3450	23,26	175,74	3327,3	1,11
3475	23,51	175,26	3350,2	1,26
3500	23,83	174,87	3373,1	1,42
3525	24,14	174,55	3396	1,34
3550	24,53	173,97	3418,7	1,83
3575	24,8	173,16	3441,5	1,73
3600	25,14	172,39	3464,1	1,88
3625	25,37	171,48	3486,7	1,81
3650	25,76	170,69	3509,3	2,07
3675	26,07	169,7	3531,8	2,13

3700	26,37	168,73	3554,2	2,09
3725	26,82	167,59	3576,5	2,72
3750	27,1	166,29	3598,8	2,61
3775	27,55	164,98	3621	3
3800	27,83	163,56	3643,2	2,87
3825	28,18	162,19	3665,3	2,93
3850	28,48	160,72	3687,3	3,04
3875	28,72	159,25	3709,2	2,97
3900	29,01	157,69	3731,1	3,23
3925	29,24	156,12	3752,9	3,19
3950	29,43	154,59	3774,7	3,09
3975	29,78	153,36	3796,5	2,8
4000	30,08	152,03	3818,1	2,91
4025	30,44	150,78	3839,7	2,9
4050	30,93	149,74	3861,2	2,89
4075	31,46	148,9	3882,6	2,74
4100	31,96	148,06	3903,9	2,67
4125	32,62	147,44	3925	2,95
4150	33,14	147,12	3946	2,19
4175	33,87	146,54	3966,9	3,19
4200	34,51	146,28	3987,5	2,63
4225	35,13	146,09	4008,1	2,52
4250	35,87	145,65	4028,4	3,13
4275	36,35	145,35	4048,6	2,05
4300	37	145,22	4068,7	2,62
4325	37,58	145,06	4088,6	2,35
4350	38,14	145,24	4108,3	2,28
4375	38,31	145,36	4127,9	0,74
4400	38,47	145,74	4147,5	1,14
4425	38,71	146,51	4167,1	2,15
4450	38,85	147	4186,6	1,35
4475	39,13	147,65	4206	1,98
4500	39,5	148,02	4225,3	1,75
4525	39,87	148,27	4244,6	1,61
4550	40,21	148,29	4263,7	1,36
4575	40,47	148,06	4282,8	1,2
4600	40,64	147,7	4301,8	1,16
4625	40,97	147,08	4320,7	2,09
4650	41,15	146,4	4339,5	1,93
4675	41,26	145,76	4358,3	1,74
4700	41,41	145,05	4377,1	1,97
4725	41,47	144,43	4395,9	1,66
4750	41,55	143,52	4414,6	2,43
4775	41,57	142,89	4433,3	1,67
4800	41,8	142,23	4452	1,98
4825	41,92	141,59	4470,6	1,77
4850	42,21	141,16	4489,1	1,64

4875	42,5	140,52	4507,6	2,08
4900	42,85	140,22	4526	1,62
4925	43,11	139,73	4544,3	1,69
4950	43,46	138,91	4562,5	2,65
4975	43,8	138,2	4580,6	2,39
5000	44,08	137,6	4598,6	2,01
5025	44,48	137,02	4616,5	2,28
5050	44,84	136,68	4634,3	1,73
5075	45,16	136,64	4651,9	1,28
5100	45,48	136,55	4669,5	1,31
5125	45,77	136,64	4687	1,19
5150	46,12	136,64	4704,4	1,4
5175	46,32	136,75	4721,7	0,86
5200	46,34	136,91	4738,9	0,47
5225	46,21	137	4756,2	0,58
5250	45,86	137,03	4773,6	1,4
5275	45,63	137,34	4791	1,28
5300	45,46	137,45	4808,5	0,75
5325	45,34	137,49	4826,1	0,49
5350	45,27	137,48	4843,7	0,28
5375	45,27	137,57	4861,3	0,26
5400	45,16	137,43	4878,9	0,59
5425	45,06	137,5	4896,5	0,45
5450	44,98	137,45	4914,2	0,35
5475	44,89	137,37	4931,9	0,43
5500	44,93	137,27	4949,6	0,32
5525	44,86	137,27	4967,3	0,28
5550	44,84	137,22	4985	0,16
5575	44,89	137,08	5002,7	0,44
5702	44,32	137,39	5093,2	0,48
5800,8	42,04	139,46	5165,2	2,72
5862,5	41,1	141,6	5211,4	2,76
5956	41,92	143,99	5281,4	1,91
6046,8	40,28	149,12	5349,8	4,13
6141,5	41,26	149,86	5421,5	1,15
6236,2	39,9	150,13	5493,5	1,45
6327,1	40,18	149,42	5563,1	0,59
6424,3	39,94	149,37	5637,5	0,25
6520,4	39,53	148,34	5711,4	0,81
6611,4	39,22	148,46	5781,7	0,35
6706,9	39,38	147,65	5855,6	0,56
6801,6	39,1	145,99	5929	1,15
6894,6	38,9	141,93	6001,2	2,76
6987,2	38,9	138,35	6073,3	2,43
7080,7	39,01	134,82	6146	2,38
7174,2	38,8	130,92	6218,8	2,63
7267,1	38,64	127,65	6291,3	2,21

7361,4	36,15	124,02	6366,2	3,53
7455,7	35,24	120,79	6442,8	2,22
7549,6	34,48	117,64	6519,9	2,08
7644,5	33,49	113,84	6598,6	2,47
7736,5	32,57	110,69	6675,7	2,12
7831,7	32,55	108,67	6755,9	1,14
7924,5	32,22	105,43	6834,3	1,9
8022,3	31,54	104,1	6917,4	1
8114,1	32,09	99,11	6995,4	2,93
8208,9	32,36	94,26	7075,6	2,74
8302,3	33,27	88,84	7154,1	3,29
8395,5	34,12	83,3	7231,7	3,42
8489,4	34,29	78,58	7309,3	2,83
8583,5	35,2	74,07	7386,7	2,9
8678,2	35,07	67,6	7464,1	3,93
8769,6	35,32	62,61	7538,8	3,16
8864,2	35,97	57,1	7615,7	3,46
8957,3	37,07	53,77	7690,6	2,43
9053	38,53	49,97	7766,2	2,87
9145,1	39,81	46,28	7837,6	2,89
9240,2	41,44	45,51	7909,8	1,79
9333,5	42,89	42,67	7978,9	2,57
9426,5	43,95	42,73	8046,5	1,14
9522,8	45,16	42,09	8115,1	1,34
9617,5	45,25	40,72	8181,8	1,03
9711,2	45,06	41,43	8247,9	0,57
9804,2	45,02	40,58	8313,6	0,65
9898,8	45,04	40,26	8380,5	0,24
9992,4	45,3	40,76	8446,5	0,47
10086,5	45,5	41,83	8512,5	0,84
10177,3	45,33	41,32	8576,3	0,44
10274,8	45,2	44,15	8644,9	2,07
10367,1	45,13	43,17	8710	0,76
10461	44,96	44,04	8776,3	0,68
10553,9	45,17	41,67	8842	1,82
10649,2	43,23	39,39	8910,3	2,63
10743,3	40,39	38,06	8980,4	3,16
10837,5	37,81	38,57	9053,5	2,76
10931,8	36,24	38,94	9128,8	1,68
11026	34,32	39,32	9205,7	2,05
11119,7	32,26	38,48	9284	2,25
11214	31,81	39,09	9364	0,59
11308	32,25	38,75	9443,6	0,51
11400,6	32,38	38,08	9521,9	0,41
11495,1	32,15	37,6	9601,8	0,36
11588,4	31,78	38,12	9681	0,49
11680,9	31,83	38,1	9759,6	0,06

11745,5	31,21	38,91	9814,6	1,16
11839,9	29,94	40,66	9895,9	1,64
11933,1	29	42,64	9977,1	1,45
12027,9	27,09	47,3	10060,7	3,06
12117	24,94	50,33	10140,8	2,84
12215,9	22,11	53,35	10231,5	3,11
12311,1	20,44	53,32	10320,2	1,75
12404,4	19,06	59,61	10408	2,71
12497,2	17,54	69,99	10496,1	3,87
12582,2	18,09	72,8	10577,1	1,2
12686,5	18,08	73,63	10676,2	0,25
12776	17,45	74,28	10761,4	0,74
12906,6	16,83	75,53	10886,2	0,55

Appendix E: Centralizers

Centralizers are used when running casing in open hole and when running liner in casing. The purpose of a centralizer is to keep the casing or liner in the center of the wellbore or casing to get an even distribution of cement around the casing/liner. This is important to get a good cement job and prevents mud channeling and poor zonal isolation. Other advantages of centralizers are [34]:

- Reducing casing drag on the wellbore during casing running operations.
- Reducing the risk of differential sticking.
- Increasing fluid turbulence at the tool, helping to remove filter cake from the wellbore.

The term standoff (SO) is used to describe how centered the pipe is in the hole. A perfectly centered casing has a standoff of 100%. A casing touching the wall of the wellbore has a standoff of 0%. The goal of a centralizer is to achieve a standoff of more than 67% throughout the casing string. Conditions affecting casing standoff are [34]:

- Well path and hole size
- Casing OD and weight
- Centralizer properties
- Mud and cement slurry position and densities (Buoyancy)

For the field case in this paper, both bow-spring centralizers and spiraglider centralizers were used when running the two liners.

E.1 Bow-Spring Centralizers

Bow-spring centralizers have steel bows that act as springs to push the pipe away from the wellbore. The shape and stiffness of the bows determines the restoring force. The effectiveness of bow-spring centralizers is largely dependent on the restoring force, which is defined as the resistance force when a bow compresses 1/3 of its uncompressed height. [34] The centralizers can be run through a wellbore, an already cemented casing string with extremely tight annular clearance or other restrictions. The bows will then withdraw to the diameter of the wellbore/casing, allowing the casing/liner to be run through while still being centralized. After

passing through the restrictions, the bows expand to provide centralization in the following openhole or underreamed sections. [35]

Figure E.1 – Weatherford S-Series Bow-Spring Centralizer [36]

E.2 SpiraGlider Centralizers

SpiraGlider centralizers have straight or spiral blades and two asymmetrically beveled stop collars shaped to minimize running resistance. They can be used in vertical, inclined and horizontal wells, and are also suitable for extended-reach wells and wells with high dogleg severity. SpiraGlider centralizers are designed to give lower drag forces and require less rotational torque than conventional centralizers. The hydrodynamic shape of the spiral blades minimizes pressure drop and local turbulence across the centralizer and gives optimal mud displacement during the cement job. [37]

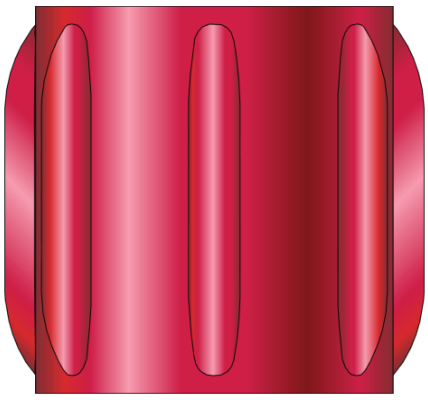

Figure E.2 – Weatherford straight bladed Spiraglider Centralizer [37]